

CLIWA-NET

BALTEX BRIDGE Cloud Liquid Water Network

Final Report

Editors:

*Susanne Crewell, Clemens Simmer (UNIBONN),
Arnout Feijt, Erik van Meijgaard (KNMI)*

<http://www.knmi.nl/samenw/cliwa-net>



CLIWA-NET is a research project supported by the European Commission under the Fifth Framework Programme within the Energy, Environment and Sustainable Development Programme.

Contract no: EVK2-CT-1999-00007

Project duration: 1 March 2000 - 28 February 2003

International BALTEX Secretariat Publication

ISSN 1681-6471

No. 26

July 2003

CLIWA-NET Participants:

Royal Netherlands Meteorological Institute (KNMI)

Arnout Feijt, Erik van Meijgaard, Andre van Lammeren, Hannelore Bloemink,
Dominique Jolivet, Anne Mathieu



Meteorological Institute, University of Bonn (UNIBONN)

Susanne Crewell, Clemens Simmer, Felix Ament, Matthias Drusch, Ulrich Löhnert,



Centre des Environnements Terrestre et Planétaires (CETP)

Cecille Mallet, Laurent Chardinal

Helsinki University of Technology, Laboratory of Space Technology (HUT)

Martti Hallikainen, Andreas Colliander



Radiometer Physics GmbH (RPG)

Thomas Rose



Deutscher Wetterdienst, Meteorological Observatory Lindenberg

Jürgen Güldner



CHALMERS

Chalmers University of Technology, Onsala Space Observatory (CHALMERS)

Gunnar Elgered, Harald Bouma, Lubomir Grdinarsky, Borys Stoew



Institute for Applied Physics, University of Bern (UNIBERN)

Christian Mätzler, Lorenz Martin



Swedish Meteorological and Hydrological Institute (SMHI)

Colin Jones, Adam Dybroe, Daniel Michelson, Ulrika Willen



Institute for Marine Research (IFM)

Andreas Macke, Heike Hauschildt



GKSS Research Center, Institute for Coastal Research (GKSS)

Markus Quante, Henriette Lemke, Oliver Sievers

Rutherford Appleton Laboratory, Radio Communications Research Unit (CCLRC)

Charles Wrench, Patrick Simpson

Subcontractor of KNMI:

Institute of Radio Engineering and Electronics, Russian Academy of Sciences (IRE)

Boris Kutuza, Gregori Shchukin, Andrej Sobachkin, Yuri Rybakov

Executive Summary

Objectives

CLIWA-NET aims at the improvement of the parameterization of cloud processes in atmospheric models with a focus on vertically integrated cloud liquid water and vertical structure of clouds. To achieve this goal a prototype of a European Cloud Observation Network (ECON) consisting of ground-based stations and satellite measurements was to be set up. It operated successfully during three enhanced observation phases (EOP) all part of BRIDGE – the major field experiment of BALTEX. The potential of this data for the objective evaluation of atmospheric models for weather forecasting and climate simulations was to be demonstrated. Furthermore, the observations should be analysed for their potential as an adequate observing system for the detection of aircraft icing conditions. As microwave radiometry is the most accurate way to measure liquid water path existing radiometers from different partners in Europe were incorporated in ECON. In order to allow such a system to become operational in the future the design of a *low-cost* microwave radiometer in co-operation with industry (SME) was another CLIWA-NET objective.

Scientific achievements

The prototype of a European Cloud Observation network (ECON) was successfully implemented during three enhanced observational periods (CNNI: August/September 2000; CNNII: April/May 2001 and BBC: August/September 2001). To successfully implement ECON existing observation systems (microwave radiometer and auxiliary instruments) were distributed in a continental scale over the BALTEX modelling region and a regional scale network in the Netherlands.

- Harmonized retrieval algorithms to derive the liquid water path (LWP) and the integrated water vapour (IWV) were developed for all stations and campaigns. Quality checked time series of LWP, IWV, cloud base height, infrared temperature and different rain flags for all stations during all campaigns were produced.
- For the three campaigns about 1400 AVHRR satellite overpasses were processed to obtain cloud type classifications.
- Fields of LWP, optical depth and effective radius were derived from NOAA-AVHRR satellite measurements. Several hundred overpasses were selected for quantitative cloud analysis. The selection was based on quality of the AVHRR instrument, sun elevation and viewing angle.
- The microwave inter-comparison campaign (MICAM) performed in the second project year verified the good quality of liquid water path measurements during the previous CNN campaigns. However, the uncertainty of current gas absorption models and the inherent retrieval ambiguities limit the accuracy of standard dual frequency systems to about 30 g m^{-2} . These models need to be further constrained.
- The combination of different advanced remote sensing instruments at the Cabauw site during the BBC campaign allowed the application of a newly developed synergetic algorithm to derive simultaneously temperature, humidity and liquid profiles and their respective uncertainties.
- Based on lidar ceilometer measurements a climatology of super-cooled layers over the Netherlands was derived. The combination of cloud radar with microwave radiometer measurements allowed the identification of some of their properties: Often ice crystals fall out of thin layers consisting of super-cooled water. Most of these layers contain little water ($<25 \text{ g m}^{-2}$). However, measurements within the regional network during the BBC campaign showed that these layers can extend over more than 100 km and last several hours long.
- For a future long-term implementation of ECON a low-cost microwave radiometer, which also takes into account requirements from the modelling community, has been designed. Due to external funding the first systems were already built and sold.
- The large reference data set from ground-based measurements allowed for a statistical evaluation of the accuracy of the LWP retrieval. This is a novelty in Europe and thus a scientific achievement in itself. It was found that the newly developed retrieval method using the $1.6 \mu\text{m}$ channel information is a significant improvement relative to the original KLAROS-scheme used by KNMI.

CLIWA-NET: BALTEX BRIDGE Cloud Liquid Water Network

Methodologies focusing on the evaluation of model predicted cloud parameters with CLIWA-NET inferred observations have been developed and examined in various applications, e.g. a statistical evaluation of LWP, the representation of vertically distributed liquid water content, and a comparison of a model predicted LWP-field with satellite retrieved spatial distributions. Furthermore, the horizontal resolution aspect and a number of parametric issues have been investigated. The main findings are:

- Models overpredict frequency and duration of precipitation. Models overpredict the amount of liquid water clouds. On average, models predict LWP in the right order of magnitude, but the spread among the models is considerable.
- On average, models provide a reasonable representation of the LWC vertical distribution, but variations among the models in amount and height of the maximum value are huge. For individual events, model predictions of the LWC vertical structure have no prediction value.
- Numerical experiments have investigated the sensitivity of cloud and precipitation parameters on the horizontal resolution in the range of 10 to 1 km. Domain averaged LWP, and, in particular, precipitation are found to be strongly enhanced by increasing horizontal resolution. Size distributions of model resolved convective cells depend strongly on the employed horizontal resolution. There are indications that the application of fully parametrized turbulence without horizontal exchange between grid boxes is no longer adequate in this range of grid spacings.
- Total cloud amounts derived from two satellite systems, i.e. ISCCP and AVHRR, are found to be significantly different with the ISCCP cloud amount being much larger than the AVHRR cloud amount. The AVHRR amounts, in turn, are found to be larger than ground-based (synop) estimates. Model predicted cloud amounts from different cloud schemes appear to be closer to the AVHRR amount or even lower. Refinement of the vertical model mesh results in a better resolution of cloud processes. In general, it also results in a better representation of macroscopic cloud parameters like cloud amount and the vertical distribution of clouds. Typical errors like a tendency to simulate cloud base height at too low altitudes are not remedied completely.

Conclusions

Within CLIWA-NET we have successfully operated the prototype of an European Cloud Observation Network during three enhanced operational campaigns. In order to allow such a network to become operationally in the future a low-cost microwave radiometer was designed and a first prototype has already been built. The data from the measurement campaigns allowed the evaluation of the full cloud cycle in numerical models along with cloud interactions with other portions of the water and radiation cycles. In some areas where the representation of clouds in numerical models has been improved, problems have been identified and work is ongoing to develop these parameterizations further.

Dissemination of results

In the future, the CLIWA-NET observations will form a key dataset for a number of applications: to further develop and test parameterization techniques for clouds and cloud interactions in climate and weather forecast models; to develop and test algorithms for ground-based and space borne remote sensing; to study super-cooled water layers, to derive statistics for attenuation at higher microwave frequencies; etc. The low-cost microwave radiometer offers the potential to make a permanent European Cloud Observation Network possible.

CLIWA-NET: BALTEX BRIDGE Cloud Liquid Water Network

TABLE OF CONTENTS

1.	Introduction	1
2.	Objectives	1
3.	Scientific achievements	2
3.1	Ground-based network	2
3.1.1	CLIWA-NET Network Campaigns	3
3.1.2	BBC Campaign.....	6
3.1.3	Added value product – LWC profiles.....	8
3.1.4	Super-cooled water layers.....	10
3.1.5	Low-cost microwave radiometer	12
3.2	Satellite measurements and integration of observations	14
3.2.1	Data acquisition	14
3.2.2	Cloud classification	15
3.2.3	Quantitative cloud analysis using AMSU.....	18
3.2.4	Quantitative cloud analysis from AVHRR	21
3.2.5	Comparison of LWP retrieved from satellite and ground observations.....	24
3.2.6	Statistical validation.....	25
3.3	Model evaluation and improvement.....	28
3.3.1	Model evaluation	28
3.3.2	Horizontal resolution	35
3.3.3	Parameterization development and assessment	39
4	Conclusions.....	44
5	References.....	46
6.	Literature produced in CLIWA-NET	48

CLIWA-NET: BALTEX BRIDGE Cloud Liquid Water Network

1. Introduction

Clouds affect our daily life in many ways. Much more than air temperature, clouds dominate our perception of weather and thus have an enormous influence on our daily activities and our health. This fact is completely at variance with our knowledge about clouds, their representation in climate and weather forecast models and our ability to predict clouds. It is their high variability in time and space, which makes clouds both hard to monitor and to model. It is well-known, that clouds are directly linked to the dynamics of the atmosphere. The most important parameter linking dynamics to clouds, in both the real world and in forecast models is the water content of clouds. Passive microwave remote sensing is by far the most direct and accurate method to estimate cloud water content. Over the oceans microwave remote sensing from satellites has been proven to be the most accurate method to determine this parameter (Grody, 1993). Unfortunately, over land areas this technique fails. Here remote sensing methods must rely on very indirect information taken from cloud reflection of solar radiation. Thus, important cloud information does not get into our models in the area where people live.

As stated by the Intergovernmental Panel on Climate Change (IPCC)'95: "the most urgent scientific problems requiring attention to determine the rate and magnitude of climate change and sea level rise are the factors controlling the distribution of clouds and their radiative characteristics....". The same was concluded in the AMIP project (e.g. Gates et al., 1999) in which the outputs of 30 atmospheric models were compared for a ten-year run. Furthermore, the latest IPCC report (2001) states that "there has been no apparent narrowing of the uncertainty range associated with cloud feedbacks in current climate simulations" and moreover that "there are particular uncertainties associated with clouds and their interaction with radiation and aerosols"; as a result it further recommends that "the only way to obtain progress in this complex area of atmospheric science is by consistently combining observations with models" and that "a more dedicated approach is needed".

The CLIWA-NET project aims to contribute to a better cloud representation in atmospheric models by an advanced observational program leading to improved parameterizations. For this purpose a prototype of a European cloud observing system was established by co-ordinating the use of existing, ground-based passive microwave radiometers and profiling instruments. The data from the ground-based remote sensing instruments were used to improve the satellite-based estimates of cloud water content. New procedures have been and will further be developed to fully exploit this synergy.

2. Objectives

CLIWA-NET focuses on observations of cloud liquid water and its vertical structure to evaluate and improve model cloud parameterizations. The specific CLIWA-NET objectives are:

- *Contribute to the development and implementation of the Global Observing System with a focus on cloud observations*
This was to be achieved during three observational campaigns by implementing a prototype of a European Cloud Observation Network which made use of existing ground-based and satellite measurements. Such a network can also be used as a validation tool for current and future satellite cloud missions.

- *Objective evaluation of atmospheric models for weather forecasting and climate and improvement of the parameterization of cloud processes, with a focus on vertically integrated cloud liquid water and vertical structure of clouds*

The importance of cloud water observations and the information on the vertical structure of clouds was demonstrated by the evaluation/ improvement of state-of-the-art cloud parameterizations. Because of the known poor representation of clouds in the NWP models, the quality of cloud forecasts from models is limited. This has large socio-economic impacts for business areas like: airports, solar energy, road construction, tourism, breweries, ice industry, etc.

CLIWA-NET made significant steps towards the improvement of cloud processes in models.

- *Development of an adequate observing system for the detection of icing conditions for aircraft*
The combination of measurements within the CLIWA-NET network can detect super cooled water layers which are a major risk in today's aviation as they can lead to icing on the aircraft frame.
- *Design of a "low cost" microwave radiometer in co-operation with industry (SME)*
Cloud liquid water is an important parameter for characterizing clouds. It can only be measured with sufficient accuracy over land by ground-based passive microwave radiometry. Up to now the costs of purchasing a microwave radiometer suitable for low maintenance operation are extremely high. In order to enable the use of microwave radiometers in an operational network the design of such a system was an innovative objective of CLIWA-NET.
- *Contribution to BALTEX/BRIDGE*
The BALTEX programme is an international effort under the World Climate Research Programme with the objective to understand and predict the hydrological cycle in the Baltic Sea region. This work also includes the prediction of extreme events such as river flooding.
BALTEX conducted its main modeling and observational experiment BRIDGE from October 1999 - February 2002. The central aim of BRIDGE was to generate comprehensive data sets for process understanding and budget studies of the entire Baltic Sea (modeling) area. All CLIWA-NET campaigns were coordinated with enhanced observation periods of BRIDGE. The CLIWA-NET project was the leading project within BRIDGE for clouds and radiation studies.

3. Scientific achievements

In order to fulfil the CLIWA-NET objectives research focussed on three aspects: 1) the implementation and analysis of observations within a **ground-based network** during three observational campaigns, 2) the derivation of macro- and microphysical cloud properties from **satellite measurements** and their integration with ground-based measurements and 3) a comprehensive **modelling** effort for the evaluation/improvement of cloud parameterizations based on the observational data set.

3.1 GROUND-BASED NETWORK

The prototype of a European cloud observing system was successfully operated in near real-time during three measurement campaigns. It encompassed measurements within a ground-based network of cloud observing stations comprising microwave radiometers as prime instruments to derive liquid water path (LWP). Due to their relatively high cost, use was made of existing mainly experimental microwave radiometers from different research groups across Europe. In order to investigate the vertical cloud structure, auxiliary measurements with highly operational low-cost instruments, e.g. lidar ceilometer and infrared radiometer, were performed. Cloud radars are even more expensive and less operational as microwave radiometers; therefore, only limited observation by these instruments could be performed in CLIWA-NET. Two **CLIWA-NET** Network (CNN) campaigns covered North Central Europe while the BALTEX BRIDGE Campaign (BBC) took place in the Netherlands:

- **CNN I:** August-September 2000
- **CNN II:** April-May 2001
- **BBC:** August-September 2001

3.1.1 CLIWA-NET Network Campaigns

The ground-based network for the CNN campaigns consisted of 12 individual stations located within the Baltic Sea Experiment (BALTEX) area (Fig. 1). The primary goal of the ground-based stations was the continuous observation of cloud liquid water path from multi-frequency passive microwave measurements. In order to derive information about the vertical cloud structure and to enhance LWP accuracy the stations were equipped with additional instruments, e.g. lidar ceilometer, infrared radiometer, or cloud radar. Details of the instruments at the individual stations can be found at <http://www.knmi.nl/samenw/cliwa-net>.

The liquid water path can be estimated from atmospheric emission measurements in the microwave region since in this spectral region the cloud contribution strongly increases with frequency (Fig. 2). Therefore, standard dual-channel systems measuring at two frequencies with one close to the 22.235 GHz water vapour line and the other in a window region at higher frequencies can simultaneously observe LWP and the integrated water vapour (IWV) (Westwater, 1993). Within CLIWA-NET existing microwave radiometers of very different design and specifications

were used. For each radiometer the uncertainty of the direct observable, the brightness temperature, was determined. Algorithms for LWP and IWV individually adapted to the different instruments were derived. For each station long-term radiosonde data sets were used as a statistical basis. However, the radiosondes do not measure cloud liquid water content (LWC) and realistic profiles needed to be diagnosed from the humidity and temperature sounding. As a too simplified treatment of clouds can lead to systematic errors (Löhnert and Crewell, 2003) an advanced cloud model was employed (Karstens et al., 1994). Most of the microwave radiometers involved in CLIWA-NET have estimated accuracies in brightness temperature better than 2 K. For dual frequency systems this translates to a LWP accuracy of about 30 g m^{-2} . A rough estimate shows that about 10 g m^{-2} error are caused by the measurement error while the remainder can be attributed to the ill-posed retrieval problem. The additional use of the 90 GHz channel can further constrain the problem and improve accuracy to better than 15 g m^{-2} (Crewell and Löhnert, 2003). The accuracy in IWV is in the range of $1\text{--}2 \text{ kg m}^{-2}$. Uncertainty estimates for the specific radiometer and campaign are included in all retrieved data files.

While the microwave radiometers were relatively diverse in design, infrared radiometer (IR) and lidar ceilometer were more or less standardized. The combination of a lidar ceilometer and IR radiometer is quite useful in characterizing cloud base height to an accuracy of $\sim 30 \text{ m}$ and cloud base temperature to

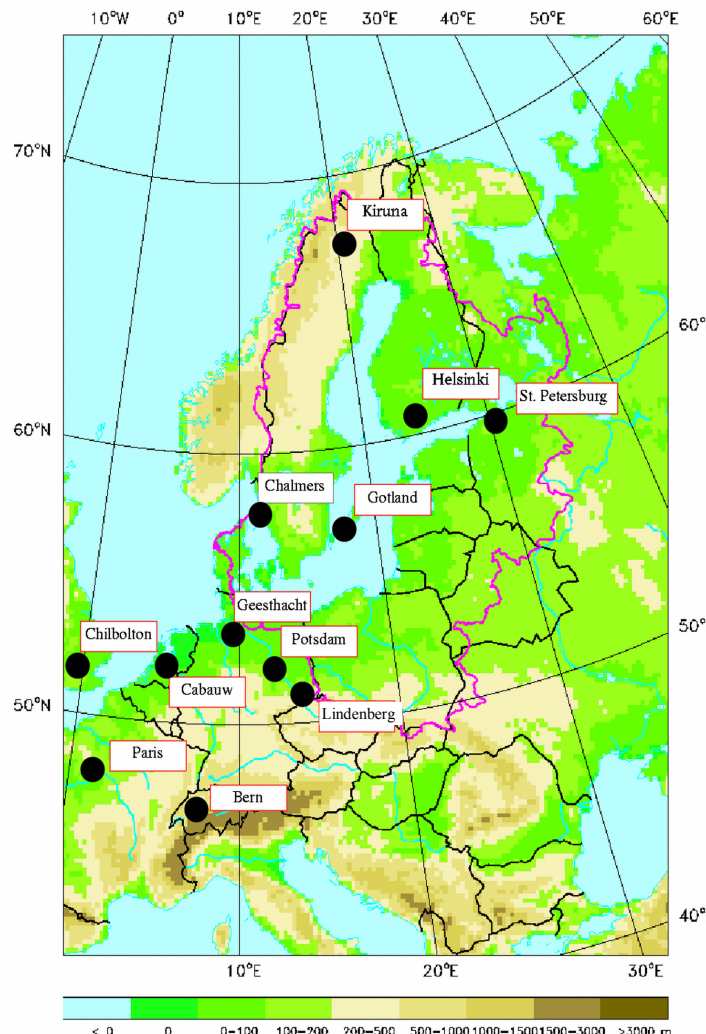


Figure 1: Position of stations during the CLIWA-NET observation periods (CNN I and II)

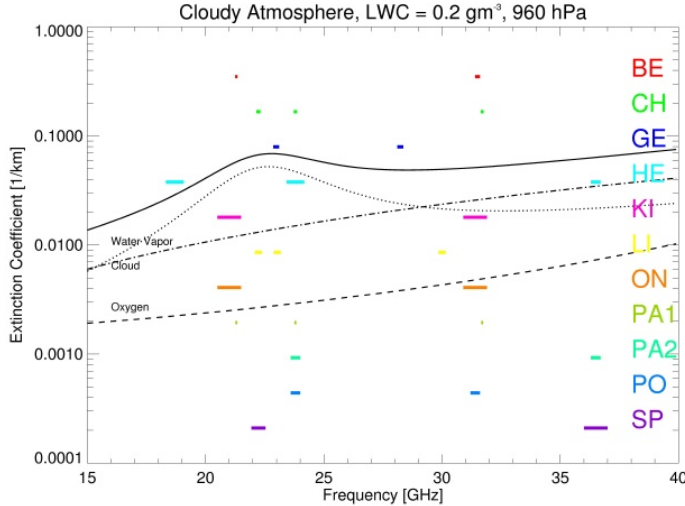


Figure 2: Frequencies of the microwave radiometer involved in the CLIWA-NET observational campaigns CNN I and II. See Table 1 for the station abbreviations.

(e.g., 1–9 GHz) and continuously scan the horizon at very low elevation angles. The Baltex radar network (BALTRAD, Koistinen and Michelson, 2002) covers nearly the whole BALTEX area. Time series of the radar reflectivity factor for the BALTRAD pixel closest to a CLIWA-NET station were made available for rain detection.

All raw data was submitted in near real time to the central processing unit in Bonn. The data was quality checked, and LWP and IWV were derived using the above mentioned algorithms. Graphical presentations for every day and every station were also available for the general public within a week on the CLIWA-NET web site. An example can be seen in Fig. 3. In order to achieve good spatial coverage over the BALTEX modelling area (Fig. 1) and to get a most complete set of instruments several rearrangements of instruments from their home stations were necessary (Table 1).

Table 1: Overview of the instrumentation employed in the CNN campaigns. Ownership of the different instruments is indicated by the colour code.

	Station	Microwave Radiometer		Infrared Radiometer		Lidar Ceilometer		Cloud Radar [v in GHz]		BALTRAD
		CNN I	CNN II	CNN I	CNN II	CNN I	CNN II	CNN I	CNN II	
BE	Bern	X	X	X	X					
CA	Cabauw		X	X	X	X	X			
CH	Chilbolton	X		X	X	X		94	94	
GE	Geesthacht	X		X		X	X	95	95	X
GO	Gotland		X	X		X	X			X
HE	Helsinki	X	X	X	X	X	X			X
KI	Kiruna	X	X	X	X	X	X			X
LI	Lindenberg	X	X	X,X	X,X	X	X			X
ON	Onsala	X	X	X	X	X	X			X
PA	Paris	X	X	X	X	X	X			
PO	Potsdam	X	X			X	X			X
SP	St. Petersburg	X	X	X	X	X	X	3, 9.6	3, 9.6	X

KNMI **UNIBONN** **Chalmers** **IFM** **Vaisala** **CETP**

an accuracy of 1–2 K after subtracting the atmospheric contribution from the IR measurement (Feijt and van Lammeren, 1996). At three stations cloud radars were operated. In order to detect small cloud droplets, cloud radars usually operate at higher (for example 95 GHz) microwave frequencies. Because attenuation is relatively strong at these frequencies cloud radars typically point vertically and gather time-height series. The radar signal is proportional to the sixth moment of the drop size distribution (DSD) and therefore the derivation of the liquid water content, which is proportional to the third moment of the DSD, is highly uncertain. Weather radars, intended for precipitation measurements, use much lower frequencies

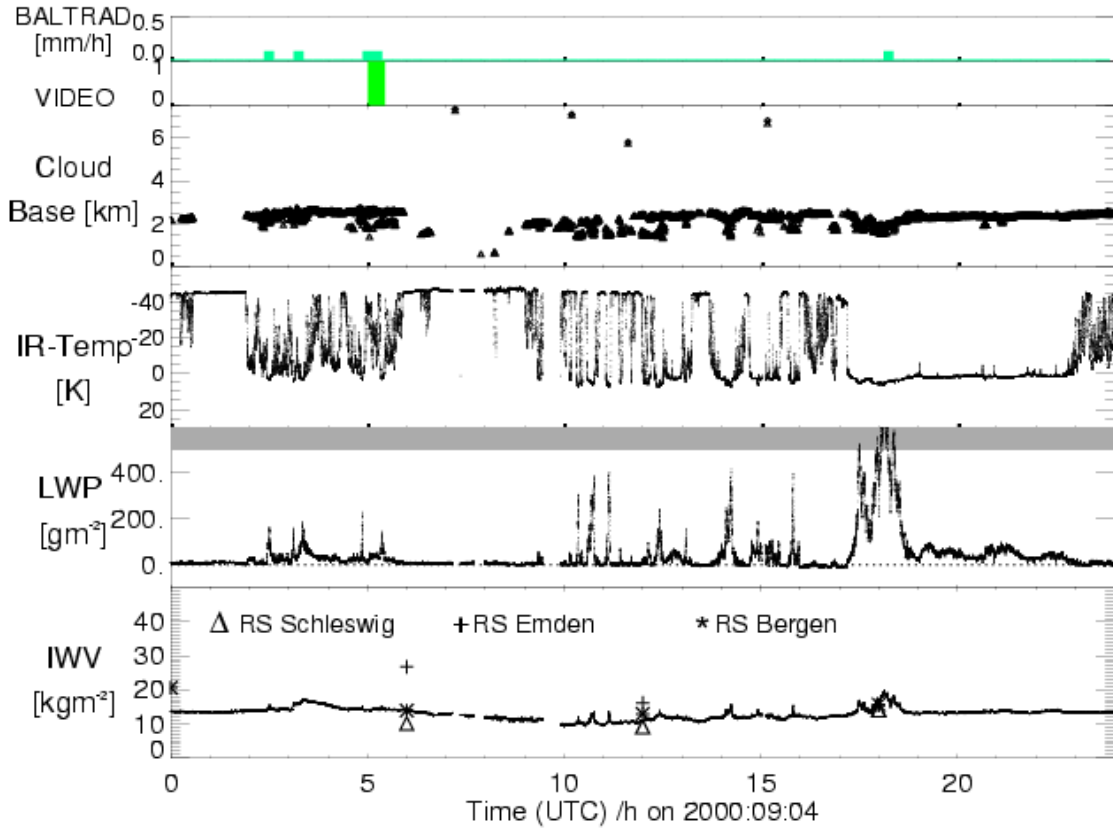


Figure 3: Example of a daily time series observed at Geesthacht on 4 September 2000 during CNNI.

The microwave and IR measurements at Geesthacht (Fig. 3) were performed with 1 s integration time and reveal cloud variability on different scales. Therefore, most measurements within CLIWA-NET were performed with integration times less than one minute. As expected, the correlation between cloud base height and IR temperature is high. During the presence of clouds, IR temperatures are high, while in the absence of clouds the IR temperature of the atmosphere drops to -30 to -55°C . From 17:30 to 19:00 UTC cloud base height increases and the IR temperature decreases. As ceilometer and IR radiometer measurements contain the cloud base information, they can not be compared directly with cloud LWP, which is a vertically integrated quantity. For example, the periods from 13:45 to 14:30 UTC and 17:30 to 18:30 UTC in the time series are characterized by almost identical values for the cloud base height (1.5 to 2.5 km) and IR temperatures (0 to 10°C). The corresponding peak LWP value for the first period varied between 0.31 and 0.42 kg m^{-2} , while for the second period they varied between 0.50 and 0.82 kg m^{-2} . Ice clouds are transparent at the microwave frequencies used in this study; they do not contribute to the microwave radiances. For the validation of the IWV time series we integrated water vapour profiles from radiosondes. Since no useful LWP and IWV retrievals can be performed during rain, these conditions have to be identified. Therefore, measurements of an upward looking visible wavelength video camera were analysed to detect the onset of precipitation. Additional information comes from the BALTRAD time series (grid box is $2 \times 2 \text{ km}^2$) with 15 min resolution. Better information is available for other stations from the rain shutter of some IR radiometers which is far more sensitive than conventional rain gauges. Furthermore, Fig. 3 shows IWV derived from radiosonde ascents at the German upper-air stations of Schleswig, Emden, and Bergen. The closest station, Bergen at a distance of ~ 75 km, shows IWV in good agreement with the microwave derived IWV. These comparisons are an indirect validation of the microwave radiometer observations.



Figure 4: Set-up of the remote sensing site in Cabauw showing the microwave radiometer MICCY (far left) and three cloud radars. The 200 m tower is visible in the background.

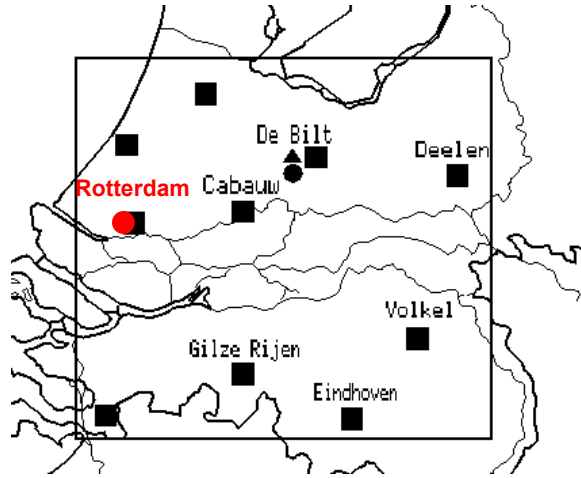


Figure 5: Distribution of stations in the Cloud Detection System. Stations labelled in black were additionally equipped with microwave radiometers. Airports were based in Rotterdam.

3.1.2 BBC Campaign

The BBC campaign (Fig. 4) included intensive remote sensing observations at the Cabauw site including three cloud radars. A detailed list of the instrumentation can be found in Table 2. Within a regional network ($120 \times 120 \text{ km}^2$) lidar ceilometers, infrared radiometers and pyranometers were operated at six stations (Fig. 5). After a microwave radiometer inter-comparison campaign (MICAM) during the first two weeks of August at Cabauw the radiometers were distributed to the stations in the regional network. Originally initiated by CLIWA-NET, the campaign grew considerably larger through the participation of e.g. four aircrafts and two tethered balloons by other European partners. A data base for the BBC campaign has been set up to transfer data from the Cabauw experimental site to systems outside KNMI and to store the final data products and quicklooks of the campaign.

Microwave Intercomparison Campaign. In total 8 radiometers participated in MICAM which significantly differed in design and specifications. The results of this unique inter-comparison were intended for a final evaluation of LWP/IWV accuracy. Because seven of the radiometer had already operated during the CNN campaigns the accuracy of these measurements could also be verified. Additionally, the MetOffice (UK) participated with the MARSS radiometer (McGrath und Hewison, 2001) and the launch of about 30 radio soundings. For a direct comparison of brightness temperatures (TB) 24 GHz is of most interest because four of the CLIWA-NET radiometers measured close to this frequency which is also used by the satellite instrument AMSU (see section 3.2.3). The simultaneous

Table 2: Instrumentation at Cabauw during BBC. Instruments brought to the regional network after the microwave inter-comparison campaign are denoted in *italics*.

Radar	Microwave radiometer	Lidar	Radiation
1.2 GHz windprofiler + RASS (KNMI)	2ch CONRAD (Chalmers) 2ch DRAKAR (CETP)	1064nm, 532 nm (RIVM) Vaisala CT75K (KNMI)	radiative fluxes (KNMI)
3 GHz TARA (TU Delft)	2ch IRE (Russia)	LD40 (KNMI)	O ₂ -A band spectrometer (UHEID)
35 GHz radar (KNMI)	5ch MARSS (Met Office)	Vaisala CT25K (UNIBONN)	KT19.85 (UNIBONN)
95 GHz MIRACLE (GKSS)	22ch MICCY (UNIBONN) 2ch TROWARA (UNIBE) 2ch WVR 1100 (DWD) 12ch WVP/TP 3001 (DWD)		KT15 (KNMI) IR-rad (UBERN) Sunphotometer (IFT) Albedometer (IFT)
Auxillary measurements			
200 m tower: temperature, dew point temperature, wind direction, wind speed, every 30 m (KNMI)			
10 m mast, sonic, Ly-a: sensible and latent heat flux (UUtrecht)			
GPS receiver (TUDelft)			
Digital Video Camera (KNMI, TUDresden)			
Radio soundings, RS-90, 34 launches during MICAM (Met Office); RS-80 afterwards about 100 launches (Dutch Army)			

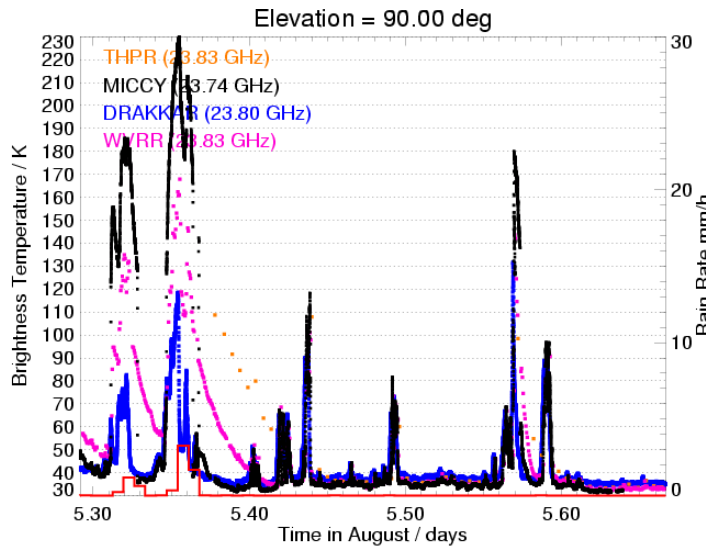


Figure 6: Time series of 24 GHz brightness temperatures and rain rate from 9 to 17 UTC on 5 August 2001 at Cabauw.

was invested to filter CLIWA-NET measurements from these effects. The use of a rain shutter (MICCY) or a strong blower (DRAKKAR) can strongly reduce the drying time.

Due to the high cloud variability, quantitative comparison of TBs was carried out in cloud free situations only. Correlation between TBs is excellent (>0.95) in these situations. For example, the 24 GHz channels of WVHR and MICCY have a correlation of 0.99, RMS of 0.5 and Bias of 1.1 K. This illustrates that radiometric noise is not the limiting factor in TB and hence LWP observation, however accurate calibration and high stability are required instead.

LWP algorithms assume a perfect knowledge about the radiative transfer in the atmosphere. To investigate this issue radiative transfer calculations of all involved brightness temperatures were performed for all radiosondes launched during the campaign employing three different gas absorption models. Meaningful comparisons can only be performed during cloud free conditions because it is not possible to exactly model the liquid water content from radio soundings. Figure 7 shows one example for 2 August, 2001. The spectral characteristics along the 22 GHz line and the 60 GHz oxygen complex are depicted well by the radiometers. Obviously, the 23.8 GHz channel of the DRAKKAR radiometer overestimates the brightness temperatures measured by three other radiometers at similar frequencies (see also Fig. 6). A calibration problem has been identified. At 90 GHz the largest discrepancies between measurements occur. Unfortunately,

observation of a broken cloud situation (Fig. 6) reveals that slight differences between radiometers can occur due to different integration times and beamwidths, which can lead to smoothing of cloud peaks. In case of precipitation, vertically pointing microwave radiometers are strongly disturbed and cannot perform useful measurements. Depending on the design and situation it can take several hours time after a rain event until the radiometer is completely dry (Fig. 6). Without any additional information it is difficult to judge whether these measurements are useful or still affected by water on the radiometer antenna/radome. Significant work

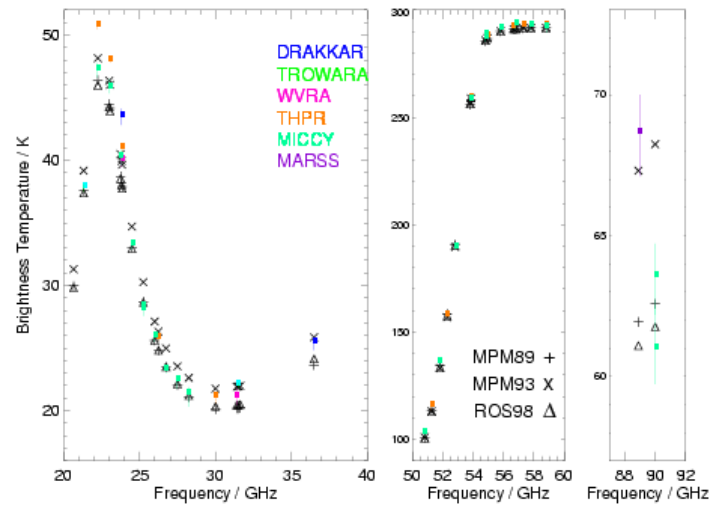


Figure 7: Simulated (black) and measured (colour-coded) brightness temperatures for a radio sounding on August 2, 2001 at 11 UTC. Radiometer measurements were averaged over 10 minutes past launch and the thin lines connect maximum and minimum within this interval. Simulations were performed using the gas absorption models according to Liebe et al. (1989) MPM89, Liebe et al. (1993) MPM93 and Rosenkranz (1998) ROS98.

the differences are in the same range as the uncertainties of the gas absorption models thus allowing no further constraint of these models. Further investigations are necessary. In general the accuracy of brightness temperature measurements was found to be well within the estimated range which gives us trust for the estimates of LWP accuracy.

3.1.3 Added value product – LWC profiles

As already pointed out *active* and *passive microwave remote sensing* both provide information about microphysical properties of clouds. In the past methods have been developed which combine collocated microwave radiometer and cloud radar measurements to infer LWC profiles (e.g. Frisch et al. 1998, Löhnert et al. 2001). In principal, such methods use the microwave-derived LWP to scale the LWC derived from the cloud radar reflectivity (Z) measurements at each height. Multi-channel radiometers such as MICCY can provide additional information on the vertical profiles of temperature, humidity and to very limited degree on LWC. During BBC long-term, simultaneous measurements of the cloud radar MIRACLE and the microwave radiometer MICCY were performed and combined with a newly developed technique

Integrated Profiling Technique. The Integrated Profiling Technique (IPT) was developed, which applies optimal estimation theory (e.g. Rodgers et al. 2000) to simultaneously retrieve profiles of temperature (T), humidity (q) and LWC from six different types of measurements. In contrast to the methods mentioned above, IPT directly combines 19 MICCY brightness temperatures with 95 GHz cloud radar reflectivity profiles, lidar ceilometer cloud base, ground-level measurements of temperature, humidity, and pressure, nearest-by radiosonde profiles, and a LWC a priori profile obtained from a microphysical cloud model. IPT bears the following advantages compared to common LWC profiling methods:

- All three retrieved profiles are “physically consistent”. This is accomplished by the fact that the retrieved profiles constrained to the ground-level measurements, fulfill the condition of saturation within the detected cloud boundaries from ceilometer (base) and cloud radar (top), and their forward-modeled brightness temperatures are constrained to the measured values.
- IPT results are independent of LWP retrieval errors because within IPT the MICCY brightness temperatures are directly inverted to the atmospheric parameters.
- IPT explicitly includes temperature, humidity and pressure information obtained from the closest operational radiosonde site. This is of crucial importance for all passive microwave methods when inferring cloud liquid water, because temperature and humidity are dominant factors contributing to the brightness temperature signals at all frequencies.

The optimal estimation equations (derived from a special case of Bayesian theory) can be applied to combine an independent set of measurements when the forward model relating the atmospheric parameter to the measurements, its error, and the error of the measurements themselves are known. After i iterations leading to convergence, the optimal solution for the desired profile ($\mathbf{x}_{op}=\mathbf{x}_{i+1}$, bold face characters indicating a vector) of temperature, humidity, and LWC can be written as

$$\mathbf{x}_{op} = \mathbf{x}_i + (\mathbf{K}_i^T \mathbf{S}_e^{-1} \mathbf{K}_i + \mathbf{S}_a^{-1})^{-1} \times [\mathbf{K}_i^T \mathbf{S}_e^{-1} (\mathbf{y} - \mathbf{y}_i) + \mathbf{S}_a^{-1} (\mathbf{x}_i - \mathbf{x}_a)].$$

with

\mathbf{y} Measurement vector consisting of \mathbf{Z} , \mathbf{TB} , and ground-level T and q

\mathbf{K}_i Jacobian matrix, or $\partial\mathbf{y}_i/\partial\mathbf{x}_i$

\mathbf{S}_e Error covariance matrix of the measurement vector \mathbf{y}

\mathbf{x}_a A priori profile consisting of \mathbf{T} , \mathbf{q} (radiosonde) and \mathbf{LWC} (cloud model)

\mathbf{S}_a Covariance matrix of the a priori profile

In principal IPT is applicable anywhere, however, the covariance matrix \mathbf{S}_a must be adjusted according to the distance (space and time) to the closest operational radiosonde site.

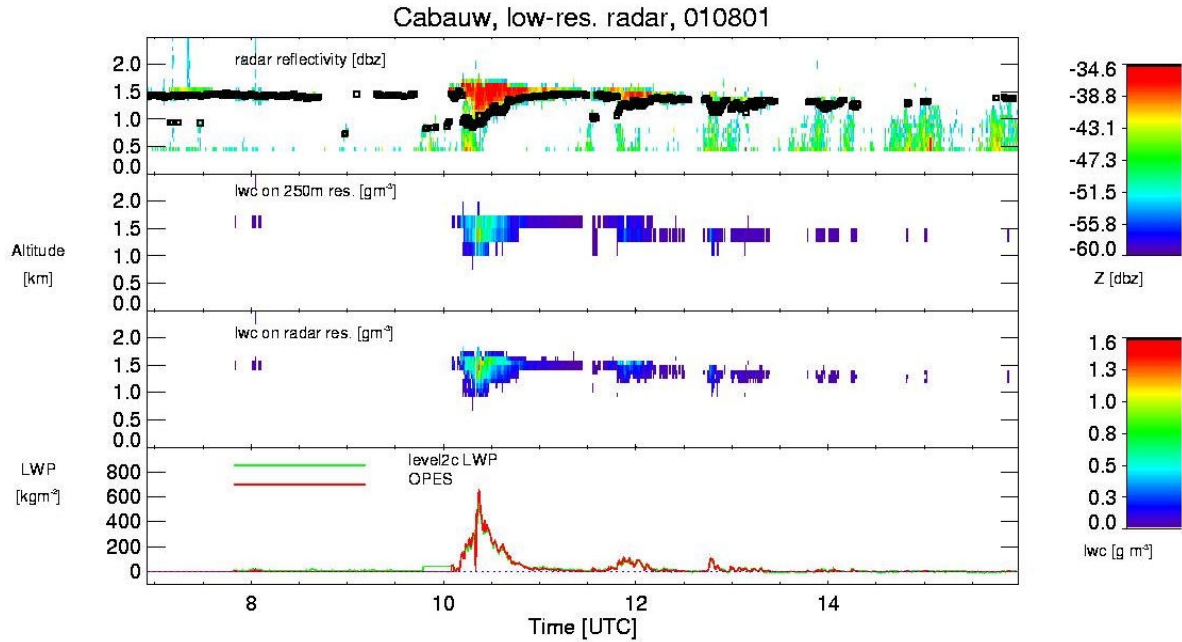


Figure 8: Top panel: time series of radar reflectivity and lidar-ceilometer cloud base (diamonds), LWC on 250 m resolution (second from top panel), LWC on radar resolution (third from top panel), and LWP (bottom panel) on August 1, 2001 at Cabauw, The Netherlands. The green line in the lower panel shows the LWP retrieved from MICCY alone by means of a statistical algorithm. The red line (IPT) shows the vertical integrated values of LWC resulting from the middle panel. The vertical red lines indicate the times when the retrieval algorithm was not applicable.

Algorithm applicability. The IPT is applied to time series of measurements obtained during the BBC campaign in August and September 2001 at the Cabauw site. To determine the cloud boundaries most accurately, lidar-ceilometer measurements are used to obtain cloud base and the highest reflectivity bin of the cloud radar with a significant signal-to-noise-ratio is used as cloud top. To be able to apply the IPT the radar reflectivities on their original resolution are averaged to IPT resolution of 250 m. Cloud base height is also interpolated to the 250 m grid by locating the nearest 250 m level. Subsequently the IPT results can be easily used to derive a product on radar range resolution.

In order to apply the IPT to the BBC data, *certain measurement conditions must be fulfilled*. For example, during cloudy conditions the measurements of microwave radiometer, cloud radar, and lidar-ceilometer must be available simultaneously. When a cloud base is detected the observed cloud top must be higher than cloud base. A crude operational procedure for classifying cloud phase was developed for the BBC campaign data. Hereby it was assumed that clouds above 7 km consist totally of ice and thus do not contribute to the *TBs* meaning that the algorithm can be applied to simultaneously existing lower liquid clouds. The height range from 3.5 to 7 km was classified as the mixed range denoting that clouds here can consist of liquid, ice or a mixture. Additional temperature checks were performed and clouds were also considered as pure ice if the temperature was less than -20 °C. Because the IPT in its present form is only applicable to pure liquid cases, it cannot be used in cases with mixed phase clouds. Due to this fact IPT was only applied to clouds below 3.5 km. However, ice can also exist in layers below 3.5 km (15-20 % of the time). A sufficient condition for the presence of ice clouds is a threshold of ~-26 dB in the linear depolarization ratio of the cloud radar MIRACLE. Such cases are mainly measured during precipitation, where the rain droplet formation involves ice-nucleation. The last condition to be met is that no precipitation is present during retrieval application. If all of these limiting factors are considered IPT can be applied to ~15 % of the time MIRACLE measured during BBC. Because MIRACLE was only operating roughly in 30 % of the total BBC time, this corresponds to ~4.5 % total time coverage.

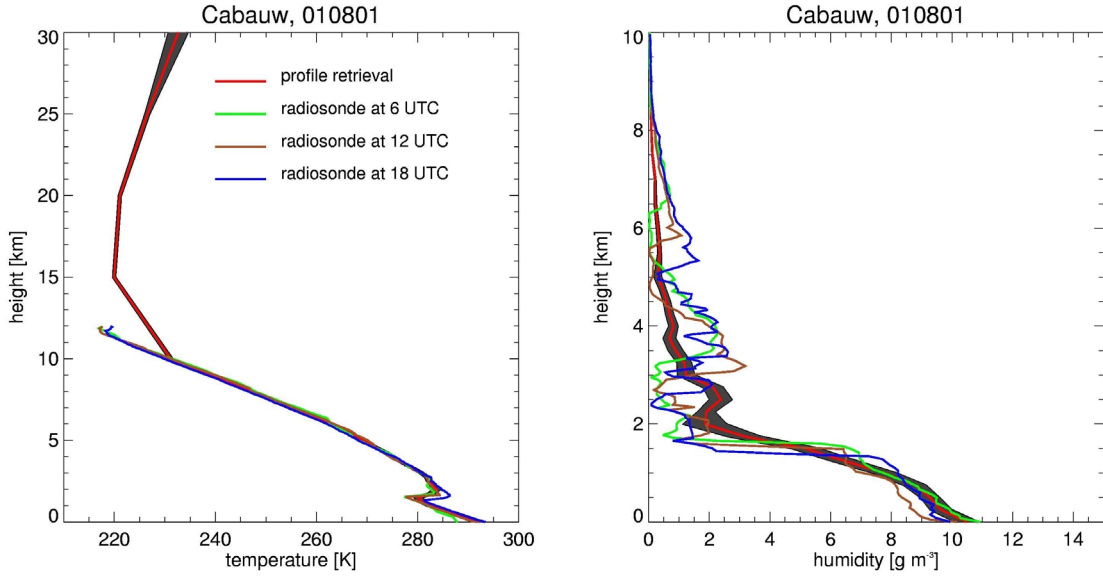


Figure 9: Mean values of temperature (left panel) and humidity (right panel) derived during the time series shown in Fig. 8. The grey shaded areas denote the retrieval standard deviation. Also shown are the corresponding radiosonde measurements from DeBilt.

Retrieval example. An example of a retrieved LWC time series with a relatively thick cumulus cloud observed on August 1, 2001 from 10 to 11 UTC with LWC values of up to 1.1 g m^{-3} and LWP values peaking at 700 g m^{-2} (Fig. 8). Afterwards, from 11 to 14 UTC, only scattered clouds with much less water content occur. It is interesting to note, that the independently retrieved LWP from MICCY measurements via a statistical algorithm (level2 added-value product) coincides very well with the LWP that results from the vertical integral of the retrieved LWC (IPT). Due to the cloud detection scheme by lidar-ceilometer and radar measurements, the IPT sets LWP to zero if no cloud is present, whereas the statistical regression can generate negative LWP in cloud-free cases or even in cases within very thin clouds. Note that this makes the LWC IPT retrieval a sophisticated LWP retrieval. The retrieved temperature and humidity profiles together with the corresponding radiosonde measurements are shown in Fig. 9. The temperature profile and especially the inversion is captured adequately and the basic characteristics of the absolute humidity profile are also retrieved and are as good as one would expect. Due to the high variability of q in the vertical (horizontal) and the limited number of highly correlated TB observations, the retrieved q profile will always be smoothed significantly. Due to this fact strong humidity gradients at the top of the boundary layer will be very difficult to capture.

As a next step it is suggested to incorporate additional measurements encompassing different spectral ranges. Instead of using the lidar-ceilometer only for cloud base determination, including the measured backscatter profile and its forward model could be used to infer cloud parameters such droplet number concentration or LWC in the lowest cloud level. Similar calculations could be carried out with an additional infrared sensor. Another possibility to be looked into is the inclusion of higher microwave frequencies (e.g. around 150 GHz) which attenuate sooner within the cloud than the MICCY frequencies. Thus, more vertical information may be obtained.

3.1.4 Super-cooled water layers

Hogan et al. (2003) developed a method for the detection of super cooled water layers (SCL) based on the backscatter profile of a ceilometer and temperature information, e.g. from radio soundings. In order to detect a super cooled layer, there are four conditions the backscatter profile must meet:

- A cloud base must be detected (using the algorithm from the ceilometer)

- The maximum backscatter β_{max} has to be larger than a certain threshold ($6 \times 10^{-5} (\text{sr m})^{-1}$).
- The backscatter coefficient at 300 m above the altitude where the maximum backscatter has been detected should be at least 20 times weaker than β_{max} .
- The temperature of the cloud base must be below 0 °C.

This method was developed to give the best agreement with layers identified subjectively (by eye). For more details about the method and its applicability, see Hogan et al. (2003). For this method to work, the ceilometer should preferably be pointing a few degrees off zenith in order to eliminate specular reflection from oriented ice crystals. During all three CLIWA–NET campaigns (CNN I, CNN II, and BBC), a CT75K ceilometer was operated continuously at the Cabauw site and a climatology of the occurrence (Table 3) and properties of these layers generated. Averaged over all campaigns super-cooled water layers occurred in more than 10 % of all times.

Table 3: Percentage of detected occurrence: cloud bases, cloud bases below 0 °C, SCLs, cloud bases below 0 °C if a cloud base is detected, SCLs if a cloud base is detected and SCLs if a cloud base below 0 °C is detected.

Period	Base/time (%)	<0 C/time (%)	SCL/time (%)	<0 C/base (%)	SCL/base (%)	SCL/<0C (%)
Aug 2000	43	10	8	22	19	85
Sep 2000	62	11	9	18	15	81
Σ CNN I	52	10	9	20	16	83
April 2001	61	34	30	55	49	90
May 2001	36	13	12	36	33	90
Σ CNN II	49	23	21	48	43	90
Aug 2001	46	13	11	29	23	81
Sep 2001	66	15	13	23	20	84
Σ BBC	56	14	12	26	21	83

During the BBC campaign simultaneous measurements of the CT75K and the 95 GHz radar reveal interesting properties of a layer occurring on 24 September 2001. The combination of the two measurements, the lidar being proportional to the 2nd moment of the DSD and the radar being proportional to the sixth moment, can yield microphysical information. Employing the algorithm by Donovan and van Lammeren (2001), shows that the cloud is topped by a layer of small liquid water drops with ice crystals falling out (Fig. 10). The lidar ceilometer within the regional network showed that this layer extended over more than 100 km and lasted for several hours. Simultaneous measurements with the microwave radiometer MICCY showed maximum LWP of 35 g m⁻² for these clouds. During CNN II and BBC more than 60 % of these super-cooled clouds had LWP values of less than 25 g m⁻². These low values are not of danger for aviation but can significantly change the radiative budget of the atmosphere (Hogan et al., 2003).

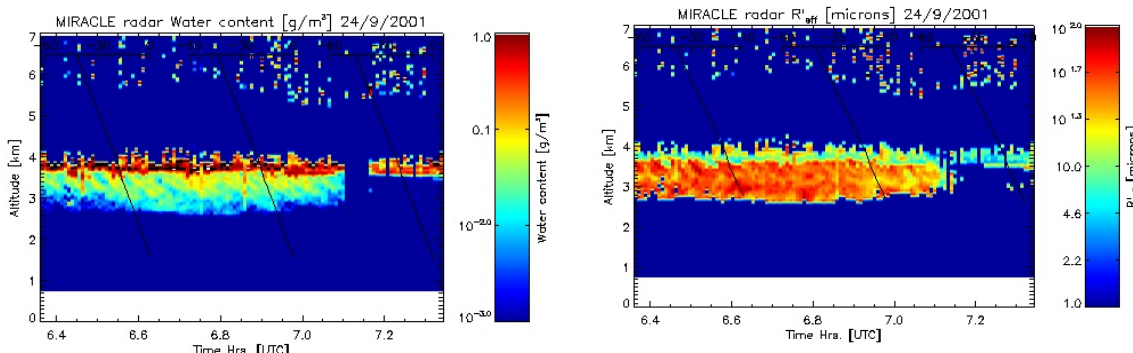


Figure 10: Liquid water content (left) and effective radius' (right) derived from lidar backscatter and radar reflectivity by applying the algorithm according to Donovan and van Lammeren (2001).

3.1.5 Low-cost microwave radiometer



Figure 11: RPG-LWP and RPG-TEMPO90 in a Master/Slave configuration. Both instruments are operated by the same host computer and configure themselves automatically as Master or Slave instruments due to their interface connections.

of different radiometers (configuration as master/slave). This was possible due to a new optical layout (Fig. 12) employing a beam splitter which allows the flexible combination of arbitrary frequency pairs: e.g. 23.8/36.5 GHz (dual-channel) or 22-30 GHz/ 50-58 GHz (profiler). Additionally, a 90 GHz radiometer can be added which improves LWP quality significantly.

To fulfil the requirements for use in an operational network the low-cost radiometer was equipped with the following specifications:

- low maintenance level (absolute calibration (liquid nitrogen) every 3 months only, cleaning of radome every 2 months)
- wide operating temperature range from -30°C to $+45^{\circ}\text{C}$
- automatic radome protection from rain, hail, snow, and dew
- robust construction of the radiometer box and stand (strong winds)
- synchronisation of all measurements to UTC (via satellite)
- automatic calibrations (gain calibration, noise standard calibration, and sky tipping)
- full built in retrieval support with online retrieval results
- backup of measurement data inside the instrument
- easy update of new radiometer software
- standard data interface to host computer network (RS-232 or Ethernet)
- portability (total mass < 70 kg)

In order to automatically protect the microwave radome from rain and snow a new shutter system was designed (compare Fig. 6). A specifically developed rain detector controls the shutter. A dew blower with 7 radial fans prevents the formation of dew on the radome. A software defined humidity threshold is used to turn on and off a 600 W heater inside the dew blower for even more efficient dew protection. Dew formation on the radome can cause significant errors (several K) in the measurement of brightness temperatures. A GPS clock defines the time standard of the instrument so that all measurement data is perfectly synchronized to satellite measurements, no matter where the radiometer is located on earth. This is highly important for the synergy with other instruments (see 3.1.3).

The implementation of an operational network of microwave radiometers – as it was set up during CLIWA-NET – is presently hampered by the cost and complexity of the available microwave radiometers. Furthermore, the analysis of CLIWA-NET data sets and their use for model evaluation has revealed several possibilities for improvement. For these reasons, the definition and design of a low cost microwave radiometer suitable for automatic, high-quality LWP measurements in an operational network was a CLIWA-NET objective. Due to internal funding and an order from outside the CLIWA-NET community, the first radiometers based on the CLIWA-NET low-cost design have already been fabricated and delivered (Fig. 11). In order to address as much user needs as possible a modular design was developed which allows the combination

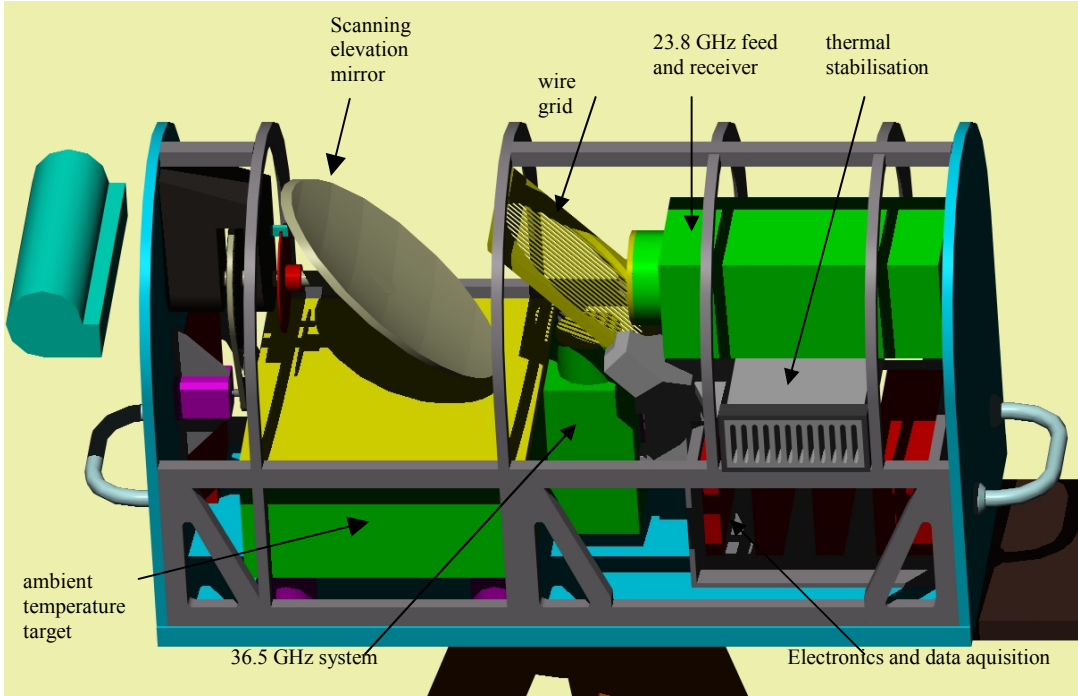


Figure 12: Internal structure of the 2-channel radiometer (cover removed).

The system performs many automatic tasks like data interfacing with the external host, data acquisition of all housekeeping channels and detector signals, controlling of elevation stepper and shutter system, backup storage of measurement data, automatic and absolute calibration procedures, retrieval calculations etc. In addition, it manages the Master/Slave interfacing between two instruments when required. These tasks are handled by a built-in embedded PC with 250 Mbyte disk on the module (DOM) for data storage. This PC is designed for operating temperatures from -30°C to 60°C and is therefore ideal for remote application. Therefore the radiometer can be either operated in the field (only power necessary) or it can be connected to the internet via the host computer to allow online access to the measurements. The latter would allow an online evaluation of model forecasts and could also be used within data assimilation.

3.2 SATELLITE MEASUREMENTS AND INTEGRATION OF OBSERVATIONS

Within CLIWA-NET a prototype of the space based component of the European cloud observing system for liquid water path fields was developed. Instruments involved were the passive imager onboard of the NOAA polar orbiting satellites, Advances Very High Resolution Radiometer (AVHRR) and the microwave radiometer onboard the same platform, AMSU. The workpackage was built-up of the following parts:

- Satellite data acquisition
- AVHRR cloud classification
- AVHRR quantitative analysis
- AMSU analysis
- Combination of satellite and ground measurements

The final aim was to obtain fields of spatial distributions of liquid water path from a combination of satellite images and time-series from the ground-based network. Based on these observations, cloud parameterizations in atmospheric models were evaluated in detail and recommendations for future improvements are given.

3.2.1 Data acquisition

The basic processing of AVHRR satellite data from the HRPT level 0 to the level 2 products Cloud Mask and Cloud Type, was successfully carried out for all three EOP periods. The processing from the raw data, HRPT level 0, to navigated and calibrated level 1b data was done using the AVHRR and ATOVS Processing Package (AAPP). To achieve best possible navigation accuracy, the software package for the Automatic Navigation Adjustment (ANA) technique, developed at Météo-France and recently made compatible with AAPP, was installed during spring 2001 (Dybbroe et al., 2003). ANA was applied to the data of the two last EOPs CNN II and BBC. Processing for CNN I was done for the entire BALTEX area, fully covering the Baltic Sea drainage basin. Due to practical reasons the area was divided into two equally sized areas. The map projection used is an *azimuthal equal area* projection centred at 60°N and 20°E. The pixel resolution is 1000 meters.

CNN I. During CNN I (August-September 2000) the AVHRR on the NOAA 15 satellite was malfunctioning and thus no useful AVHRR data are available from this period. Therefore only data from the NOAA 12 and 14 satellites was available, both having almost coinciding overpass-times during CNN I. The overpass times were concentrated in the early morning around 4-5 UTC (94 overpasses) and in the early afternoon around 14-15 UTC (151 overpasses), thus providing a rather inappropriate coverage in time for studies of diurnal effects. A total of 245 satellite overpasses were processed and analysed. At the time of CNN I ANA was not yet installed and therefore no post-navigation was performed with the satellite data. If the default navigation with AAPP using TBUS data is applied, navigational errors of up to 10 km and more are not uncommon.

CNN II. During CNN II we enlarged the processing domain to include a large part of northern Europe including parts of the Atlantic. All CLIWA-NET surface stations were covered together with a sufficiently large area for comparison with output from NWP models. For computational reasons the area was divided into four parts. During CNN II data from four different NOAA satellites was available (NOAA 12, 14, 15 and 16). In total 681 satellite overpasses (318 during April and 363 during May) were available during CNN II divided into 130 night time, 216 morning, 207 afternoon, and 128 evening orbits. For studies of the diurnal cycle, post-navigation using ANA proved to have a significant positive effect on the navigation accuracy of the data. ANA only failed to deliver a post-navigation in about 16 % of all satellite overpasses processed. The average geo-location error was reduced from 7 to 1.5km.

BBC. Processing during BBC was done on the south-western sub-area of the CNN II processing domain, defined above. A total of 472 satellite overpasses were received and processed during August and September 2001, which classified into 95 night time, 169 morning, 106 afternoon and 102 evening overpasses. All four NOAA satellites provided useful data.

3.2.2 Cloud classification

The basic cloud parameters, Cloud Mask and Cloud Type, were derived for all three extensive observing periods (CNN I, CNN II and BBC). Both are important input for the derivation of other cloud parameters from satellite data, like the cloud top temperature – but they also provide fairly independent means to evaluate cloud parameterization schemes of Numerical Weather Prediction (NWP) or Climate Models.

Algorithms. In the framework of the EUMETSAT Satellite Application Facilities (SAFs) SMHI is developing new methods and software to retrieve cloud and precipitation information from present and the coming generation of meteorological satellites (MSG and EPS/NOAA). The Cloud Mask scheme is a multi-spectral thresholding algorithm taking AVHRR data as input. The scheme employs smoothly varying thresholds separating cloudy and snow cover from cloud free conditions. Tabulated thresholds as a function of the satellite-sun viewing geometry and the state of the atmosphere and the earth surface have been derived from off-line radiative transfer model (RTM) simulations. The Cloud Type classification is a multi-spectral thresholding algorithm applied to all cloudy pixels as provided by the Cloud Mask. The main approach is that IR and short-wave IR imagery may be used to separate opaque from semi-transparent or fractional clouds, and that opaque clouds may be vertically subdivided by use of 11 μm imagery. A more elaborate description of the algorithms can be found in the second annual report.

Cloud Classification. The main output of the Cloud Mask algorithm is a pixel classification into 6 classes (non-processed, cloud free, snow/ice contamination, cloud contaminated, cloud filled, and undefined) and a set of 13 different processing/quality flags. The Cloud Type algorithm takes this as input, and produces a pixel classification into 16 classes and a set of 12 processing/quality flags. The 16 classes of the Cloud Type output include the two classes: non-processed (typically data points outside the satellite swath) and undefined (not used in the present version of the algorithm). The 14 remaining classes include 4 surface (cloud free) classes and 10 different cloud types (Fig. 13).

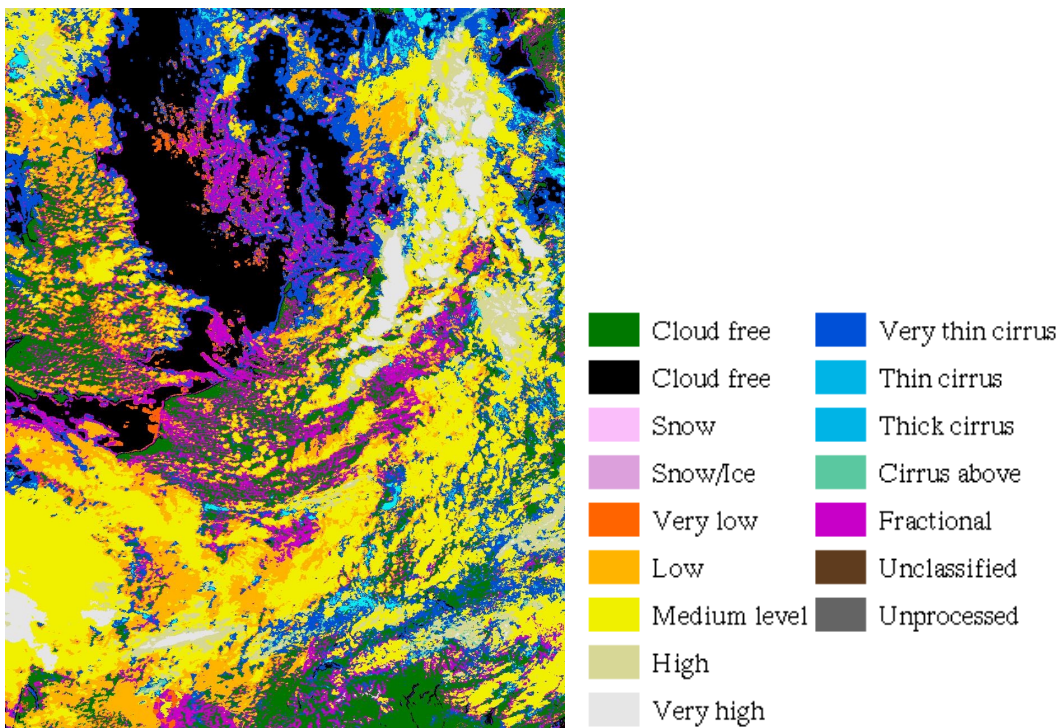


Figure 13: An image of the Cloud Type product (left) on August 5, 2001, 12:08 UTC (NOAA 16). The applied colour legend is shown on the right.

Precipitation. Although it is well known that precipitation on the ground (or in the case of the radar data below or near the cloud base) is only weakly correlated with AVHRR data, the inter-comparison of NOAA 15 AVHRR and BALTRAD radar data does provide an important indirect objective validation of the Cloud Type product. It is encouraging that the precipitation likelihood increases with the height of the opaque clouds and with the thickness of the thin cirrus clouds. Table 4 provides indications of the relation between cloud type category and the presence of ice particles in the upper part of the cloud. In addition to the thin cirrus clouds, the very high, and high opaque clouds, also the medium level clouds have a relatively high probability of ice particle presence.

Table 4: Probability of rain for cloud free and each cloud category of the Cloud Type, derived from one year of co-located BALTRAD and NOAA 15 AVHRR data.

Cloud Type category	Probability of rain	Cloud Type	Probability of rain
All cloud free types	< 2.6 %	Very thin cirrus	4.9 %
Very low clouds	2.1 %	Thin cirrus	8.4 %
Low clouds	5.5 %	Thick cirrus	11.1 %
Medium level clouds	21.2 %	Cirrus over lower clouds	16.5 %
High opaque	38.9 %	Fractional clouds	3.5 %

Validation. The Cloud Mask algorithm has been extensively validated against surface observations from nearly three years of Synop reports from stations in central and northern Europe. The subjective validation of the Cloud Type has shown that fractional water clouds (sub-pixel cumulus and cloud edges) are often incorrectly classified as *very thin cirrus* or *thin cirrus*. To some extent the opposite is true too. Also, thin cirrus above low and mid level clouds are sometimes incorrectly classified as mid level or high level opaque clouds.

Results for CNN II and BBC. For all three EOPs we have derived the mean total cloud cover, the mean fraction of water clouds, the mean fraction of ice clouds, and the mean fraction of thin cirrus clouds. The water clouds here include the *very low clouds*, *low clouds*, and the *medium level clouds* categories, though there is a considerable likelihood/risk of ice particle presence. The ice clouds are defined as *very thin cirrus*, *thin cirrus*, *thick cirrus*, *cirrus over lower clouds*, *high opaque clouds*, and *very high opaque clouds*. The thin cirrus clouds are here defined as the two categories *very thin cirrus* and *thin cirrus*.

Based on a detailed study using the BBC data and partly supported by the extensive objective to verify of the cloud mask over sea and land, we assign a 50% coverage to all pixels over sea classified as *very thin cirrus* or *fractional*, and 100% to all other pixels. This is in order to derive consistent cloud cover fields over both land and sea. We see that the category *fractional* has been assigned a 100% coverage over land. This is motivated by an assumption that a FOV has to be substantially covered (usually more than 50% coverage) in order to be detected, and that small cumulus clouds may go undetected.

The maps of total mean cloud cover, mean water cloud cover, mean ice cloud cover, and the mean cover of thin and semi-transparent cirrus clouds without lower cloudiness beneath for September 2001 are shown in Figure 14. As seen from the map the often observed clear and partly artificial land-sea boundary is reduced and is more realistic using this post-processing. Figure 15 shows the mean cloud cover parameters for BBC divided into four time slots. The total cloud cover over land is at its minimum during night and morning and increases to a maximum in the afternoon or early evening. The increase in cloud cover over land over the day is seen first in the water clouds and later in the ice cloud coverage.

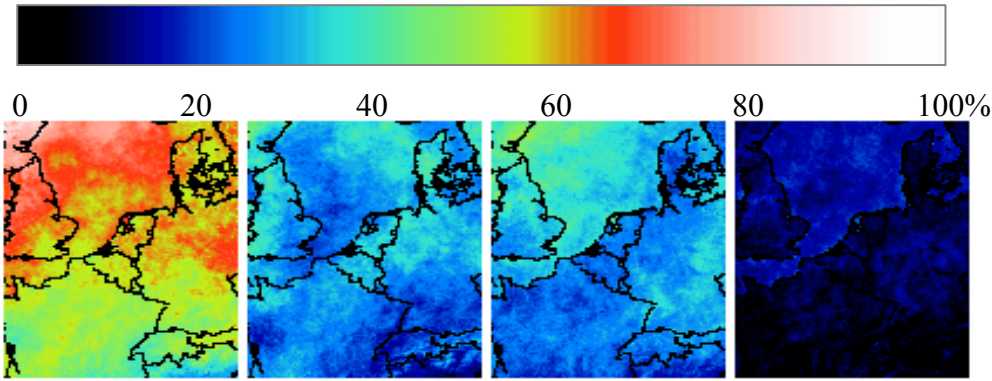


Figure 14: Total all-day mean fractional cloud cover for BBC, September 2001. From the left to right is the total mean cloud cover, the mean water cloud cover, the mean ice cloud cover, and the mean cover of thin and semi-transparent cirrus clouds without lower cloudiness beneath.

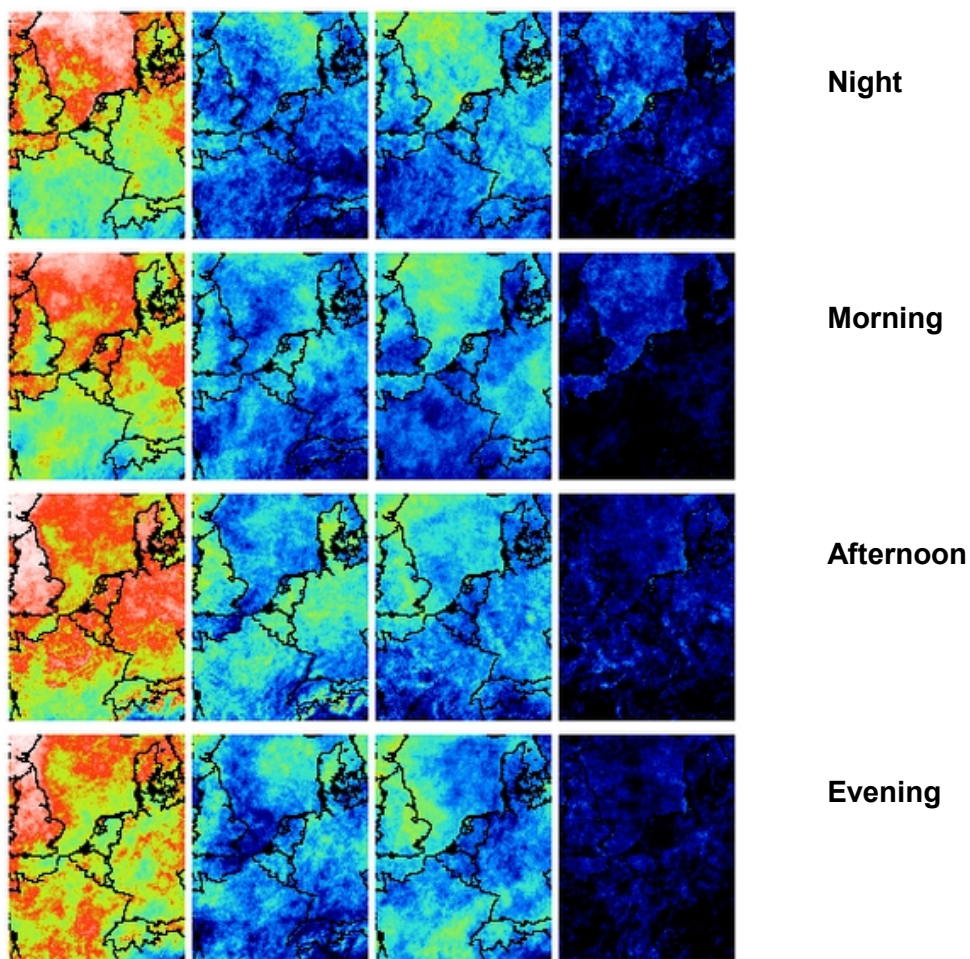


Figure 15: Mean fractional cloud coverage during August 2001 for four time periods per day. From left to right: total cloud coverage, water cloud coverage, ice cloud coverage, and thin cirrus coverage.

Comparison with surface stations. From both the low resolution dataset with frequency of cloud types inside 10 by 10 pixel boxes, and from the high resolution dataset of the Cloud Type product, it is possible to extract information around NWP Grid points or actual locations of CLIWA-NET surface stations. Figure 16 shows an example of collocated (in time and space) surface observations, weather radar, and satellite data at the station Onsala near Gothenburg, Sweden on April 4, 2001. In this case

the Cloud Type analysis is reasonably consistent with the surface observations. The only possible exception is the satellite observation early in the morning. A little before 5 UTC the satellite observes predominantly cloud free conditions, but at that time there is a rapid increase in the ground based IR radiometer temperature, which indicates cloud contamination. At the next satellite observation, less than two hours later, there is actually a layer of thin cirrus clouds observed by the Cloud Type analysis.

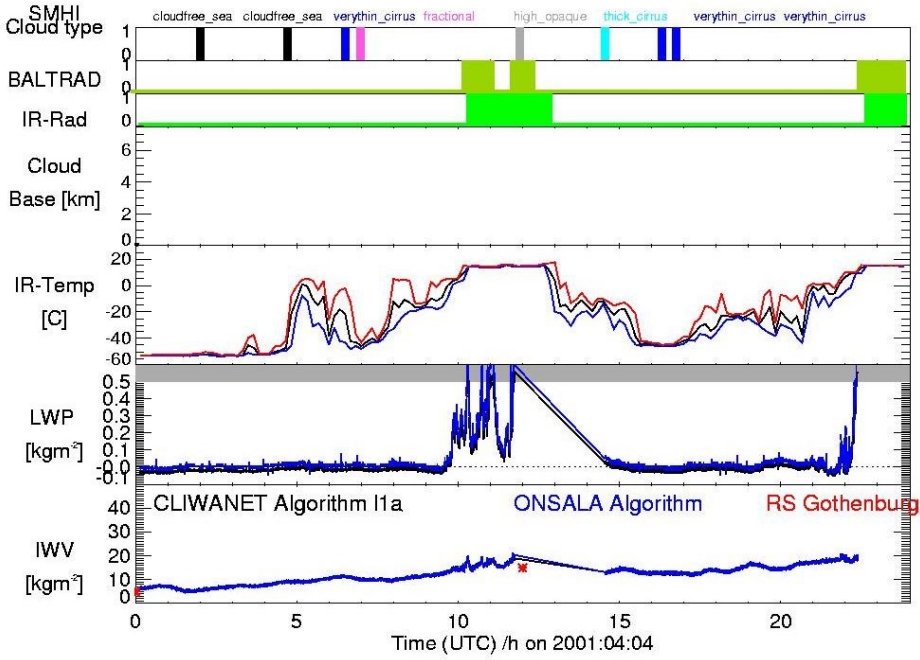


Figure 16: Surface observations at Onsala on April 4, 2001, during CNN II, with the satellite Cloud Type analysis and the rain/no rain flag from the BALTEX Radar dataset, BALTRAD. The Cloud Type categories shown here are for each satellite overpass the most frequent class observed within a 5 by 5 pixel area centred at the location of surface station.

3.2.3 Quantitative cloud analysis using AMSU

The aim of this work package is to develop remote sensing algorithms that convert microwave radiation emitted from cloudy skies into cloud liquid water path. Motivation for this arises from the fact that the intensity (or brightness temperature) at microwave frequencies is a direct measure of the amount of liquid water provided that certain boundary conditions like surface temperature and surface wind are well known. Here, data from the Advanced Sounding Microwave Unit (AMSU) have been used. The AMSU is a multi-channel microwave radiometer onboard the NOAA satellites. It is divided into two segments, AMSU-A for cloud and water vapour path measurements used in the present study and AMSU-B for sounding of temperature and humidity profiles under clear sky conditions. The NOAA satellite also carries the AVHRR which thus provides collocated measurements of solar reflected and thermal emitted radiation. AVHRR measurements are analysed in an accompanying study performed at KNMI. We note that AVHRR measurements are sensitive to cloud total water (liquid and ice) whereas AMSU is little affected by ice, except for some temperature depletion due to scattering effects.

A public available semi-empirical algorithm that translates AMSU measurements into LWP and IWV is provided by Weng et al. (1999). This method was implemented, but due to large differences of AMSU-derived LWP and collocated AVHRR LWP the method was found not suitable for our application. Therefore, during the project a new physically based AMSU cloud retrieval scheme was developed. In order to define the statistical relation between cloud liquid water path and water vapour with

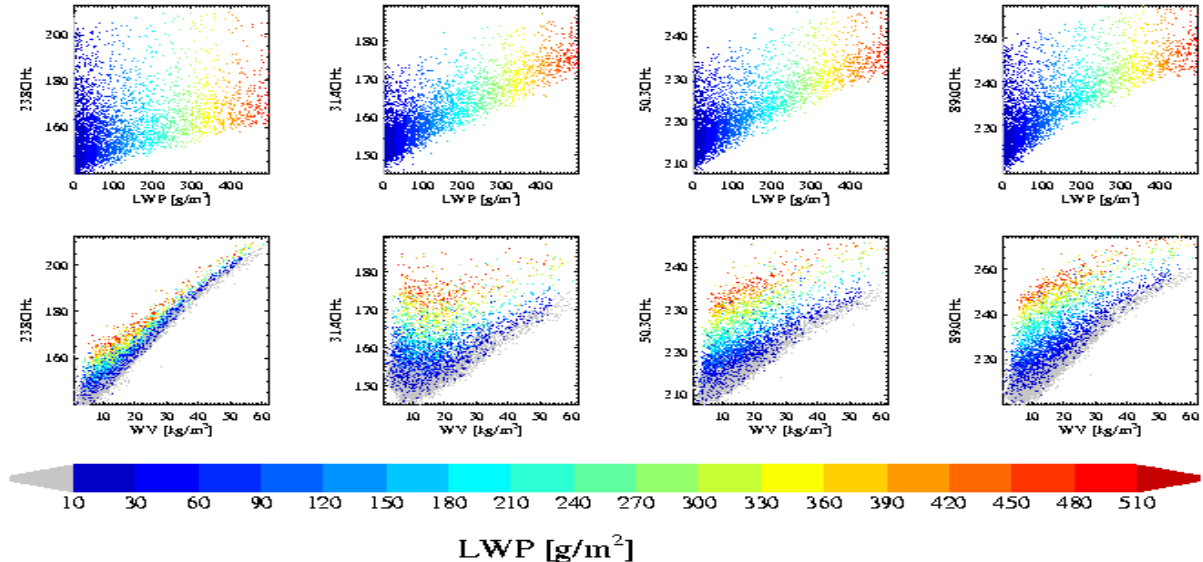


Figure 17: Simulated AMSU brightness temperature depending on LWP and I WV.

the brightness temperatures at the AMSU-A frequencies basically same technique as for the ground-based microwave radiometer was used. The only difference is the necessary assumptions about the signal contribution from the ground. Radiative transfer calculations by means of the microwave radiative transfer model MWMOD (Fuhrhop et al., 1998) were performed. Because only few measurements of vertical profiles of liquid water content exist (Löhnert et al., 2001) large set of radiosonde profiles over ocean areas under cloudy conditions have been converted into liquid water profiles. This conversion includes a number of assumptions regarding cloud height, cloud particle number concentration, and mixing processes (see Karstens et al., 1994). We assume that these assumptions do not affect the quality of the statistics of the so obtained cloud fields significantly.

The top row of Figure 17 shows the resulting relations between LWP and brightness temperatures at 23.8 GHz, 31.4 GHz, 50.3 GHz and 89.0 GHz for a satellite viewing angle of 1.6 degrees. The individual channels show a general positive correlation, though quite noisy. However, the larger microwave frequencies are more sensitive to larger LWP values. Therefore, a combination of the individual brightness temperatures may result in a strong correlation with the LWP as described below. In principle, the same is possible for the vertically integrated water vapour WV, but the present study is on liquid water.

Algorithm development. In order to account for the non-linear multivariate relation between atmospheric and radiation parameters a Neural Network (NN) approach (Jung, 1998) has been chosen for the algorithm development. The data set of LWP and corresponding brightness temperatures at the AMSU channels as described in the previous section is split into two parts: One part, the training part, is used to design the NN; the second part, the control set, is used for quality control. This quality control is required because NN tend to "learn" too close to the specific training data set on the expense of generality. A NN consists of three or more layers. The first layer represents the input signals, which in this case are the AMSU brightness temperatures. The last layer is the output layer, which provides the LWP in our NN application. The nodes in these two and a middle or "hidden" layer are associated with weighting factors. During the training process, these weighting factors are

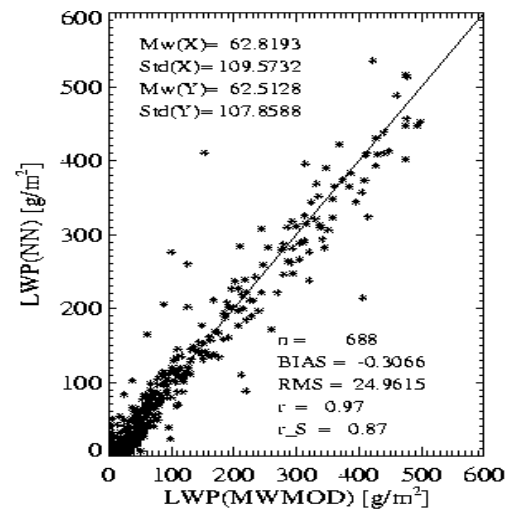


Figure 18: Neural Network LWP versus reference LWP for the validation dataset.

modified iteratively until the relation between input brightness temperatures and output LWP fields is optimised. As pointed out in 3.1, the largest improvement in LWP accuracy results from increasing the number of frequency channels from two to three. In general, the algorithm improves as the number of hidden neurons increases. However, saturation is reached at 4 hidden neurons. The neuron denoted with "-1" corresponds to a linear correlation between LWP and AMSU brightness temperatures. In order to illustrate the accuracy of the NN algorithm Figure 18 shows a scatter plot of LWP from the test data set vs. LWP as derived from the algorithm for 4 AMSU frequencies and 5 nodes in the middle NN layer. The overall correlation coefficient $r = 0.97$. If the non-uniform LWP density distribution is taken into account, the correlation coefficient is still 0.87 (Spearman correlation) from which we conclude that our NN retrieval scheme reproduces the LWP sufficiently well.

Validation. Problems with respect to the new AMSU NN algorithm arise when the results are compared to LWP from AVHRR based retrievals. The latter is done by means of the KLAROS scheme, which converts AVHRR reflectance measurements in the visible spectral range into cloud optical thickness, which in turn can be converted to LWP by assuming a certain particle effective radius. A comparison of ground based LWP from microwave radiometer (which is supposed to provide high quality results) with KLAROS LWP usually yields quantities within the same order of magnitude (section 3.2.4). However, differences are much larger when satellite based LWP fields from AMSU and from AVHRR are compared. This is illustrated exemplarily for a satellite overpass from 04/04/2001, noon. Figure 19 shows the original LWP field as retrieved with the KLAROS scheme. For comparison reasons the AVHRR results are averaged in Figure 20 along the large AMSU field of views. The spatial antenna weighting function of the AMSU has been taken into account. The retrieved AMSU LWP is shown in Fig. 21. The cloud field structure is well represented.

The two methods are compared quantitatively in Figure 22. In colour the scan position is displayed,

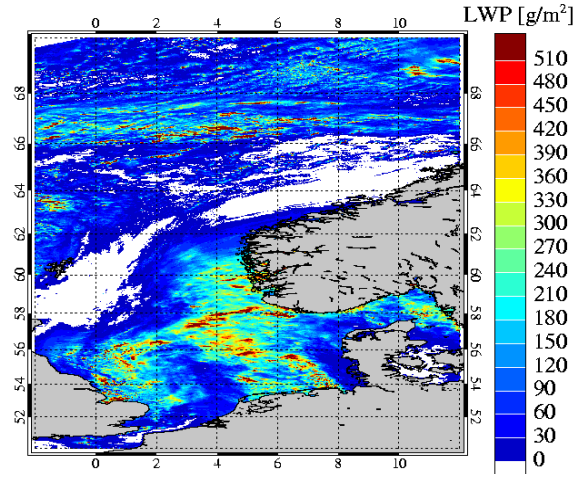


Figure 19: AVHRR LWP retrieved with the KLAROS scheme.

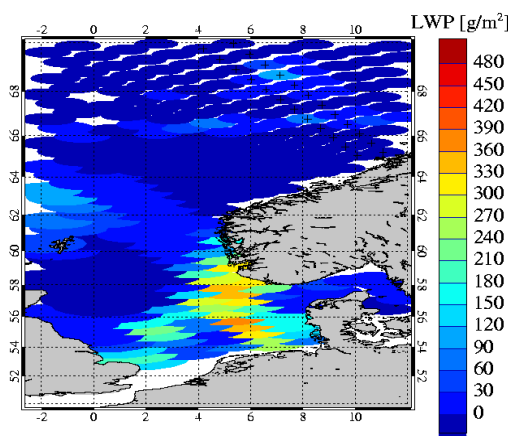


Figure 20: AVHRR LWP on the AMSU grid

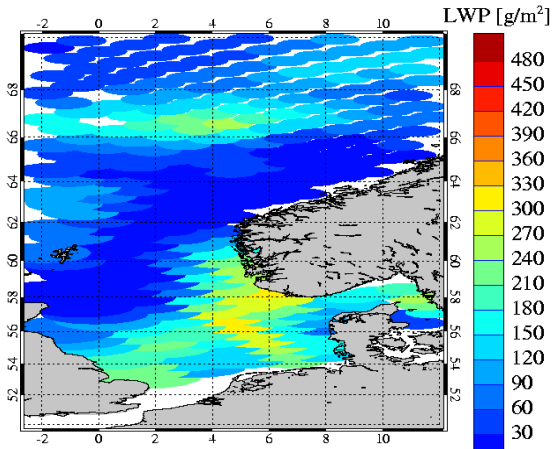


Figure 21: AMSU LWP retrieved with the Neural Network method.

whereby position 1 (purple) represents the near nadir FOV. All plotted FOVs have at least a cloud cover higher than 95%. The cloud cover is defined by the high resolution AVHRR FOV, where the LWP exceeds 5 g m^{-2} . The bordered circles depict the total cloud cover.

Using the neural network algorithm for the retrieval of LWP from measured AMSU brightness temperatures, the results are not satisfactory. AMSU tends to underestimate the LWP compared to AVHRR when looking at near nadir FOV's. The correlation seems to depend on the viewing zenith angle and varies strongly with the observed case.

The underestimation is caused by the sensitivity of the neural network to the training data. For appropriate neural network algorithms a huge data base is needed, in this case it consists of radiosonde ascents over sea. The majority of ascents used here are provided by the Alfred-Wegner Institute, Bremerhaven. The radiosondes were launched from the research vessel "Polarstern" on their way from Antarctica to the North Pole. So the data set is dominated by cold atmospheres with low amounts of water vapour, even if the used radiosondes are launched between 70 S to 70 N. The temperatures retrieved with the radiative transfer model are low in the water vapour channel. Due to this the neural network retrieval overestimates the contribution of water vapour contained within the 23.8 GHz channel, which results in a strong underestimation of LWP. The reliability of the NN algorithm strongly depends on the number of training data and as well on the distribution of possible atmospheric states contained in the radiosondes. Using the same data set and additional ground information like the surface wind, pressure and sea surface temperature from NCEP/NCAR, the correlation between the AMSU LWP and AVHRR LWP is higher and the underestimation of AMSU related to AVHRR is reduced. For our retrieval, the amount of training data is not representative, and so the algorithm is not reliable.

Another possibility for a retrieval of LWP is the derivation of a multi-linear regression. Here the ground state can also be included. A stable correlation between modelled LWP and the input data is retrieved, but using the AMSU data, the correlation with the AVHRR retrieval is even worse. We conclude that the current state of the AMSU-A instrument is not suited for getting quantitative LWP information.

3.2.4 Quantitative cloud analysis from AVHRR

AVHRR analysis was planned to provide the spatial distribution of cloud liquid water path at one moment in time. The retrieval of LWP is based on the interpretation of the amount of sunlight reflected towards the satellite. The interpretation is implemented in the KLAROS scheme. The amount of reflected sunlight does not depend on LWP alone, but also on cloud particle size, cloud 3dimensional structure, particle phase etc. These cloud properties are not taken into account in the original KLAROS scheme. Therefore, it was expected that the accuracy of the satellite analysis alone would not be sufficient for atmospheric model evaluation. Two approaches were selected to improve the accuracy of the liquid water path:

- Improvement of the AVHRR analysis using the $1.6 \mu\text{m}$ channel
- Comparison with and optimisation to the ground based microwave radiometer network.

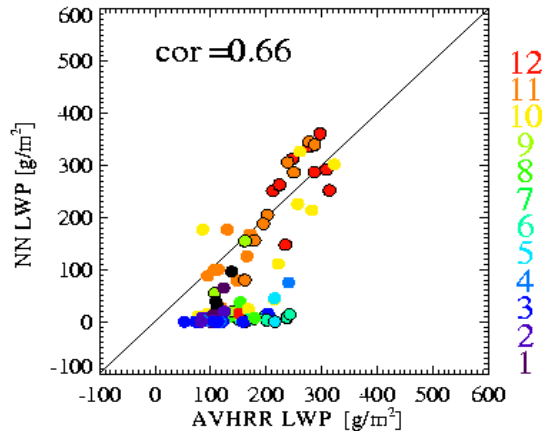


Figure 22: Neural Network LWP from AMSU data versus AVHRR LWP from KLAROS. See text for further description.

The scatter plot shows the relationship between NN LWP [g/m²] on the y-axis and AVHRR LWP [g/m²] on the x-axis. The x-axis ranges from -100 to 600, and the y-axis ranges from -100 to 600. A diagonal line represents the 1:1 relationship. Data points are colored according to their position in the near nadir FOV, ranging from purple (position 1) to red (position 12). The correlation coefficient is labeled as $\text{cor} = 0.66$. A vertical color bar on the right indicates the positions: 12 (red), 11 (orange), 10 (yellow), 9 (green), 8 (light green), 7 (cyan), 6 (blue), 5 (dark blue), 4 (purple), 3 (black), 2 (grey), and 1 (dark grey).

KLAROS. KNMI has developed an operational and automated cloud detection and cloud property retrieval scheme, referred to as KLAROS (KNMI's Local implementation of APOLLO Retrievals in an Operational System). The APOLLO cloud detection scheme is applied to discriminate cloudy from cloud free pixels (Saunders and Kriebel, 1988). The scheme is adapted and extended to include variable thresholds from atmospheric profiles and NWP surface temperature fields that operate automatically. Moreover, the scheme allows the determination of the following cloud properties: optical thickness, cloud emissivity, cloud top temperature and cloud liquid water path. Figure 23 shows a schematic representation of the steps involved in the retrieval of KLAROS optical thickness and cloud top temperature.

The properties of clouds are determined on a pixel by pixel basis for pixels that are flagged cloudy. The visible optical thickness is derived from the $0.6\text{ }\mu\text{m}$ reflectivity. The radiative transfer model Doubling Adding KNMI (DAK) is used to simulate both atmospheric absorption and scattering and the cloud scattering properties (Stammes, 1994). With DAK the top of the atmosphere reflectivity is calculated for plane parallel clouds with different optical thickness as a function of surface albedo, solar zenith angle, viewing zenith angle, relative azimuth angle, and cloud thermodynamic phase. The scattering phase function for a size distribution of liquid water droplets was calculated using Mie theory, whereby the scattering phase function for a size distribution of ice crystals was calculated by ray-tracing, assuming the imperfect hexagonal shape (Hess et al., 1998, Knap et al., 1999). This enables the retrieval of optical thickness for water and for ice clouds. The water optical thickness is the basic information to derive LWP.

The cloud liquid water path is calculated as follows:

$$\text{LWP} = 2 \cdot \tau \cdot r_e / 3,$$

whereby τ is the optical thickness and r_e the effective radius of the liquid water droplet distribution. In the original implementation of KLAROS an effective radius of $10\text{ }\mu\text{m}$ is assumed, which is the value used in the International Satellite Cloud Climatology Project (ISCCP) algorithms. KLAROS was used to process AVHRR measurements from CNN I, CNN II and BBC measurement campaigns. The quality of the radiances of the succeeding NOAA platforms differs considerably. Strengths and weaknesses of the instruments are: NOAA-12: low quality calibration; NOAA-14: indecisive vicarious calibration; NOAA-15: measurements are noisy; NOAA-16: well calibrated, including $1.6\text{ }\mu\text{m}$ channel. Clearly, the NOAA-16 measurements are superior and therefore most of the research efforts focussed on the high quality measurements of this platform.

Methods to use the $1.6\text{ }\mu\text{m}$ channel onboard NOAA-16. In the KLAROS retrieval scheme there are several assumptions. This section describes the successful effort to improve the LWP retrieval by directly measuring two cloud properties using the $1.6\text{ }\mu\text{m}$ radiances measured from AVHRR: cloud particle phase and cloud particle size. Thus, the number of unknowns is reduced and the accuracy/quality of the retrieval is improved considerably.

Cloud particle phase. Water and ice clouds have different optical properties due to the different cloud particles. Water clouds consist of spherical water droplets that move with the air-mass. In general water droplets are smaller than $20\text{ }\mu\text{m}$. Ice clouds consist of ice crystals that occur in a wide range of shapes. Of these shapes the hexagonal columns and plates are most common. Measurements of ice crystals sizes show values from $20\text{ }\mu\text{m}$ to millimetres. Snow is also a type of ice-crystal.

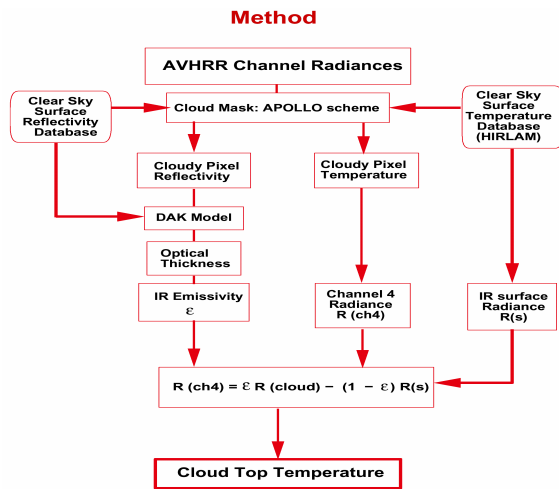


Figure 23: Flow diagram of KLAROS for cloud detection and cloud property retrieval

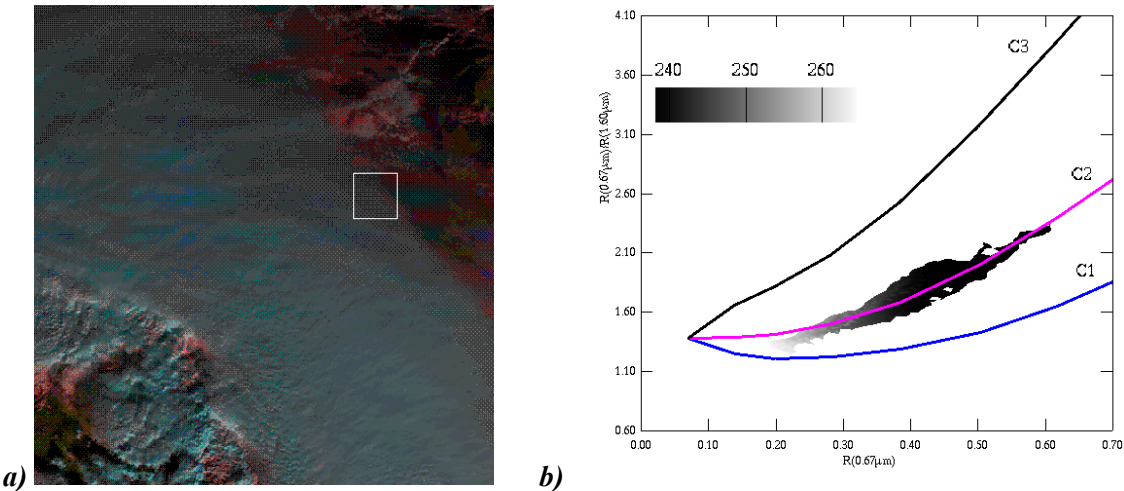


Figure 24: a) Cirrus field connected to a frontal zone. b) Corresponding scatter plot of 0.6 and 1.6 μm reflectivities.

The different sizes and shapes imply different radiative properties. The method developed at KNMI uses the reflected sunlight at 1.6 μm compared to 0.6 μm . Cloud particles hardly absorb radiation at 0.6 μm , but do absorb at 1.6 μm . The strength of absorption depends on the particle phase and size. In general, large particles absorb more than small particles. We have two unknowns: optical thickness and absorption and two measurements: 0.6 and 1.6 μm . The retrieval of particle size and phase is based on radiative transfer calculations for all possible sun-satellite-geometries and various cloud particle types. Calculations were done for 3 types of water droplets, characterized by their frequency distribution (Gamma-function), effective radius (4, 10 and 16 μm) and effective variance (0.15). The distorted ice crystal concept (Hess et al., 1998) was used to define ice particle distributions of 20 μm (C1), 40 μm (C2) and 100 μm (C3). We found that the ratio of reflectivity at 0.6 μm ($R_{0.6}$) and reflectivity at 1.6 μm ($R_{1.6}$) is a good indicator for particle type, especially if interpreted relative to $R_{0.6}$. In Figure 24 an example is given of $R_{0.6}/R_{1.6}$ versus $R_{0.6}$ for a specific sun-satellite geometry. Figure 24a shows a large cirrus field connected to a frontal zone. The reflectivities at 0.6 and 1.6 μm are shown in Figure 24b. It is clear that the cloud consists of ice crystals of the C2 type.

Cloud particle size. The method that was described above can also be used to estimate the size of water particles. As a first order effect this improves the estimates of optical thickness because the reflectivity at 0.6 μm is mainly determined by the optical thickness, but is also weakly dependent on particle size. This is illustrated in Figure 25, which gives $R_{0.6}$ versus $R_{1.6}$ for varying optical thickness and particle size for one sun-satellite geometry. As a proof of principle an example is given of a particle size retrieval. In Figure 26 a ATSR measurement of a stratocumulus deck at the Dutch coast can be seen. In Figure 26b the reflectivities are projected in a scatter plot. Clearly the particles in the cloud deck are in the order of 8 μm .

LWP retrieval. The relation between LWP, optical thickness, and particle size described in the previous section is applied to retrieve LWP. The new methods

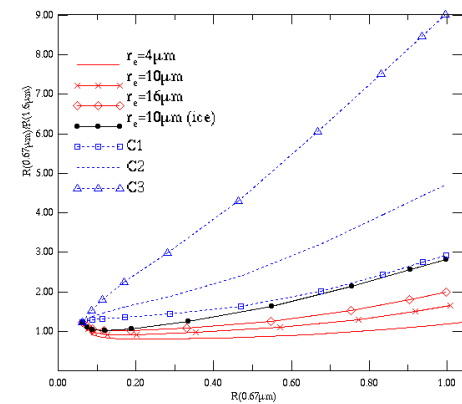


Figure 25: RTM calculation of sunlight reflectance to cloud particle of varying size and phase.

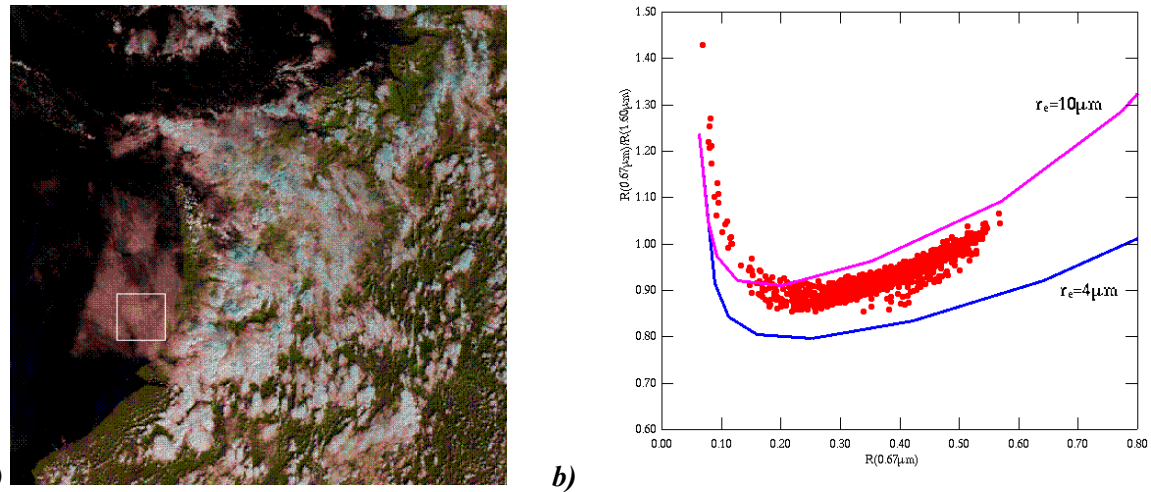


Figure 26: a) Stratocumulus field on the North Sea near the coast; b) corresponding scatter plot of 0.6 and 1.6 μm reflectivities.

that were presented give a better estimate of the optical thickness and an estimate of the particle size. These values were input to the LWP retrieval. In the following we will compare satellite derived values for LWP and measurements from the ground based microwave radiometers.

3.2.5 Comparison of LWP retrieved from satellite and ground observations

The CLIWA-NET campaigns have yielded an unprecedented set of microwave radiometer data for satellite retrieval validation. In Figure 27 only 15 days of measurements for one ground station is given. Red dots are satellite-retrieved values over a 10x10 km area around the ground station. The crosses are microwave radiometer values averaged over 40 minutes around the time of satellite overpass. For some days the values are close to each other. But on other days there are large discrepancies.

Our study shows that a large contribution to the difference originates from the co-location inconsistency. The time-series from ground based measurements is not always representative for the cloud field as seen from satellite. This is due to the fact that cloud field properties change in time and space. Therefore, we never know which part of the time series that is measured at one location is representative for which part of the spatial distribution that is measured at one moment in time. Below a method is introduced to assess the relation between these two different ways of observing clouds and two different cases are given as example.

August 13, 2001. At the time of satellite overpass there is an extended stratus field over the Netherlands. This is obvious from the satellite image (Figure 28a) and the time series (Figure 28b).

In Figure 28c the average and the variability of the satellite retrieved LWP over an area of increasing size is shown. The average ranges from 250 g m^{-2} for a small area to 180 g m^{-2} for the area of 1° by 1° (about 60x60 km^2). The observed LWP from ground is presented in Fig. 28d. The average varies between 220 and 240 g m^{-2} . The standard

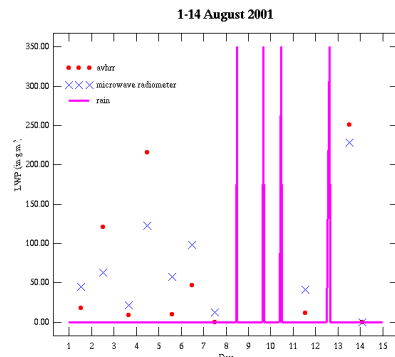


Figure 27: 15 days of ground and satellite measurements.

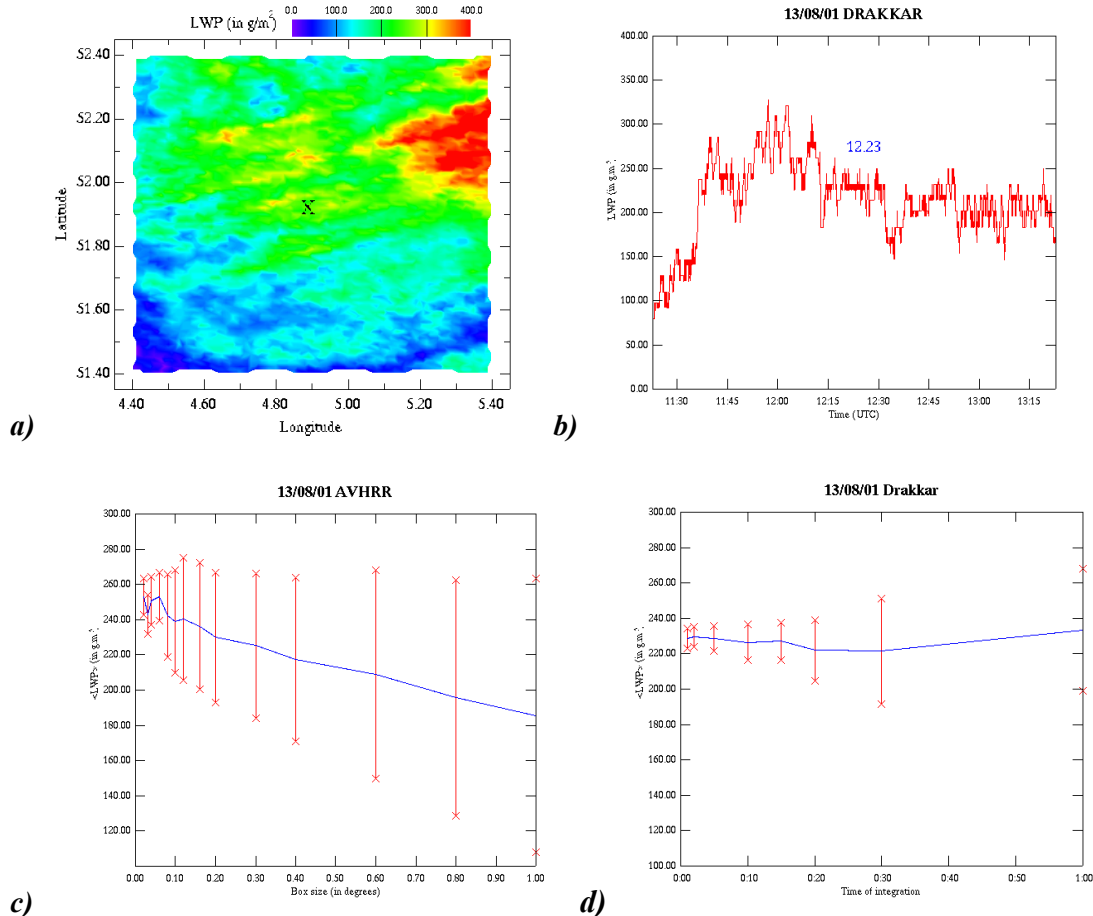


Figure 28: LWP as measured from a) satellite, b) ground averaged over c) space and d) time on August 13, 2001.

deviation is of the order of 5 g m^{-2} for small time intervals to 15 g m^{-2} for large intervals. Obviously, the cloud field is not very variable in space and over Cabauw the cloud field is very stable in time.

For stable conditions it is allowed to compare small time intervals with comparable area averages. In this case the satellite-derived value is $245 \pm 10 \text{ g m}^{-2}$ and the ground based value $230 \pm 5 \text{ g m}^{-2}$.

August 4, 2001. At the time of satellite overpass there is a field of small scale cumuli over the Netherlands. The cloud field shows high variability in space (Figure 29a) and time (Figure 29b). In Figure 29c the average and the variability of the satellite retrieved LWP over an area of increasing size is shown. The average ranges from 70 g m^{-2} to 215 g m^{-2} . The standard deviation is of the order of 100 g m^{-2} for most area sizes. The observed LWP from ground is presented in Fig. 29d. The average is about 40 for a small area, then increases to about 150 g m^{-2} for a 6 minute interval and then slowly decreases again to about 40 for large time intervals. The standard deviation is as large as the average. Obviously the cloud field is very variable in space and time. We are not able to say anything about the quality of the satellite retrieval.

3.2.6 Statistical validation

In this section the satellite retrieved values will be compared to ground based observations in a statistical sense. In the course of this project we made scatter plots for the various instruments, locations and campaigns. Figure 30 shows the results for station Lindenbergs during CNN II. Before a comparison can be made we have to reject those cases, which include ice clouds or precipitation. Ice clouds do not

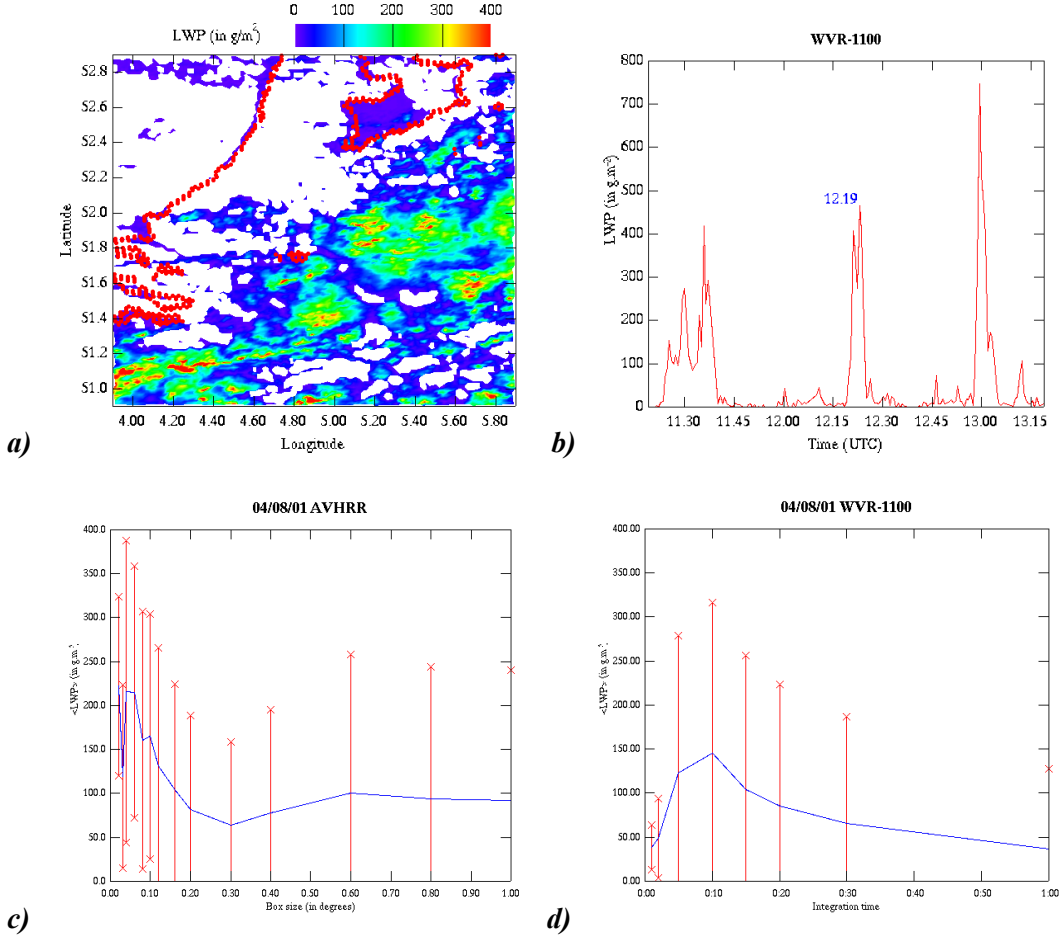


Figure 29: LWP as measured from a) satellite, b) ground averaged over c) space and d) time on August 4, 2001.

affect the ground-based measurements, but do affect the satellite radiances. In case of precipitation the ground observations are not valid/available. The scatter plots differ with location and instrument. This is partly due to the differing instrument characteristics.

For example: We found that there are large differences with respect to recover the time after a rain event. In Figure 31 the whole set of satellite versus ground-based values is given. The correlation is high (0.91). The standard deviation seems acceptable, but the scatter is still large. This is partly due to the co-location inconsistency, instrument differences, and microwave radiometer error characteristics. We find that the use of the $1.6 \mu\text{m}$ channel improved the satellite retrieval considerably. Still, the retrieval does not include 3D scattering effects and a sufficiently accurate handling of surface radiative properties.

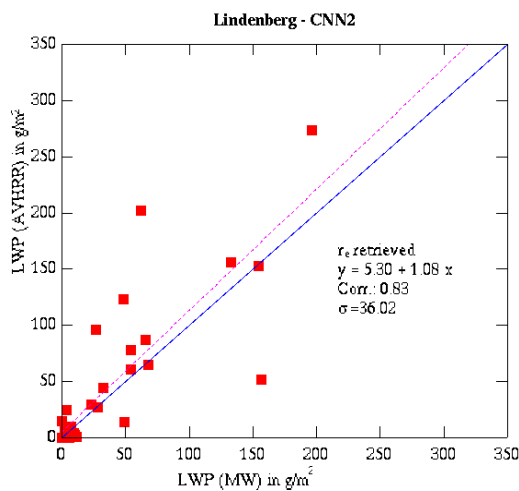


Figure 30: Ground based versus satellite derived estimates of LWP for Lindenberg.

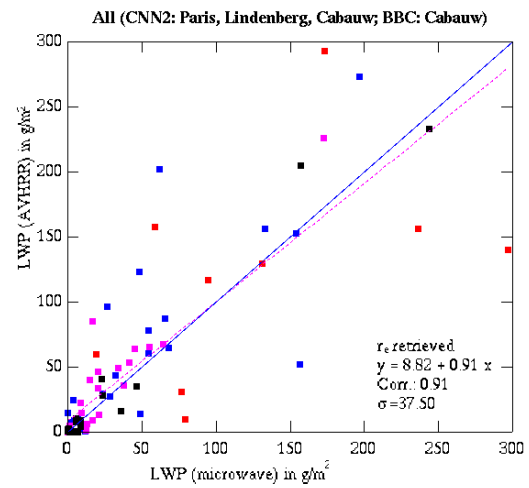


Figure 31: Ground based versus satellite derived estimates of LWP for all stations.

3.3 MODEL EVALUATION AND IMPROVEMENT

The major objective of CLIWA-NET is the demonstration of the usefulness of a European Cloud Observation such as it was set up in CLIWA-NET for the evaluation and improvement of atmospheric models. As clouds are the major uncertainty in current climate forecasts this work is of immediate benefit. Corresponding to the objective of CLIWA-NET main focus was on the liquid water path and its vertical structure.

3.3.1 Model evaluation

To prepare the inter-comparison with observations all atmospheric models needed to be set up in a similar fashion for the three observational campaigns. Methodologies focusing on the evaluation of model predicted cloud parameters with CLIWA-NET inferred observations have been developed and examined in various applications, e.g. a statistical evaluation of predicted liquid water path, the representation of vertically distributed liquid water content, and a comparison of a model predicted LWP-fields with satellite retrieved spatial distributions. Furthermore, the relation between transmissivity of solar radiation and liquid water path was investigated.

Model set up. Within the CLIWA-Net project four European institutes participated in the evaluation of model predicted cloud parameters: the European Centre for Medium-range Weather Forecast (ECMWF), Deutscher Wetterdienst (DWD), the Swedish Rossby Centre, and the Royal Netherlands Meteorological Institute (KNMI). The ECMWF participated with the global forecast model (version CY24R1) operated at an effective horizontal resolution of 40 km and with 60 layers in the vertical. It employed the prognostic cloud scheme of Tiedtke (1993) in which cloud content and cloud fraction are both treated prognostically. The DWD contributed with the recently developed Lokal Modell (LM; Doms and Schättler, 1999) operated in non-hydrostatic mode at a resolution of 7 km and with 35 layers in the vertical. At this resolution convection is still parameterised, but stratiform clouds are assumed to be resolved, implying that the cloud fraction of an entire grid box is determined by an all-or-nothing scheme. The Rossby Centre has developed a climate version of the numerical weather prediction model HIRLAM, hereafter referred to as the RCA-model (Jones, 2001). In this model cloud parameters are represented by the convection scheme of Kain and Fritsch (1991) and a stratiform cloud scheme proposed by Rasch and Kristjansson (1998). KNMI operated a regional version of the ECHAM4 GCM, hereafter referred to as RACMO (Regional Atmospheric Climate Model; Christensen *et al.* 1996). Cumulus convection is represented by a mass-flux scheme and stratiform processes by a modified version of a scheme originated by Sundqvist *et al.* (1989) in which cloud content is prognosed. Details can be found in Roeckner *et al.* (1996).

Model time series were calculated for sub-domains centered around the CLIWA-NET site. The sub-domain size was chosen to be in the order of 50x50 km². For ECMWF this leads to just one grid cell, for RCA and RACMO to 3x3 grid cells, and for the LM to 7x7 grid cells. The model output refers to a 12 to 36 hour window taken from each daily forecast initiated at 12:00 UTC the previous day. The RCA-model and RACMO were operated in as much an identical fashion as possible. The two models shared the same domain, where the horizontal resolution was 18 km and the number of model layers was 24. For the BBC-campaign the RCA vertical mesh was increased to 40 levels. Both models used the same set of ECMWF analyses to initialise the atmospheric component of the model and to drive the model from the lateral boundaries. The LM initialization has its own data-assimilation; the LM boundaries are forced from large-scale forecasts operated by DWD. For the BBC campaign integrations with the Lokal Modell have been carried out by UNIBONN.

Liquid water path and integrated water vapour. To obtain insight in the climatology of observations and model predictions we have studied the frequency distributions of the liquid water path and water vapour column. Figure 32 shows histograms of occurrence of mean LWP and IWV observed at Cabauw during the BBC-campaign. Using information from multiple instruments a number of atmospheric conditions have been probed on the basis of 10-minute sampling intervals. For this purpose, observation retrieved from raw MRAD-measurements are integrated in 10-minute intervals by straight averaging which removes the fluctuations on time scales of minutes or less. Precipitation is indicated from the rain shutter mounted on the IR-radiometer. Once precipitation is detected in a 10-minute

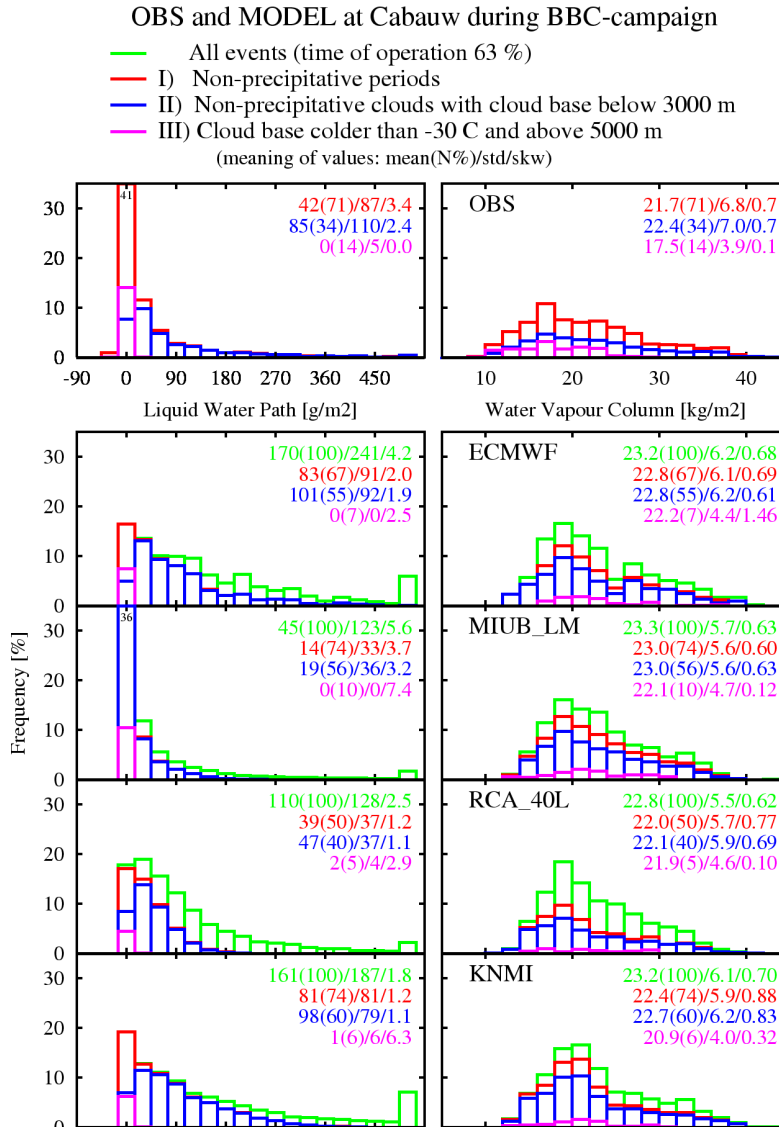


Figure 32: Histograms of observed and model predicted LWP and IWV at Cabauw during BBC. (LWP-values > 500 g/m² are collected in one bin.)

I) is difficult to characterize, and may contain mixed phase clouds, super cooled water clouds, or clouds with high variability within the 10-minute integration time. Likewise, Figure 32 contains the corresponding parameters derived from the model predictions. Processing of the model forecast series is restricted to time slots with valid measurements. This favours the model sample of large-scale flow patterns to be close to the observed sample in which the local cloud measurements were embedded.

Figure 33 summarizes the model evaluation of LWP and IWV for both CNN-campaigns. For each CLIWA-NET site the mean values for LWP and IWV inferred from observations and derived from model predictions are depicted for the three types of atmospheric conditions introduced above. In case cloud base height observations were absent (stations Bern, Palaiseau, and Gotland) the conditions under II) and III) were redefined to cloud base temperature only, while the reverse was done for non-observed cloud base temperature (Potsdam). In case a site was not operational (Cabauw, Chilbolton and Gotland during CNN I and Geesthacht during CNN II) the model predictions apply to the entire campaign without restriction. In general, sites returned a high measurement rate. The low rate at Helsinki reflects that measurements were restricted to the working hours on working days. Conditions at Kiruna during CNN II were subject to frost. Low measuring rates at the other sites were in general due

interval observations from this interval are rejected from further analysis. The displayed frequency distributions of retrieved LWP and IWV are given as a percentage of the total measuring time. In the BBC-campaign, the total measuring time amounts to about 63 % of the total campaign time (61 days). The loss of measuring time is almost entirely due to the MRAD-instrument not having been operated, mainly for reasons of maintenance.

Figure 32 presents results for three classes of atmospheric conditions discriminated as follows: I) non-precipitating periods, II) non-precipitating water clouds which were assumed whenever the minimum lidar-ceilometer cloud base height during a 10-minute interval was below 3000 m, the maximum cloud base temperature was above 0°C, and no precipitation was indicated by the rain-shutter, and III) free of liquid water clouds which was assumed whenever the maximum cloud base temperature was below -30°C and cloud base height above 5000 m. Classes II) and III) are exclude each other and both fall within class I). The residual in class

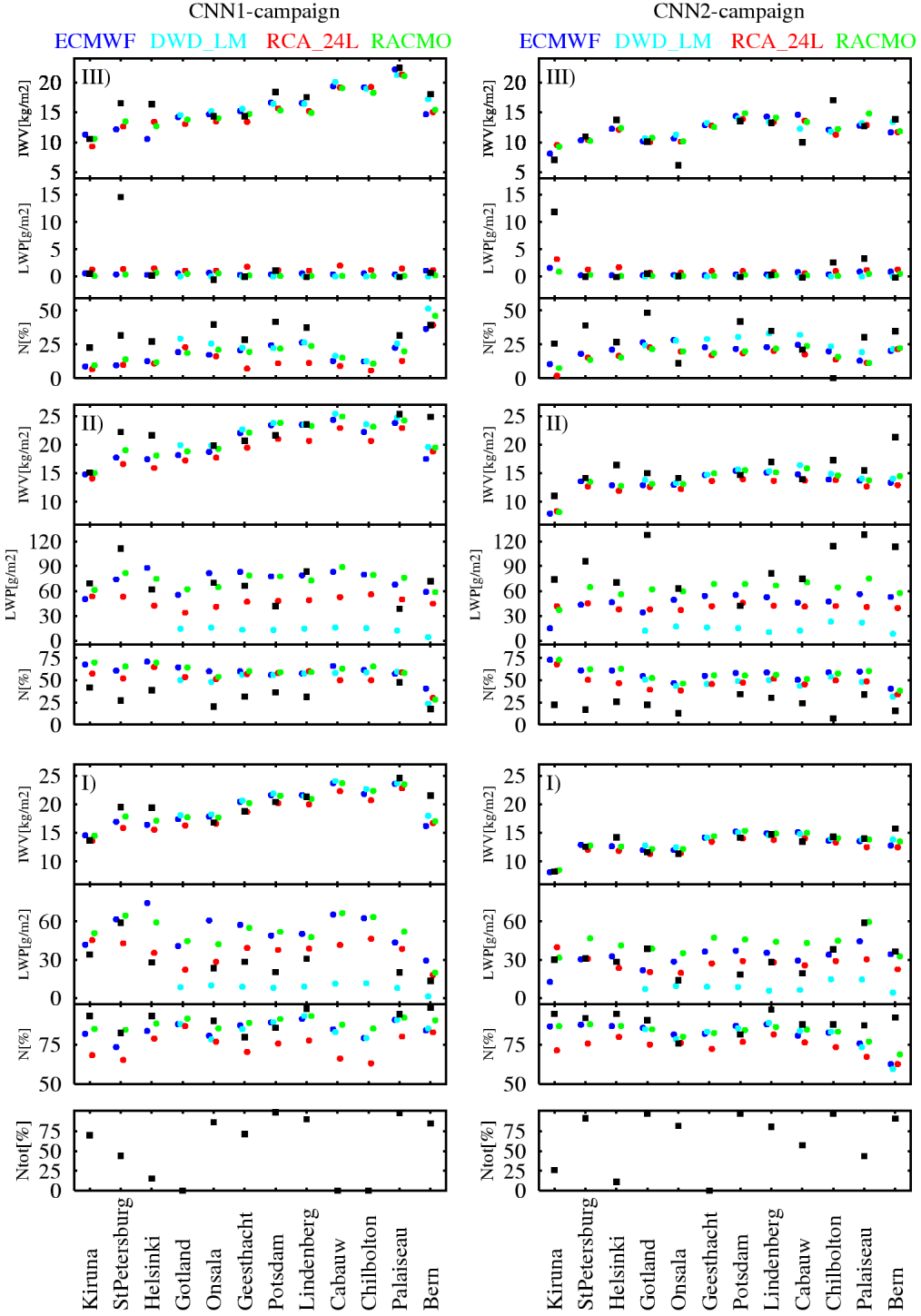


Figure 33: Observed and model predicted mean LWP and IWV and frequency of occurrence for three classes of atmospheric conditions (see text) at 12 stations during CNN I (left panels) and CNN II (right panels).

to instrumental problems.

With regard to the observations, IWV during CNN II is lower than during CNN I and BBC as springtime conditions are colder than in late summer. Occurrence of precipitation, being the complement of condition I, varies from 25 % at Onsala (CNN II) and 18 % at Cabauw (BBC) to almost dry conditions in Lindenberg (both CNNS) and Bern (CNN I). During non-precipitating periods mean LWP is

mostly between 15 and 45 g/m² (exceptions are St Petersburg (CNN I) and Palaisseau (CNN II)). For non-precipitating water clouds, mean LWP values are between 40 and 80 g/m² (exceptions are again St Petersburg (CNN I and CNN II) and Palaisseau and Bern (CNN II)), while the frequency of occurrence is between 10 and 40% (at Chilbolton (CNN II) it was less than 5%, at Palaisseau (CNN I) almost 50%, but the conditions were less strict owing to the absence of a ceilometer). In conditions free of water clouds most sites indeed return a mean LWP close to 0 g/m² (exceptions are St Petersburg (CNN I) and Kiruna (CNN II), and to somewhat lesser extent Chilbolton and Palaisseau during CNN II). The occurrence of cloud free periods shows more variability as it ranges from 0 % at Chilbolton (CNN II) to nearly 50% at Gotland (CNN II). All together, the picture emerging from the observations seems coherent, although question marks remain on the reliability of the measurements at St. Petersburg (CNN I in particular) and Chilbolton (CNN II).

With regard to the model predictions the picture is surprisingly unequivocal. Predictions from all models show a persistent tendency to overestimate the frequency of occurrence of precipitation. This applies in particular to the RCA-model. Predictions of IWV are reasonably accurate. The models tend to group together even when a deviation from the observations is substantial, like for instance at Bern. Model predicted IWV has been corrected for the difference in model orography and site elevation, but for Bern the correction turned out to be quite large and a mismatch continued to exist. Concerning LWP, at all instances ECMWF and RACMO are on the high side compared to observed values, while RCA is on the low side. The LWP prediction from the LM is manifestly wrong. Part of the reason is that sub-grid scale liquid water content was not incorporated in the model output (see section 3.3.2). It is indeed found that for typical synoptic scale events the LM estimate for LWP turns out to be in the proper range of magnitude. In applying the LM to the BBC-campaign UNIBONN has exported the liquid water contents used in the radiation calculations rather than the amounts produced by the thermodynamics, however these LWP estimates are still found to be much smaller than indicated by the observations (see Fig. 32). Concerning condition II) predictions from all models at all sites (considerably) overestimate the occurrence of liquid water clouds. Part of this deviation might be related to the length of the time slots (10 minutes) at which the observed parameters are sampled from the raw measurements. But given the considerable size of the overpredictions it is unlikely that choosing a larger time slot size (e.g. one hour) will entirely make up for the found differences. For condition III) a reverse result is found. In general, conditions free of water clouds are observed more often than predicted, although for a number of sites the predicted rate of cloud free conditions turns out to be fairly accurate (Onsala, Geesthacht and Bern (CNN I) and Cabauw(CNN II)). Only at Onsala during CNN II the amount of periods free of water clouds was found overpredicted. IWV-predictions in condition III) range from underestimating through accurately reproducing to overestimating the observed values.

Vertical distribution of cloud liquid water. Model predicted vertical structure of cloud liquid water has been evaluated on the basis of observations retrieved in Cabauw during the BBC-campaign. As has been outlined in section 3.1.3, the retrieval of the vertical distribution of cloud liquid water is the synergistic result of measurements from microwave radiometer, cloud radar and lidar ceilometer. In essence, information from the multi-channel microwave radiometer (MICCY) is used to infer a profile of liquid water content normalized to the liquid water path, while ceilometer and cloud radar are used to constrain the vertical position and extent of the cloud. Owing to the required presence of three instruments and given the fact that, like in the evaluation of LWP, a meaningful retrieval is only possible in non-precipitating conditions including the absence of drizzle, the relative number of retrievals turned out to be rather limited. In the present analysis retrievals are available for 7 % of the BBC campaign, always confined to the daylight period in correspondence to the operational hours of the GKSS clouds radar.

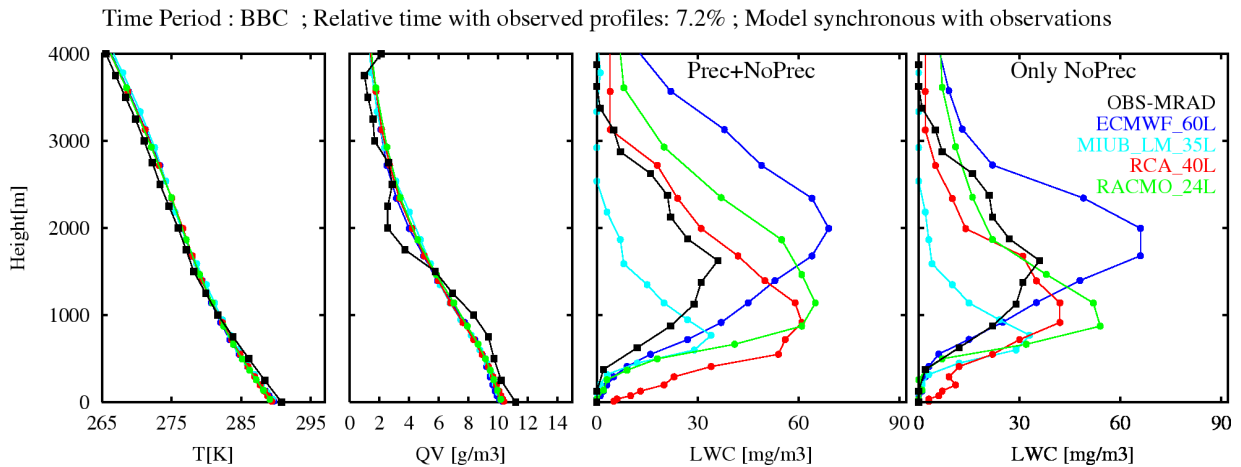


Figure 34: observed and model predicted profiles of temperature, absolute humidity and liquid water content at Cabauw averaged over 7.2% of the BBC-campaign.

Model predicted profiles are shown in Figs 34. The model predictions are confined to the time slots for which profile information was successfully retrieved from the measurements. Furthermore, to indicate the effect of precipitation the figure on the cloud liquid water profile is duplicated with respect to the occurrence of precipitation at the surface in either of the model predictions. The result is consistent with the finding in an earlier paragraph of this section, i.e. ECMWF and RACMO have similar amounts of LWP, RCA somewhat smaller, and LM much smaller. A significant difference can be seen in the position of the maximum liquid water content. RCA and RACMO predict this height to occur at about 1000 m, whereas the ECMWF model puts the position of maximum LWC at almost 2000 m, which is somewhat closer to the observed height of about 1600 m. LM, on the other hand is below 1000 m. If we restrict to non-precipitative events the main characteristics remain, but the details change. LWP reduces, the position of maximum LWC comes down, and the amount of LWC above the maximum reduces. Interestingly, for temperature and humidity all four models are mutually very comparable, but fail to reproduce the observed vertical structure in humidity related to the position of the boundary-layer height.

Comparison of model derived LWP with satellite retrieved LWP. One of the focal points of Work package 3000 has been the development of an algorithm to retrieve spatial distributions of LWP from satellite observations. A detailed description of the applied methodology can be found in section 3.2.4. In evaluating model predicted spatial distributions of LWP a pilot study has been devoted to a case of thick stratocumulus that occurred over the Netherlands on 4 May 2001 during the CNN II-campaign (Feijt et al., 2002).

Here we discuss the recent findings of a statistical evaluation for the entire BBC-campaign. For this purpose, satellite inferred spatial distributions (resolution ~ 1 km) have been projected on the RACMO model grid (resolution 18 km). For the portion of ice cloud flagged pixels within a model grid box it is assumed that the LWP content is equal to the mean value found for liquid water cloud flagged pixels. A pixel is flagged as an ice cloud when the cloud top temperature is below -13°C . Once the number of pixels with ice clouds is more than half the number of pixels with liquid water clouds the result for the model grid box is flagged ice-cloud. For the model prediction a similar procedure is applied: when cloud top temperature, i.e. 5% of the cloud cover profile is below -13°C the model result for that specific grid box is flagged ice cloud. Figure 35 shows mean values of satellite inferred and model predicted LWP along a north-south and an east-west transect across Cabauw. Averaging is done over the number of successful retrievals of LWP. When a specific grid box sees an ice cloud either in a satellite sense or in a model sense it is removed from the averaging. The relative number of successful retrievals (see Figure 35) is 73 % and varies between 60 and 80%.

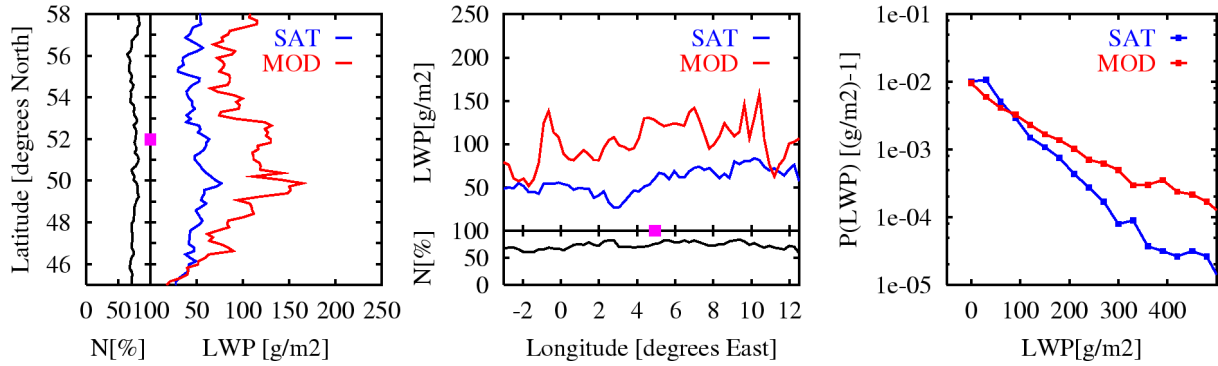


Figure 35: Transects across Cabauw (magenta square) of mean LWP and relative amount of successful retrievals. The right-hand panel shows the frequency distribution of satellite inferred and model predicted LWP.

It is found that at almost all points along the transects the mean model predicted LWP is larger than the satellite retrieved value. The frequency distributions shown in the right-hand panel in Figure 35 nicely show the reason why. The satellite retrieved distribution falls off much steeper than the model predicted distribution. On average the satellite retrieved LWP value for the two transects together during the BBC-campaign is 54 g/m². The equivalent model value is 98 g/m². The satellite retrieved distribution peaks at low but non-zero values for LWP. Apparently the occurrence of pixels with small, but non-zero amounts of liquid water is in abundance over the number of pixels entirely free of liquid water clouds when integrated over domains with the size of a model grid box. This is not found in the model predicted distribution implying that, in a statistical sense, the parameterizations cannot reproduce such sub-grid scale effect.

Transmissivity of solar radiation and liquid water. The vertical distribution of cloud liquid water is crucial to the atmospheric radiative budget. In this contribution we have examined the relationship between the SW transmissivity and LWP inferred from measurements and derived from model predictions. The measured relation is shown in Figure 36 (left panel). Transmissivity is defined as the ratio of incoming solar radiation at the surface and at the top of the atmosphere. Observed values are based on synchronous and collocating measurements in Cabauw during the BBC-campaign. The huge scatter in the observations is essentially due to the always present short-scale inhomogeneity in cloud condensate, also in overcast conditions. Moreover, the presence and amount of ice clouds are not considered.

Also shown in Figure 36 (right panel) is the average relation between transmissivity and LWP employed by the models. The measured relation is reasonably well represented in cloud free conditions but at higher LWP values the model relations start to deviate.

The diurnal cycle of SW transmissivity during the BBC-campaign inferred from the radiation measurements and derived from the model predictions is shown in Figure 37. Evidently, the RCA prediction fits best to the data. The RACMO prediction strongly under-predicts the measurements, implying that this model operates with a reduced radiative forcing at the surface. The LM provides a reasonable reproduction of the amount of solar radiation reaching the surface. This is a nice example of compensating errors. Although the relation between radiation and liquid water path is totally wrong as shown in Figure 36, the underestimation of LWP by the LM eventually results in a reasonable prediction of incoming solar radiation. Finally, the ECMWF curve is a bit low. The rigid shape of the ECMWF curve is due to the fact that the full radiation in the ECMWF model, including the effects of clouds, are only invoked once every three hours. At intermediate time steps, information on changes in the atmospheric model state is not accounted for in the short wave radiation.

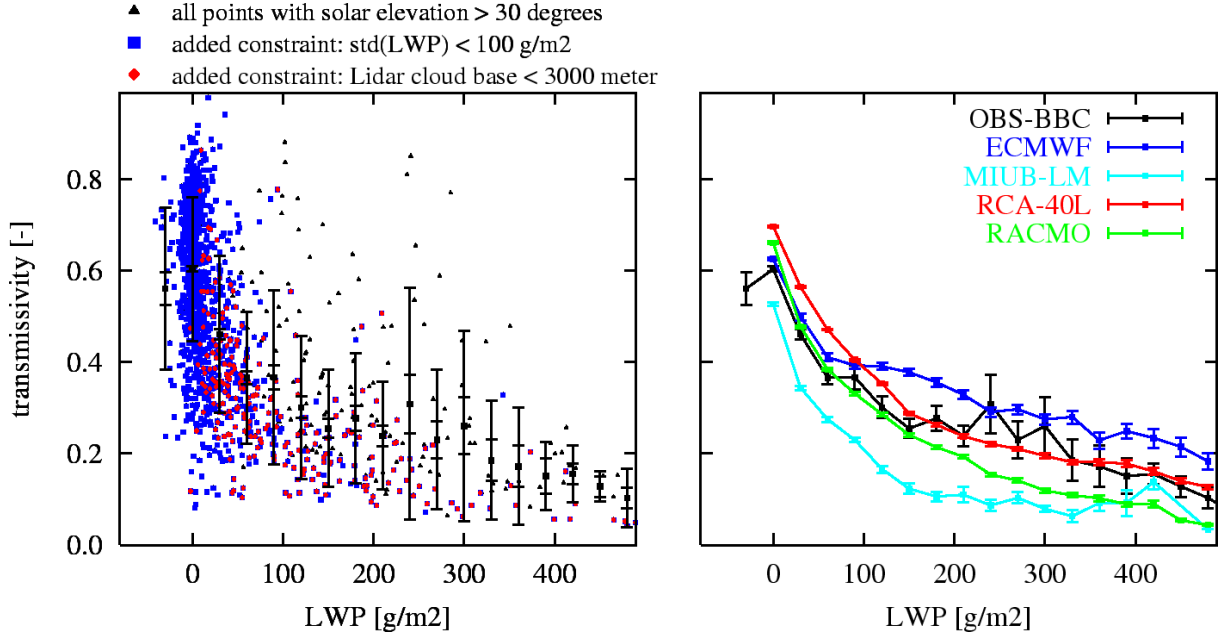


Figure 36: Observed and model predicted relations between transmissivity of solar radiation at the surface and liquid water path. The left panel shows measurements averaged over 10-minute intervals. Additional constraints: i) the 10-minute standard deviation of LWP is less than 100 g/m^2 , ii) the minimum ceilometer cloud base height is below 3000 m (5% threshold of 10-minute time series). The right panel includes model predicted relations.

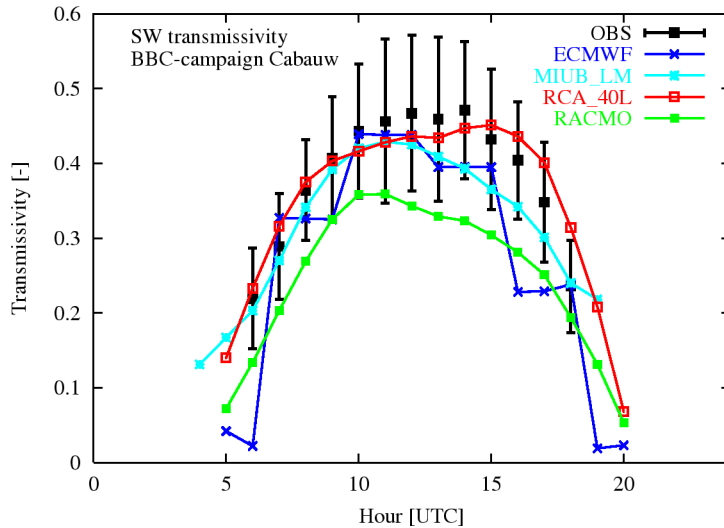


Figure 37: Diurnal cycle of SW transmissivity from measurements and model predictions during BBC.

3.3.2 Horizontal resolution

The objective of this work package is to examine the role of the horizontal grid refinement in the mesoscale regime (10 down to 1 km) in the representation of cloud parameters. We use the operational mesoscale model “Lokal-Modell” (LM) of the German weather service. Since model integrations at the 1 km scale are extremely expensive in computational time, we have restricted the analysis to case studies instead of longer time periods. In total six cases were investigated using exactly the same model domain at all resolutions, because we had found that it was otherwise impossible to decide whether differences had to be attributed to the refinement or to differences in the boundary conditions. Additional model integrations of one case during the CNN II campaign and two during the BBC campaign were performed. Simulations with parameterized convection to study differences between resolved and parameterized convection accomplished these new runs. More advanced analysis tools, especially an objective cell detection algorithm, were developed.

Model set-up. Table 5 gives an overview of all LM simulations performed in the frame work of WP4200. The two model domains we used cover an area of 440x440 km and are centered on Potsdam and Cabauw respectively. To avoid spin up effects all simulations are started at 12 UTC the day before. Depending on the resolution, the integration time step varies between 40 s and 6 s. Boundary data is provided every hour from LM analyses and interpolated on finer grids using a newly developed interpolation routine, which was implemented into the LM input module. This algorithm has proven to be superior to the old interpolation program “lm2lm” because it conserves average quantities like e.g. total water content.

Four different types of output data are provided by each simulation run: standard output of all prognostic and many diagnostic variables at the whole model grid (hourly), model domain averages of cloud related quantities like liquid water path and cloud height (10 min intervals), mean profiles of humidity, temperature etc. (10 min intervals) and information about convective cells which are identified by the cell detection algorithm described in the next section.

Analysis of model runs. A perfect model will add small scale features without changing the coarse scale structure, if grid spacing is reduced. Consequently area averaged quantities are expected to be insensitive to changes in resolution. The integrated water vapour, which is one of the key variables defining the probability of cloud formation, obeys this rule very well, as shown in Table 6. In contrast, liquid water path, precipitation and, to a smaller extent, ice water path (IWP) have significant trends; these quantities increase as grid spacing is reduced. Surprisingly, parameterised as well as resolved cloud cover seems to be consistent in terms of mean values. As a consequence hardly any deviations in the net surface radiation occur, because cloud cover is the most relevant parameter modifying radiative fluxes. Since not only the energy input but also the boundary layer stability remains unchanged, the surface energy budget is not affected by the refinement. The feedback of rainfall on evaporation by wetting the soil seems to be negligible on short time scales less than one day considered in this study.

As observed trends in LWP, IWP and precipitation reveal serious model deficiencies, it is important to identify the underlying mechanisms. The increase in cloud water, i.e. LWP and IWC, can be mostly

Table 5: Selected cases and model configurations.

Date	Campaign	Synoptic situations	Area	Configurations
2000/08/02	CNN I	cold front, deep convection	Potsdam	convection scheme off; Δx=7.0, 5.5, 2.8, 2.2, 1.1 km; diagnostic ice scheme
2000/08/25		high pressure system, shallow convection		
2000/09/04		moderate convection in the cold sector of a meso-cyclone		
2001/04/13	CNN II	advection of cold air from North sea	Cabauw	without convection scheme: Δx=7.0, 2.8, 1.1 km, with convection scheme: Δx=7.0, 2.8 km; prognostic ice scheme
2001/08/02	BBC	advection of extreme moist air from south, warm front		
2001/09/23		high pressure system, penetrative convection		

Table 6: Deviation of mean quantities (averaged over model domain and 24h) simulated at different resolutions relative to the 7km run. Mean values of all cases in bold letters, smallest (largest) deviation indicated above (below). Convection scheme is always switched off.

	Integr. water vapour	Liquid water path	Ice water path	Precipi- tation	Total cloud cover	Grid scale cloud cover	Net sur- face ra- diation	Sensible heat flux	Latent heat flux
2.8 km	1,00	1,10	1,02	1,26	0,98	0,96	0,95	0,92	0,97
	1,01	1,33	1,14	1,93	1,04	1,05	1,00	0,99	1,00
	1,02	1,74	1,27	4,26	1,10	1,16	1,05	1,08	1,02
1.1 km	1,00	1,03	0,77	1,36	0,96	0,89	0,94	0,88	0,96
	1,01	1,54	1,09	2,25	1,01	1,02	0,99	0,97	0,99
	1,02	2,38	1,31	5,49	1,07	1,24	1,09	1,07	1,02

ascribed to the lack of a sub-grid condensation scheme. The condensation scheme implemented in the LM follows the concept of saturation adjustment: if the average water content of a pixel exceeds water vapour saturation, the oversaturated portion is converted into cloud water, while a non-saturated pixel can not contain any cloud water.

Nevertheless, due to sub-grid scale humidity fluctuations saturated areas connected with positive cloud water content may occur within a box that is on average unsaturated. Since cloud water content is a positive definite quantity, this type of sampling error will result in a systematic underestimation of cloud water content at coarse scales. Figure 38 clearly demonstrates that LWP systematically increases when using smaller grid spacing, but if the saturation adjustment is applied on the 7 km scale for all runs, the differences nearly vanish. Derived from the three case studies over the “Cabauw” area, an increase of cloud water content due to resolved water vapour fluctuations in the order of 25% at the 2.8 km scale and of 80% at the 1.1 km can be expected. More cloud water will directly result in more rainfall, but precipitation may be enhanced also by a second type of nonlinear sampling error. Figure 39 shows that the increase in rain rate caused by a positive anomaly in LWP is not fully compensated by the decreased rain rate due to negative LWP anomaly with the same amplitude. The more LWP

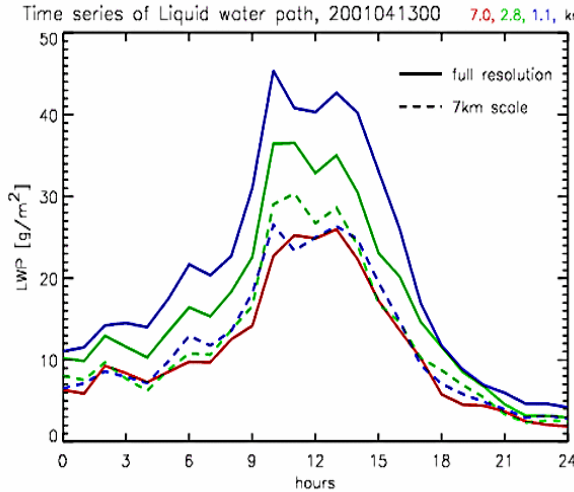


Figure 38: Time series of area averaged LWP at different resolutions (solid lines. Dashed lines show LWP obtained when water content and temperature are averaged on 7 km grid boxes before saturation adjustment is applied.

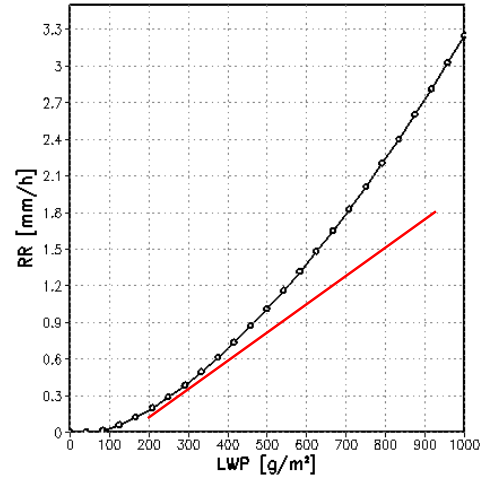


Figure 39: Rain rates simulated by the LM cloud-microphysical module using idealized profiles with constant cloud geometry and varying LWP. The red tangent serves as a guide to the eye to illustrate the nonlinearity.

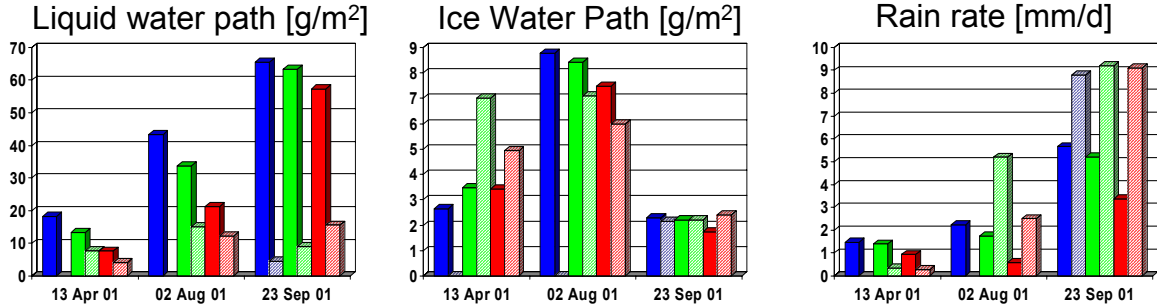


Figure 40: Daily mean values averaged over the model domain for all “Cabauw” cases. Solid bars show results without parameterized convection, dashed including the Tiedtke mass-flux convection scheme (7 km runs (red), 2.8 km (green) and 1.1 km (blue)).

fluctuations are resolved, the higher the rain rate.

It is expected that simulations at 1 km horizontal scale can resolve at least deep convection and that consequently a parameterization of convection becomes superfluous or less important. Therefore it is of great interest to compare simulations with and without parameterised convection. As far as mean quantities are considered, IWV, cloud cover and net surface radiation show no sensitivity, small differences occur in sensible and latent heat flux and significant discrepancies can be observed with respect to LWP, IWP and precipitation, as depicted by Figure 40. The Tiedtke mass flux convection scheme implemented into LM assumes stationarity neglecting all storage terms. Supersaturation is directly converted into rain without producing cloud water. Consequently LWP values of simulations with parameterised convection are dramatically reduced. This relation is not valid in terms of IWP because there is little interference between cloud ice production and convective rain formation as they are usually bound to different altitudes. The results concerning precipitation give no clear picture. Nevertheless, relying more on the stronger precipitating cases, one might expect, that explicitly resolved convection produces less rain but the differences become smaller as the resolution is increased. The remaining gap may be traced back to the lack of sub-grid scale condensation at scales smaller than 1 km.

The most important effect of condensation modifying the atmospheric development on longer time ranges is the stabilization due to vertical transport. This transport seems to differ between resolved and parameterised convection as Figure 41 indicates. Humidity deviations in the order of 10 % appear and differences of potential temperature with the magnitude of 1 K can be observed. It is worthwhile to note, that simulations at different resolutions with resolved convection are in much closer agreement than compared to the simulation with parameterised convection. A detailed analysis of these findings and explanation of underlying mechanism is still missing.

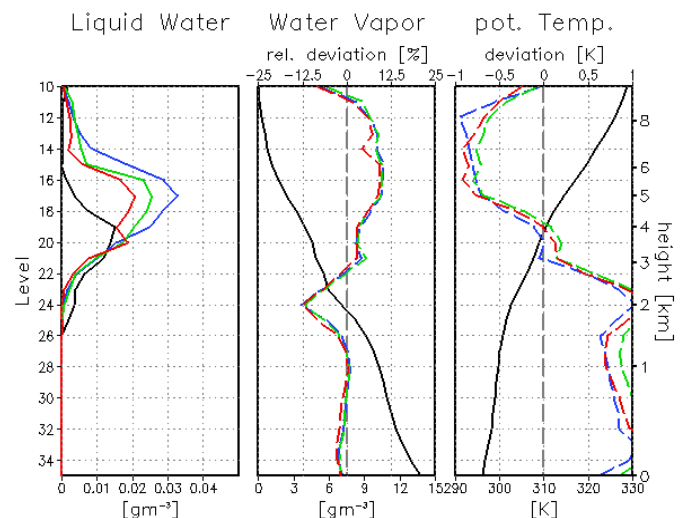


Figure 41: Domain averaged profiles at 12 UTC, September 23, 2001. A 7 km run with convection scheme serves as reference (black); runs without convection scheme: 7 km (red), 2.8 km (green), 1.1 km (blue); deviations are dashed.

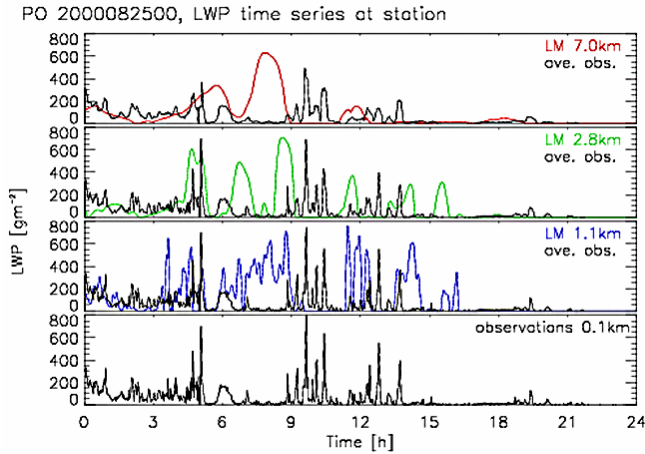


Figure 42: Time series of LWP at station Potsdam. Microwave radiometer measurements (black lines) are filtered with the advective timescale to be representative for each model resolution.

size of cells remains nearly constant in number of grid points but not in physical units. A reason might be that the turbulence scheme is based on the boundary-layer approximation, which assumes no horizontal exchange. This approximation is well justified, as long the horizontal grid spacing is large compared to the boundary-layer height. The lack of horizontal exchange allows the development of locally confined convective updrafts at the pixel scale. The only type of horizontal diffusion implemented in to the LM is a computational mixing to numerically stabilize the leapfrog integration scheme. A sensitivity study varying the strength of computational mixing proved the dependence between cell size distribution and horizontal diffusion. A 3D turbulence scheme is currently being implemented in the LM. Size distributions of convective cells inferred from CLIWA-NET data, in particular from AVHRR LWP retrievals, might help to evaluate and calibrate such a scheme.

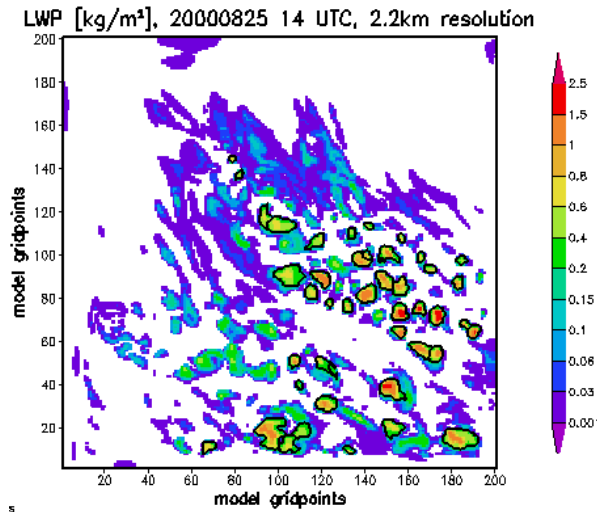


Figure 43: LWP field at one time step, detected cells are encircled by black lines.

The time series of LWP in Figure 42 give reason to suppose that high resolution simulations improve the representation of small scale variations in time and consequently in space, too. The statistical behaviour of clouds, especially the intermittency, is better represented at high resolutions. This encouraging result should be substantiated by more quantitative methods of time series analysis.

Concerning cloud structures, it was realized that the size of resolved convective cells seemed to shrink systematically as the grid spacing was reduced. The development of an objective cell detection algorithm, which uses certain LWP thresholds to identify pixels in the surrounding of local LWP maxima as part of a convective cell (see Figure 43), enabled us to quantify this effect. Normalized cell size distributions plotted in Figure 44 clearly indicate that the

size distributions of convective cells inferred from CLIWA-NET data, in particular from AVHRR LWP retrievals, might help to evaluate and calibrate such a scheme.

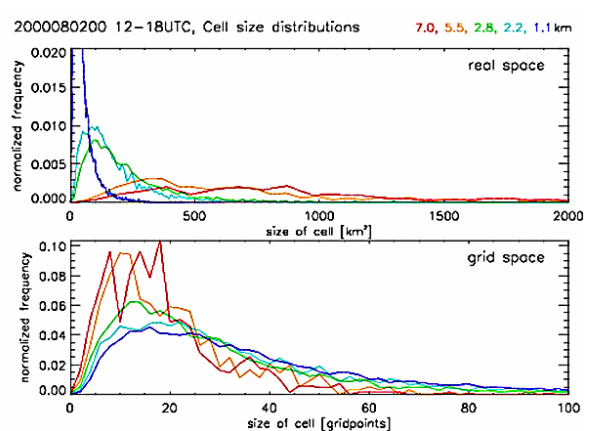


Figure 44: Normalized cell size distribution in physical units (top) and in number of grid points (bottom).

Findings and conclusions. Undergoing a horizontal refinement the LM is consistent in terms of mean IWV, mean cloud cover and averaged surface fluxes. The systematic trends in LWP, IWP and rain rate, which occur in simulations without convection scheme, are mainly caused by neglecting sub-grid scale variability of water vapour and cloud water. If the LM will become operational at 2.8 km resolution without or only partial parameterised convection, as it is planned by German weather service, the implementation of sub grid scale condensation is highly recommended. Such schemes are well documented in literature and can be implemented as an extension of the current microphysical package. The observed shrinking of resolved convective cells can be counteracted by introducing physically motivated horizontal diffusion. A 3D turbulence scheme is currently implemented into LM and CLIWA-NET measurements may show useful data for evaluation and calibration. We found significant differences concerning the vertical stratification and consequently vertical transport between resolved and parameterised convection. As these differences may affect the quality of forecasts in all variables, it is important to investigate these effects in future. In general, the six case studies performed in WP4200 provide a huge data set, which we could not entirely exploit in the time frame of the CLIWA-NET project. Besides the vertical convective transport, the variability at small scales and the benefits of high resolution simulation in contrast to current resolutions should be topics of further research. CLIWA-NET measurements should be used more intensively to judge which model formulation is in best agreement with reality.

3.3.3 Parameterization development and assessment

Within the parameterization work package we have tried to identify a number of key weaknesses in the present representation of cloud processes in climate and NWP models. We have evaluated these processes in the CLIWA-NET models, using a suite of observations and where possible indicated avenues for improvement in representing these processes. To make a meaningful evaluation of model clouds sets great demands on cloud observing systems. Here we will use a combination of land based point measurements (e.g. cloud penetrating radars and ceilometers) and satellite retrievals (e.g. AVHRR cloud amounts) to evaluate the model cloud fields.

We will concentrate on the sensitivity of simulated cloud fields and associated cloud process (e.g. diurnal cycle of clouds, cloud-radiation interaction) to increasing model vertical resolution. It is generally expected that a more accurate representation of cloud processes will occur as model vertical resolution increases. As motivation, Figure 45a shows the vertical structure of the cloud field, observed by the KNMI radar over Cabauw, through the day of September 18, 2001. The raw KNMI radar reflectivities have been temporally averaged to produce a cloud fraction representative of ~20 km spatial resolution. During the day a frontal system passed over Cabauw, this is clearly seen in the gradual transition from high clouds to low clouds as the day progressed. Early in the morning a fog layer was present gradually turning into a low-level clouds layer. This layer lifted and thinned through the morning, attaining a cloud base of ~750 m by 12 noon. Late in the evening a second period of upper level clouds (above 5 km) was observed.

Figure 45b-e shows the simulated cloud field for this day by some of the CLIWA-NET models. All models simulate the 3 observed cloud structures with varying degrees of success. In the plot, RCA24 and the RACMO models used identical vertical layering (24 levels) while RCA40 and ECMWF both used an identical 40 layer structure. The RCA model was the exact same model in both simulations except for the increased vertical resolution. The improvement in the RCA simulation of the frontal cloud system, as vertical resolution is increased, is clearly visible, especially in the mid-troposphere. In fact, the model cloud fields look more common grouped by vertical resolution, ECMWF with RCA40 and RACMO with RCA24, than if they were grouped by common model physics (in this case the two RCA models). We would like to ascertain if this improvement holds for more days in the BBC campaign and over wider regions than this single point.

Cloud sensitivity to vertical resolution using cloud penetrating radars. To address this issue we begin by comparing the mean diurnal cycle of vertical cloud structure observed over Cabauw for the period 8-17th of August 2001. Figure 46 shows the KNMI radar derived cloud fraction, aver-

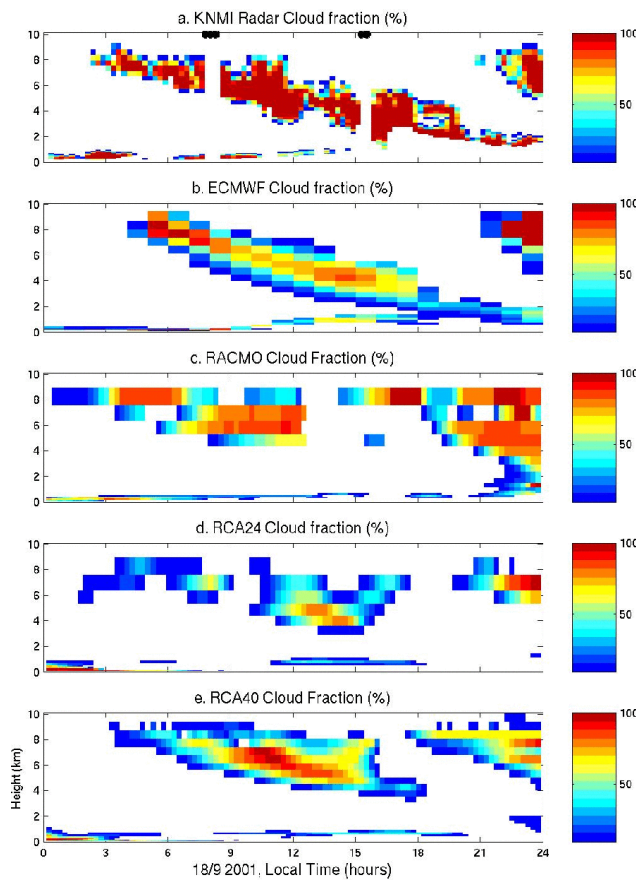


Figure 45: Diurnal cycle of cloud fraction over Cabauw during September 18, 2001. Panel a) Cloud fraction derived for ~20 km spatial resolution from KNMI Cloud Radar b-e) CLIWA-NET model derived cloud fractions for grid box collocated with Cabauw.

period. We believe this is partly related to a more active sub-grid scale vertical turbulence scheme in RACMO compared to the RCA model. The RCA60 model shows a slightly better diurnal cycle of low-level clouds when compared to RCA24 and the radar data. The low-level cloud amounts are reduced, towards observations and the predominant cloud base appears to lift to slightly higher levels as the day progresses. There is also some sense that the cloud amounts around 2-4 km are increased and improved in RCA60 over RCA24 and the relative minimum seen in the radar clouds at ~5 km is better represented in the RCA60 model.

Use of satellite observations. We would like to determine if the improvements in the cloud field seen with increasing vertical resolution in the previous section, is evident over wider, more varied geographic regions. To ascertain this we must turn to satellite derived clouds to get a better spatial coverage of the observed cloud fields. In this section we compare monthly mean RCA simulated clouds to monthly mean clouds derived from the AVHRR sensor on the NOAA satellites, for the BBC period (see section 3.2.2).

Figure 47 shows the mean total cloud cover from the RCA24 model and as seen by the AVHRR satellite. For further comparison we also include the ISCCP satellite clouds for the same period (Rossow and Garder 1993). While the ISCCP and AVHRR clouds are both derived from satellite observed radiances, it is important to note that very different retrieval techniques are used in the two datasets, which are also at different spatial resolutions. For more details see Karlsson 2001 (for AVHRR) and Rossow

aged for this period, and the equivalent cloud fraction from the RCA24, RACMO24 and RCA60 simulations (The RCA60 model has a vertical resolution in the mid to upper troposphere of between 150-400 metres, it also has 14 layers below 900hpa compared to 8 layers in the RCA24 model). Cloud base in the radar ure has been determined by using the cloud base detected by a collocated ceilometer. For this period, the predominant cloud base is at ~400 metres in the morning rising to around 750 metres by early afternoon. The radar derived cloud fraction is around 20% between 1 to 3 km, reducing to very small values around 5km. It should be stressed that it is extremely difficult to derive a highly accurate cloud fraction from the cloud radar data and these values should be considered indicative values only at present.

Nevertheless, some systematic errors can be seen in the model data when compared to the radar clouds. In particular, the RCA24 model clearly overestimates the amount of low-level clouds and the cloud base remains low throughout the day. There is also a tendency for the mid-tropospheric cloud minimum, seen in the radar data, to be too low in RCA24. RACMO24 seems to do a better job in representing the amount and diurnal development of the low level clouds for this

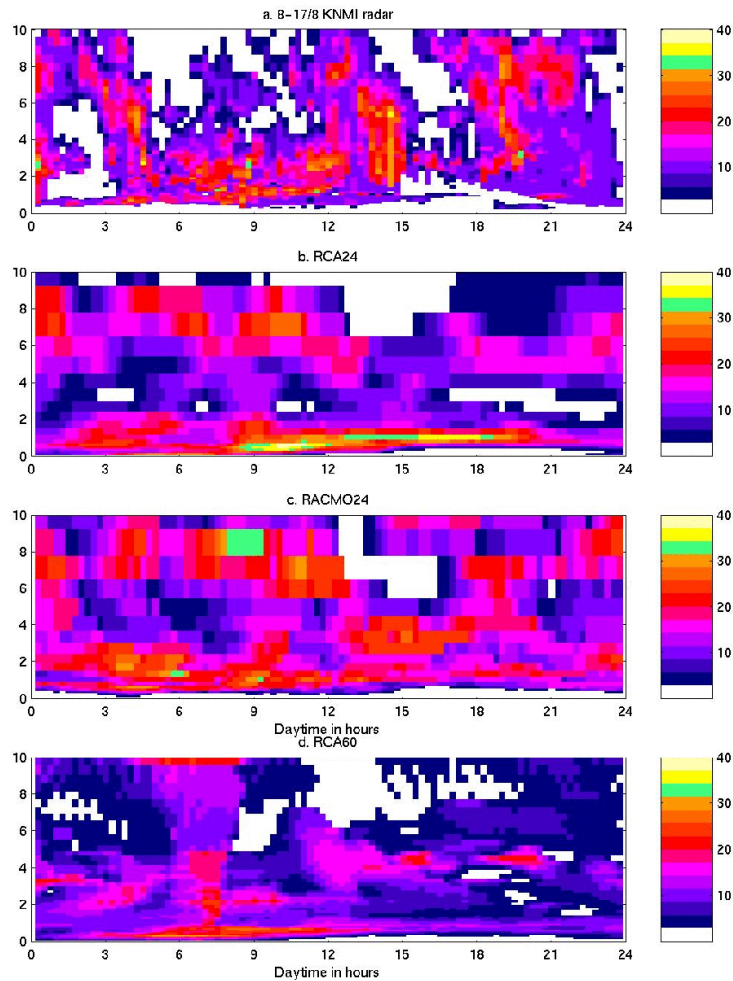


Figure 46: Mean diurnal cycle of cloud fraction at Cabauw, for the period 8-17th August 2001. Panel a) Cloud fraction derived for ~20 km spatial resolution from KNMI cloud radar. b-d) CLIWA-NET model derived cloud fractions for grid box and period collocated with radar data.

actively working to tune the Xu-Randall cloud scheme to be more appropriate to mid-latitude regions also. An important feature we have noticed in simulated clouds from the Xu-Randall scheme is the tendency for binary clouds, either zero or 100%, rather than frequent fractional cloud cover as seen in the Slingo scheme. This binary cloud structure is strongly supported by observations).

The RCA24 cloud amounts, with the present operational (Slingo) cloud scheme are fairly close to the AVHRR values. The RCA cloud cover is derived from assuming the vertical clouds are overlapped in a maximum-random manner. In particular, the August to September increase in cloud amounts is well represented as is the general North-East to South-West decrease in the cloud amounts. One area of clear disagreement is over Great Britain, with the RCA model simulating too large cloud amounts. Further analysis against the AVHRR data, has indicated this error is associated with an overestimate of low level clouds during the night/early morning period over this region (*results not shown here*). This error is analogous to the earlier mentioned low level cloud overestimate against the radar data at Cabauw. We have further verified this problem using ceilometer data over the BBC mesoscale network, to analyse model cloud bases (*results not shown here*). We note here that the RCA24 model cloud cover is much closer to the AVHRR values than are the ISCCP satellite derived clouds.

and Garder 1993 (for details of the ISCCP technique). Even taking into account these differences, it is rather disappointing to see that the mean cloud covers in the two satellite data sets are so different. Monthly mean differences of between 10-25% can be seen, with ISCCP systematically having more clouds. The AVHRR clouds have been evaluated against collocated surface observations in this region and have a slight positive bias, relative to the surface based (synop) observations, of ~5-10%. Given the positive bias in the ISCCP clouds relative to the AVHRR clouds, we must conclude the ISCCP cloud amounts are grossly overestimated in this region, during the BBC period.

Figure 47 (2nd and 3rd rows) shows the mean cloud cover simulated by the RCA24 model using either the Slingo (relative humidity based) cloud scheme (Slingo 1987) or the semi-prognostic scheme due to Xu & Randall (1996), the latter using both prognostic cloud water and diagnostic relative humidity in the calculation of the cloud fraction. (The Xu-Randall cloud scheme was originally derived using Cloud resolving Model data for the tropical ocean regions. Using the CLIWA-NET observations we are

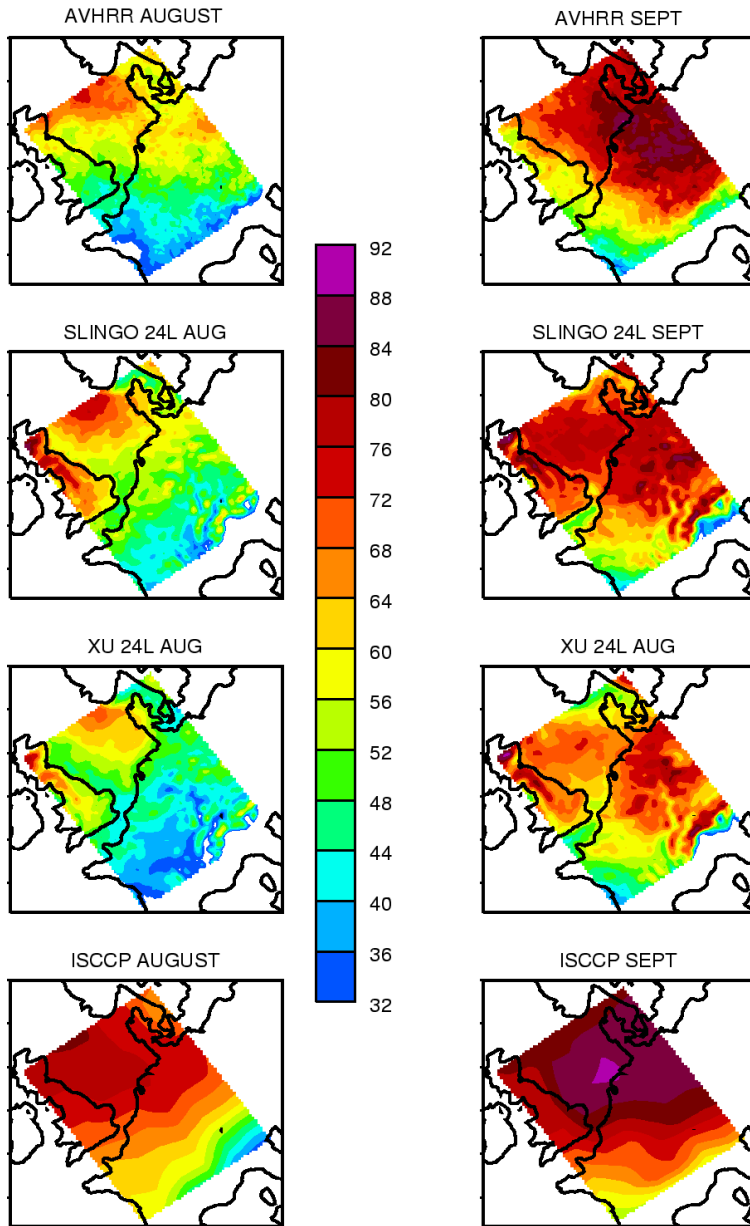


Figure 47: Monthly mean total cloud cover BBC-campaign (Aug-Sep 2001)

Figure 48 shows the August and September monthly mean total cloud cover error (RCA24-AVHRR) also shown is the bias in the cloud cover above ~ 500 hPa (labelled high clouds) and cloud cover below ~ 500 hPa (labelled low clouds). High clouds from RCA are derived using maximum-random overlap of clouds downward from the model top until 500 hPa is reached. Low-level clouds from the model are derived in the following manner. Starting from the level closest to 500hpa we perform a maximum-random overlap of all cloud layers down to the lowest model level. We then assume this low cloud cover is maximally overlapped by the earlier derived high cloud (This procedure we believe mimics most closely the satellite viewed cloud covers). The comparison suggests the model slightly underestimates high cloud amounts, but has a larger magnitude overestimate in low cloud cover (Some portion of the positive low level cloud bias seen in the model is due to the lack of shading by the under predicted high clouds). With respect to the total cloud cover these errors compensate each other and indicate that it is important that the vertical structure of clouds is evaluated as well as just the total cloud cover. This is particularly true considering the opposing radiative effects low and high clouds have on the climate system.

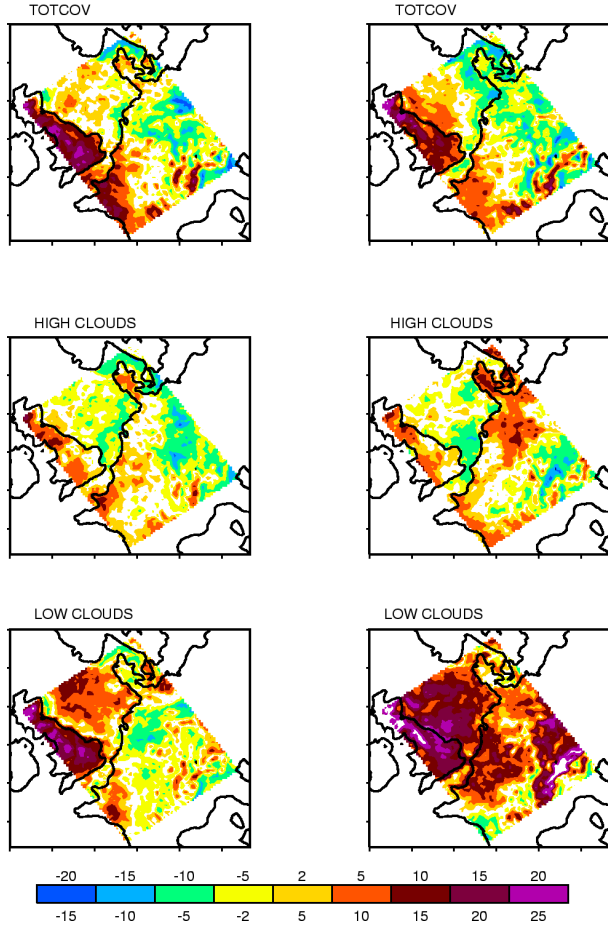


Figure 48: Bias in monthly mean cloud amount (RCA24-AVHRR). Left column: Aug 2001; Right column: Sep 2001

järvi 1990 and Sass et al. 1994) is extremely fast but also heavily parameterised.

Here we illustrate a simple modification to the RCA radiation code that tries to represent the effect of cloud inhomogeneities on the transmission and reflection of solar radiation. In the RCA radiation code, the cloud fraction and scaled in-cloud water are treated following plane parallel assumptions (meaning the cloud is assumed to be a single homogenous layer of cloud fraction and water). It is well known from observations, that clouds are not homogenous, rather normally broken up into a number of separate entities, at the scale of a model grid box (~ 20 km), due to mesoscale variability in the vertical circulation. Furthermore, water inside clouds is distributed in an extremely non-homogeneous manner (Cahalan et al., 1994). Detailed radiative calculations show that a heterogeneous distribution of water,

The positive bias in RCA24 low-level clouds supports the results from the radar comparison. Further analysis of the diurnal cycle of the model and satellite clouds indicates the low-level cloud error is weighted towards an overestimate in the low level cloud amounts in the morning period (results not shown here). Parallel analysis suggests this tendency for excessive low level clouds in the night/early morning is related to an under active sub-grid scale turbulence scheme in the RCA model.

Cloud-radiation interaction and representation of inhomogeneous cloud fields. The primary role clouds play in the climate system is through their interaction and modification of the incoming solar radiation flux and outgoing terrestrial radiation. Accurately representing cloud-radiation interaction is of fundamental importance in models that are to be used in climate prediction. This is by no means a simple task, accurately modelling cloud-radiation interaction is computationally very demanding, simplifications to the basic physics are needed if the parameterization is to be tenable from a computational perspective. The RCA model is perhaps extreme in the level of simplification applied to the calculation of radiation. The present radiation code (detailed in Savijärvi 1990 and Sass et al. 1994)

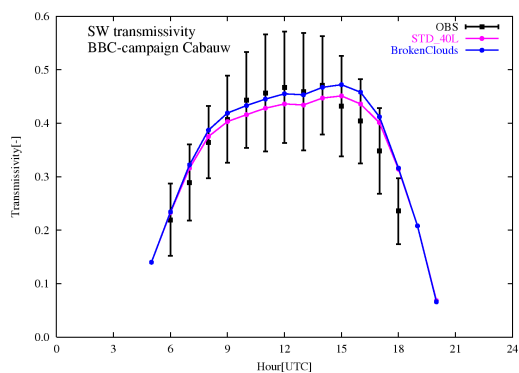


Figure 49: Total atmospheric transmissivity as observed over Cabauw during the BBC-campaign and as simulated by standard RCA40 and by RCA40 plus inclusion of parameterization for broken cloud effect on solar radiation.

within a given cloud, always leads to lower cloud albedos than an equivalent cloud with a homogeneous distribution of water (Cahalan et al., 1994).

In the RCA radiation code, we have introduced a simple parameterization that mimics the findings of more detailed radiation codes, with respect to the effect of non-homogeneity of water and cloud brokenness, on cloud reflectivity and transmissivity. The modification increases the transmission of solar radiation (reducing the amount reflected) as a function of the cloud fraction and solar zenith angle. It is developed from a number of observational studies (Coakley 1991, Hignett and Taylor, 1996) and Monte Carlo radiation studies (Jonas, 1994). Figure 6.49 shows the effect of introducing this modification into the radiation code of the RCA40 model. The total model atmosphere solar transmissivity, for the standard RCA40 model and RCA40 with the broken cloud parameterization, is plotted. The modification appears to improve the total model transmission of solar radiation and leads to an improved surface short wave radiation budget.

4 Conclusions

The CLIWA-NET project was very productive. The major achievements and conclusions drawn from the project are summarised below:

Observational aspects

The prototype of European Cloud Observation network (ECON) was successfully implemented during three enhanced observational (CNNI: August/September 2000; CNNII: April/May 2001 and BBC: August/September 2001). To successfully implement these existing observation systems, microwave radiometers and auxiliary instruments were distributed in a continental network over the BALTEX modelling region and a regional scale network in The Netherlands.

- Harmonized retrieval algorithms to derive the liquid water path (LWP) and the integrated water vapour (IWV) were developed for all stations and campaigns. Quality checked time series of LWP, IWV, cloud base height, infrared temperature of the atmosphere and different rain flags for all stations during all campaigns were produced.
- The microwave inter-comparison campaign (MICAM) performed in the 2nd project year verified the good quality of liquid water path measurements during the previous CNN campaigns. However, the uncertainty of current gas absorption models and the inherent retrieval ambiguities still limit the accuracy of standard dual frequency systems to about 30 g m^{-2} . These models need to be further constrained.
- The combination of different advanced remote sensing instruments at the Cabauw site during the BBC campaign allowed the application of a newly developed synergetic algorithm to derive simultaneously temperature, humidity, and liquid water profiles and their respective uncertainties.
- Based on lidar ceilometer measurements a climatology of super-cooled layers over the Netherlands was derived. The combination with cloud radar and microwave radiometer measurements allowed the identification of some new properties: Often ice crystals are falling out of thin layers consisting of super-cooled water. Most of these layers contain very little water ($<25 \text{ g m}^{-2}$). However, measurements within the regional network during the BBC campaign showed that these layers can extend over more than 100 km and last several hours long.
- For a future long-term implementation of ECON a low-cost microwave radiometer which also takes into account requirements from the modelling community has been designed. Due to external funding the first systems were already built.

Satellite and integration aspects

Satellite measurements were analysed to provide spatial information about cloud parameters. Main focus was on LWP and the transfer the temporal information from the ground-based stations to larger areas. For this purpose NOAA-AVHRR and NOAA-AMSU data was combined.

- The quality of satellite data was found to be insufficient for the CNN I campaign while significant progress was made for the later campaigns as higher quality satellite data from NOAA-16 were available.
- The satellite data acquisition system obtained data from nearly all possible satellite overpasses. Cloud classification was performed for more than 1000 scenes. The cloud classification scheme showed in general a very high quality during all observational campaigns. Problems in the estimation of cloud coverage mainly occur during twilight where the cloud amount from AVHRR is less reliable and mostly tends to be slightly underestimated. In addition there is an inherent difference in the cloud scheme and in the AVHRR sensitivity in general between land and sea surfaces, resulting in a slight overestimation but higher reliability over sea and a slight underestimation and lower reliability over land. This inherent discrepancy between sea and land in cloud amount combined with an observed ambiguity between separation of fractional water clouds (small cumuli and cloud edges) and thin cirrus, made post-processing necessary before the data could be used for studies of diurnal cloud cover and model comparison in general.
- The improvement of satellite estimates of LWP from NOAA-AVHRR was possible due to the newly developed analysis methods that utilize the additional information from the near infrared channel of NOAA-16. The new methods include analysis of the cloud thermodynamic phase (ice or water) and estimates of the size of the cloud particles.
- The additional use of AMSU LWP estimates was not possible due to the limited quality and coarse resolution of AMSU and retrieval difficulties.

Modelling aspects

Methodologies focusing on the **evaluation of model predicted cloud parameters** with CLIWA-NET inferred observations have been developed and examined in various applications, e.g. a statistical evaluation of predicted liquid water path (LWP), the representation of vertically distributed liquid water content (LWC), and a comparison of a model predicted LWP-fields with satellite retrieved spatial distributions. The main findings are:

- Models over-predict frequency and duration of precipitation. Models over-predict the amount of liquid water clouds. On average, models predict LWP in the right order of magnitude, but the spread among the models is considerable.
- On average, models provide a reasonable representation of the LWC vertical distribution, but variations among the models in amount and height of the maximum value are huge. For individual events, model predictions of the LWC vertical structure have no prediction value.
- Satellite retrieved frequency distributions of LWP fall off much steeper than models predict.
- Model relations between solar transmissivity and LWP are compared with the observed relation. Some models represent inadequate relations with transmissivity falling off to steeply with increasing LWP. Owing to a compensating error, i.e a significant under-prediction of LWP, one model still provides a reasonable radiative forcing at the surface.

Numerical experiments have been conducted with a meso-scale model, e.g. the Lokal-Modell, to examine the sensitivity of cloud and precipitation parameters on the **horizontal resolution** in the range of 10 to 1 km. The main findings are:

- Domain averaged LWP, and, in particular, precipitation are found strongly enhanced by increasing horizontal resolution.
- Domain averaged IWV, cloud cover, and surface energy fluxes are hardly affected by the resolution refinement for short-term integrations in forecast mode.
- Size distributions of model resolved convective cells depend strongly on the employed horizontal resolution. The dominant size scales with the grid spacing rather than a model-independent physical scale. At the smallest grid-spacing a resolution independent distribution starts to develop. There are indications that the application of fully parameterized turbulence without horizontal exchange between grid boxes is no longer adequate in this range of grid spacing.

In a number of **parametric issues** have been addressed concerning the diurnal cycle of clouds, the effect of model vertical resolution, the capability of cloud schemes to reproduce spatial distributions of cloud amount, the sensitivity of solar transmissivity to parametric assumptions on cloud in homogeneities, and the role of cloud overlap assumptions applied in vertically stacked clouds.

The main findings are:

- Total cloud amounts derived from two satellite systems, i.e. ISCCP and AVHRR, are found to be significantly different with the ISCCP cloud amount being much larger than the AVHRR cloud amount. The AVHRR amounts, in turn, are found to be larger than ground-based (synop) estimates. Model predicted cloud amounts from different cloud schemes appear to be closer to the AVHRR amount or even lower.
- Refinement of the vertical model mesh results in a better representation of cloud processes. In general, it also results in a better representation of macroscopic cloud parameters like cloud amount and the vertical distribution of clouds. Typical errors like a tendency to simulate cloud base height at too low altitudes are not remedied completely.
- One of the CLIWA-NET models, e.g. the RCA-model, is found to considerably overestimate the amount of low-level clouds and somewhat underestimate high-level cloud amount. Due to compensating errors the total cloud amount is reproduced fairly well, but in a radiative sense both errors result in a net cooling tendency of the climate system in the model.

The CLIWA-NET User's Requirement Document has been produced. The content is based on the discussion between members of the CLIWA-NET management team and the individual members of the User's Advisory Group. An evaluation by the members of the User Advisory group was performed close to the end of the project and the progress within CLIWA-NET was appreciated. An important conclusion is that the results of the CLIWA-NET project are relevant for a wide diversity of applications.

5 References

- Cahalan R., W.Ridgway, W.J.Wiscombe, T.Bell and J.B.Snider, 1994: The Albedo of Fractal Stratocumulus Clouds. *Journal of Atmos. Sci.*, 51, 2434-2455.
- Coakley J.A, 1991: Reflectivities of uniform and broken layered clouds. *Tellus*, 43B, 420-433.
- Christensen J.H., O.B. Christensen, P. Lopez, E. van Meijgaard & M. Botzet, 1996: The HIRHAM4 Regional Atmospheric Climate Model. DMI Scientific Report 96-4, 51 pp. [Available from DMI, Lyngbyvej 100, DK-2100 Copenhagen.]
- Crewell, S, M. Drusch, E. van Meijgaard and A. van Lammeren, 2002: Cloud observations and modeling within the European BALTEX Cloud Liquid Water Network, *Boreal Env. Res.* 7: 235-245.
- Crewell, S. and U. Löhner, 2003: Accuracy of cloud liquid water path from ground-based microwave radiometry. Part II. Sensor accuracy and synergy, *Radio Science*, Vol. 38, No. 3, 7-1 - 7-10.
- Dybbroe, A., Thoss, A., and Karlsson, K.-G. 2001. Mean Cloudiness Derived from Satellite Data over the Baltic Sea Drainage Basin During CLIWA-NET Campaigns. *3rd Study conference on Baltex. Conference Proceedings, International BALTEX Secretariat publication No. 20, Geesthacht*, 51-52.
- Dybbroe, A., Brunel, P., Marsouin, A., and Thoss, A. 2003. Accurate real-time navigation of AVHRR data at high latitudes. In Proc. 12th Int. TOVS Study Conference, Lorne, Australia, March 2002.
- Doms, G. and U. Schättler, 1999: The Nonhydrostatic Limited-Area Model LM (Lokal-Modell) of DWD - Part I: Scientific Documentation, DWD, 155 pp. [Available from Deutscher Wetterdienst, Postfach 100645, D-63004 Offenbach, Germany].
- Donovan, D. P. und A. C. A. P. van Lammeren, 2001: Cloud effective particle size and water content profile retrievals using combined lidar and radar observations. 1. Theory and examples, *J. Geophys. Res.*, 106, 27425-27448.
- Feijt, A.J., D. Jolivet, and E. van Meijgaard, 2002: Retrieval of the spatial distribution of liquid water path from combined ground-based and satellite observations for atmospheric model evaluation. *Boreal Env. Res.*, 7, 265-271.

- Feijt, A. and A. van Lammeren, 1996: Ground-based and satellite observations of cloud fields in the Netherlands. *Mon. Wea. Rev.* 124: 1914-1923.
- Frisch, A. S., G. Feingold, C. W. Fairall, T. Uttal und J. B. Snider, 1998: On cloud radar and microwave measurements of stratus cloud liquid water profiles, *J. Geophys. Res.*, 103, 23195-23197.
- Grody, N. C., 1993: Remote sensing of the atmosphere from satellites using microwave radiometry, in *Atmospheric Remote Sensing by Microwave Radiometry*, edited by M. A. Janssen, pp. 259-334, John Wiley, New York,.
- Fuhrhop et al., 1998: MWMOD User manual, Version1.12., Institute of Marine Research, University Kiel, Germany, 82p.
- Hignett P and J.P. Taylor, 1996: The radiative properties of inhomogeneous boundary layer clouds: Observations and modelling. *Q.J.Royal Met. Soc.*, 122B, 1341-1364.
- Hogan, R.J., A. J. Illingworth, J. P. V. Poiares Baptista and E. J. O'Connor, 2003: Characteristics of mixed-phase clouds: Part II: A climatology from ground-based lidar, *Q. J. Meteorol. Soc.* 129, accepted.
- Jonas P.R., 1994: On the reflectance of cellular cloud layers. *Q.J.Royal Met. Soc.*, 120, 221-229.
- Jones, C.G., 2001: A brief description of RCA2 (Rossby Centre Atmosphere Model Version 2) In: SWECLIM Newsletter 11, 9-15. Available from the Rossby Centre SMHI, Sweden.
- Jung, T., E. Ruprecht and F. Wagner, 1998: Determination of Cloud Liquid Water Path Over the Oceans From SSM/I Data Using Neural Networks. *J. Appl. Meteorol.*, 37, 832-844.
- Kain, J.S. and M. Fritsch, 1991: A 1D entraining/detraining plume model and its application in convective parameterization. *J.Atm. Sci.*, 47, 2784-2802.
- Karlsson K., 2001: A NOAA-AVHRR cloud climatology over Scandinavia covering the period 1991-2000. *SMHI Reports Meteorology & Climatology* No.97 95pp
- Karstens, U., C. Simmer, and E. Ruprecht, 1994: Remote sensing of Cloud Liquid Water , Meteorology and Atmosph. Physics, 54, 157-171.
- Koistinen, J. and D. B. Michelson, 2002: BALTEX radar products and their accuracies, *Boreal Env. Res.*, 7, 265-253-263.
- Liebe, H. J., T. Manabe and G. A. Hufford, 1989: Millimeter-wave attenuation and delay rates due to fog/cloud conditions, *IEEE Trans. Antennas Propag.*, 37, 1617-1623, 1989.
- Liebe, H. J., G. A. Hufford, und M. G. Cotton, 1993: Propagation modelling of moist air and suspended water/ice particles at frequencies below 1000 GHz, *Proc. AGARD 52nd Specialists Meeting of the Electromagnetic Wave Propagation Panel*, Palma de Mallorca, Spain, AGARD, 3-1-3-10.
- Löhnert, U. and S. Crewell, 2003: Accuracy of cloud liquid water path from ground-based microwave radiometry. Part I. Dependency on Cloud model statistics, Radio Science, Vol. 38, No. 3, 6-1 - 6-11.
- Löhnert, U., Crewell S, Simmer C, Macke A, 2001: Profiling cloud liquid water by combining active and passive microwave measurements with cloud model statistics, *J. Atmos. Oceanic Technol.*, 18 (8): 1354-1366.
- McGrath, A. und T. Hewison, 2001: Measuring the accuracy of MARSS – An airborne microwave radiometer, *J. Atmos. Oceanic Technol.*, 18, 2003-2012.
- Roeckner, E.; and Coauthors 1996: The atmospheric general circulation model ECHAM-4: Model description and simulation of present-day climate. Report 218, pp 90. [Available from Max Planck Institute for Meteorology, Bundesstrasse 55, D-20146, Hamburg, Germany.]
- Rasch, P.J., and J.E. Kristjansson, 1998: A comparison of the CCM3 model climate using diagnosed and predicted condensate parameterizations. *J. Climate* 11: 1587-1614.
- Rodgers, C. D., 2000. *Inverse Methods for Atmospheres: Theory and Practice*, World Sci.; Singapore, 238 pp.
- Rossow W.B. and L.C.Garder, 1993: Cloud detection using satellite measurements of infrared and visible radiances for ISCCP. *J. Climate* 6 2341-2369
- Sass B.H, L.Rontu and P.Räisänen, 1994: HIRLAM-2 radiation scheme: Documentation and test. *HIRLAM Technical Report 16*, SMHI. 43pp
- Savijärvi H 1990: Fast Radiation parameterisatin schemes for mesoscale and short range forecast models. *J. Appl. Meteor.* 29 437-447
- Slingo J., 1987: The development and verification of a cloud prediction scheme for the ECMWF model. *Q.J.Royal Met. Soc* 113 899-928
- Sundqvist, H., E. Berge & J.E. Kristjansson, 1989: Condensation and cloud parameterization studies with a Mesoscale numerical weather prediction model. *Mon. Wea. Rev.* 117: 1641-1657.

- Tiedtke, M., 1989: A comprehensive mass flux scheme for cumulus parameterization in large-scale models. *Mon. Wea. Rev.* 117, 1779-1800
- Tiedtke, M., 1993: Representation of clouds in large-scale models. *Mon. Wea. Rev.* 121: 3040-3061.
- Weng et al. ,1999 : http://orbit-net.nesdis.noaa.gov/arad2/MSPPS/html/day2/algorithm_day2.html
- Westwater, E. R., 1993: Ground-based microwave remote sensing of meteorological variables, in *Atmospheric Remote Sensing by Microwave Radiometry*, edited by M. A. Janssen, pp. 145-213, John Wiley, New York.
- Xu K.M. and D.A.Randall, 1996: A Semi-empirical Cloudiness Parameterization for use in Climate Models. *J. Atmos. Sci.* 53 3084-3102

6. Literature produced in CLIWA-NET

Peer Reviewed Articles:

- Crewell, S. and CLIWA-NET and 4DClouds team, 2003: The BALTEX BRIDGE Campaign (BBC) -An integrated approach for a better understanding of clouds, *Bulletin of the American Meteorological Society* submitted.
- Crewell, S. and U. Löhnert, 2003: Accuracy of cloud liquid water path from ground-based microwave radiometry. Part II. Sensor accuracy and synergy, *Radio Science*, Vol. 38, No. 3, 7-1 - 7-10.
- Crewell, S., M. Drusch, E. Van Meijgaard und A. Van Lammeren, 2002: Cloud Observations and Modelling within the European BALTEX Cloud Liquid Water Network, *Boreal Environment Research*, Vol 7(3), 235-245.
- Crewell, S., U. Löhnert, A. van Lammeren and M. Quante, 2000: Cloud remote sensing by combining synergistic sensor information, *Phys. Chem. Earth (B)*, 25, 1042-1048.
- Doescher, R., U. Willen, C. Jones, A. Rutgersson, H.E. M. Meier, U. Hansson, and L. P. Graham, 2002: The development of the regional coupled ocean-atmosphere model RCAO, *Boreal Environment Research*, Vol. 7(3) p. 183-192.
- Feijt, A.J., D. Jolivet, and E. van Meijgaard, 2002: Retrieval of the spatial distribution of liquid water path from combined ground-based and satellite observations for atmospheric model evaluation, *Boreal Environment Research*, Vol. 7(4), 265-271.
- Löhnert, U. and S. Crewell, 2003: Accuracy of cloud liquid water path from ground-based microwave radiometry. Part I. Dependency on Cloud model statistics, *Radio Science*, Vol. 38, No. 3, 6-1 - 6-11.
- Jolivet, D. and A. Feijt 2003 Cloud particle type determination using a 0.67 and 1.6 μm channel, *J. Geophys. Res.* submitted.
- Löhnert, U., S. Crewell, A. Macke and C. Simmer, 2001: Profiling cloud liquid water by combining active and passive microwave measurements with cloud model statistics, *J. Atmos. Oceanic Technol.*, Vol 18 (8) 1354-1366.

Conference Proceedings

- Crewell, S. and U. Löhnert, 2002: Ground-based remote sensing of cloud liquid water - A case study, *XXVII General Assembly of the International Union of Radio Science*, Maastricht, august 2002, Conference Proceedings, 3 pages.
- Crewell, S., U. Löhnert, and T. Rose, 2002: Synergetic algorithms for temperature and humidity profiling based on ground-based microwave measurements, *Workshop on COST Action 720*, Symposium Proceedings, L'Aquila, 18-21 June 2002, 2 pages.
- Crewell, S., M. Drusch, U. Löhnert, C. Simmer, A. Van Lammeren and CLIWA-NET Project Team, 2001: Cloud Observations from the Ground-Based CLIWA-NET Network I (CNN I) during BRIDGE EOP I, *3rd Study Conference on BALTEX*, Marieham, Finland, 2-6 July 2001, Conference Proceedings, Pages 43-44.

- Dybbroe, A., A. Thoss, A., and K.-G. Karlsson,, 2001: Validation of Nowcasting SAF Polar Platform Products, *EUMETSAT Data Users Conference*, Conference Proceedings, Dublin, Ireland, 2-6 September 2002, Pages 444-451.
- Dybbroe, A., Brunel, P., Marsouin, A., and Thoss, A., 2002: Accurate real-time navigation of AVHRR data at high latitudes, *12th Int. TOVS Study Conference*, Lorne, Australia, March 2002, Conference Proceedings.
- Dybbroe, A., A. Thoss and K.-G. Karlsson, 2001: Mean Cloudiness Derived from Satellite Data over the Baltic Sea Drainage Basin During CLIWA-NET Campaigns, *3rd Study Conference on BALTEX*, Marieham, Finland, 2-6 July 2001, Conference Proceedings, Pages 51-52.
- Hauschildt, H. and A. Macke, 2002: A neural network based algorithm for the retrieval of LWP from AMSU measurements, *EUMETSAT Data Users Conference*, Dublin, Ireland, 2-6 September 2002, 8 pages.
- Hauschildt, H., T. Martin and A. Macke, 2001: Cloud Liquid Water path from combined AMSU and AVHRR measurements, *3rd Study Conference on BALTEX*, Marieham, Finland, 2-6 July 2001, Conference Proceedings, Pages 81-82.
- Löhnert U. and S. Crewell, Profiling cloud liquid by combination of multi-channel ground-based passive microwave and cloud radar measurements, *Workshop on COST Action 720*, Symposium Proceedings, L'Aquila 18-21 June 2002, 2 pages.
- Martin, L. and C. Mätzler, 2001: Using a 30 GHz Radiometer and GPS to measure atmospheric liquid water, *3rd Study Conference on BALTEX*, Marieham, Finland, 2-6 July 2001, Conference Proceedings, Page 157.
- Van Meijgaard, E., A. Mathieu, A. Feijt, and S. Crewell, 2002: The European BALTEX Cloud liquid water network: An overview, *AMS Conference on Cloud Physics*, Session 2.1, Ogden, Utah, June 2002, 4 pages.
- Meywerk, J., O.Sievers, M. Quante, V. Venema and S. Crewell, 2002: Deriving water cloud properties from vertical pointing 95 GHz Doppler radar, *2nd European Conf. on Radar Meteorology*, Conference Proceedings, Delft, The Netherlands, 18-22 November 2002, 6 pages.
- Roebeling, R. A., A.J. Feijt, D. Jolivet and E. van Meijgaard ,2002: Retrieval of spatial distribution of liquid water path from NOAA-AVHRR for atmospheric model evaluation, *EUMETSAT Data Users Conference*, Conference Proceedings, Dublin, Ireland, 2-6 September 2002.

Miscellaneous

- Crewell, S. and the CLIWA-NET team, 2003: The BALTEX Cloud Liquid Water Network: CLIWA-NET, EGS - AGU - EUG Joint Assembly, Nice, France, April 2003, Poster
- Hauschildt, H., A. Macke und T. Martin, 2001: Bestimmung der horizontalen Verteilung des Flüssigwasserpades aus Daten des AMSU und AVHRR, *DACH Meteorologentagung*, 8-21 September 2001, Poster
- Hauschildt, H., T. Martin and A. Macke, 2001: Cloud Liquid Water path from combined AMSU and AVHRR measurements, *XXVI EGS General Assembly*, Nice, France, 26-30 March 2001, Poster
- Hauschildt, H., T. Martin and A. Macke, 2000: Horizontal Distribution of Cloud Liquid Water from combined AVHRR and AMSU measurements, *SAF-Training Workshop*, Dresden, Germany, 20 - 22 November 2000, Poster
- Löhnert, U., S. Crewell, C. Simmer, A. Macke, M. Quante, 2000: Extraction of Cloud Liquid Water Signals from a Combination of a Cloud Radar and a Multi-Channel Microwave Radiometer, *XXV EGS General Assembly*, Nice, France, 25-29 April 2000, Poster
- Löhnert, U. 2002: Derivation of cloud liquid water from ground-based active and passive remote sensor, University of Bonn, 103 pp, PhD thesis.
- Hauschildt, H. 2000: Bestimmung der horizont-talen Verteilung des Flüssig-wasserpades aus Daten des AMSU und AVHRR, Institute for Marine Sciences, University of Kiel,83 pp, Diploma Thesis.
- Schlüter, I. , 2002: Einfluss der horizontalen Auflösung auf die Wolkensimulation des Lokal-Modells, Meteorologisches Institut der Rhein. Friedr.-Wilh.-Universität Bonn,44 pp, Diploma Thesis.
- Simmer, C. and S.Crewell, 2002: BALTEX BRIDGE Campaign Workshop, Leipzig, BALTEX Newsletter, Page 12-13.

The CLIWA-NET web site <http://www.knmi.nl/samenw/cliwa-net> contains comprehensive information about the project, quicklooks and results. All publications including quarterly and annual reports of CLIWA-NET can be found there.

The projects highlights, quicklooks and Level2c data are distributed on DVD. The content can be found at http://cliwaftp.meteo.uni-bonn.de/CLIWA-NET/cliwa_dvd/

International BALTEX Secretariat Publication Series
ISSN 1681-6471

- No. 1:** Minutes of First Meeting of the BALTEX Science Steering Group at GKSS Research Center in Geesthacht, Germany, 16-17 May, 1994. August 1994
- No. 2:** Baltic Sea Experiment BALTEX – Initial Implementation Plan. March 1995, 84 pages
- No. 3:** First Study Conference on BALTEX, Visby, Sweden, August 28 – September 1, 1995. Conference Proceedings. Editor: A. Omstedt, SMHI Norrköping, Sweden. August 1995, 190 pages
- No. 4:** Minutes of Second Meeting of the BALTEX Science Steering Group at Finnish Institute of Marine Research in Helsinki, Finland, 25-27 January, 1995. October 1995
- No. 5:** Minutes of Third Meeting of the BALTEX Science Steering Group at Strand Hotel in Visby, Sweden, September 2, 1995. March 1996
- No. 6:** BALTEX Radar Research – A Plan for Future Action. October 1996, 46 pages
- No. 7:** Minutes of Fourth Meeting of the BALTEX Science Steering Group at Institute of Oceanology PAS in Sopot, Poland, 3-5 June, 1996. February 1997
- No. 8:** *Hydrological, Oceanic and Atmospheric Experience from BALTEX*. Extended Abstracts of the XXII EGS Assembly, Vienna, Austria, 21-25 April, 1997. Editors: M. Alestalo and H.-J. Isemer. August 1997, 172 pages
- No. 9:** The Main BALTEX Experiment 1999-2001 – **BRIDGE**. Strategic Plan. October 1997, 78 pages
- No. 10:** Minutes of Fifth Meeting of the BALTEX Science Steering Group at Latvian Hydrometeorological Agency in Riga, Latvia, 14-16 April, 1997. January 1998
- No. 11:** Second Study Conference on BALTEX, Juliusruh, Island of Rügen, Germany, 25-29 May 1998. Conference Proceedings. Editors: E. Raschke and H.-J. Isemer. May 1998, 251 pages
- No. 12:** Minutes of 7th Meeting of the BALTEX Science Steering Group at Hotel Aquamaris in Juliusruh, Island of RÜGEN, Germany, 26 May 1998. November 1998
- No. 13:** Minutes of 6th Meeting of the BALTEX Science Steering Group at Danish Meteorological Institute in Copenhagen, Denmark, 2-4 March 1998. January 1999

- No. 14:** BALTEX – BASIS Data Report 1998. Editor: Jouko Launiainen, 96 pages. March 1999.
- No. 15:** Minutes of 8th Meeting of the Science Steering Group at Stockholm University in Stockholm, Sweden, 8-10 December 1998. May 1999
- No. 16:** Minutes of 9th Meeting of the BALTEX Science Steering Group at Finnish Meteorological Institute in Helsinki, Finland, 19-20 May 1999. July 1999
- No. 17:** Parameterization of surface fluxes, atmospheric planetary boundary layer and ocean mixed layer turbulence for BRIDGE – What can we learn from field experiments? Editor: Nils Gustafsson. April 2000
- No. 18:** Minutes of the 10th Meeting of the BALTEX Science Steering Group in Warsaw, Poland, 7-9 February 2000. April 2000
- No. 19:** BALTEX-BASIS: Final Report, Editors: Jouko Launiainen and Timo Vihma. May 2001
- No. 20:** Third Study Conference on BALTEX, Mariehamn, Island of Åland, Finland, 2-6 July 2001, Conference Proceedings. Editor: Jens Meywerk, 264 pages. July 2001
- No. 21:** Minutes of 11th Meeting of the BALTEX Science Steering Group at Max-Planck-Institute for Meteorology in Hamburg, Germany, 13-14 November 2000. July 2001
- No. 22:** Minutes of 12th Meeting of the BALTEX Science Steering Group held at Royal Netherlands Meteorological Institute (KNMI), De Bilt, The Netherlands, 12-14 November 2001. April 2002
- No. 23:** Minutes of 13th Meeting of the BALTEX Science Steering Group held at Estonian Business School (EBS), Centre for Baltic Studies, Tallinn, Estonia, 17-19 June 2002. September 2002
- No. 24:** The eight BALTIMOS Field Experiments 1998-2001. Field Reports and Examples of Measurements. Editors: Burghard Brümmer, Gerd Müller, David Schröder, Amélie Kirchgäßner, Jouko Launiainen, Timo Vihma. April 2003, 138 pages.
- No. 25:** Minutes of 14th Meeting of the BALTEX Science Steering Group held at Lund University, Department of Physical Geography and Ecosystems Analysis, Lund, Sweden, 18 - 20 November 2002. May 2003
- No. 26:** CLIWA-NET: BALTEX BRIDGE Cloud Liquid Water Network. Final Report. Editors: Susanne Crewell, Clemens Simmer, Arnout Fejt, Erik van Meijgaard. July 2003, 53 pages.